A STUDY OF SECONDARY INJECTION OF GASES INTO A SUPERSONIC FLOW

Thesis by

Frank William Spaid

In Partial Fulfillment of the Requirements

For the Degree of

Doctor of Philosophy

California Institute of Technology

Pasadena, California

1964

(Submitted May 18, 1964)

ACKNOWLEDGMENTS

The author would like to express his appreciation to Professor Edward E. Zukoski of the California Institute of Technology for his help and encouragement, and his many contributions to the research which is the subject of this thesis.

Thanks are given to the Hypersonic Wind Tunnel Staff for assistance with the experiments which were carried out in the Supersonic Wind Tunnel at the California Institute of Technology.

The author would also like to thank John F. Newton, Jr., and Mack W. Dowdy of the Solid Propellant Engineering Section at the Jet Propulsion Laboratory, and the entire staff of the 20-inch Supersonic Wind Tunnel at JPL for their assistance with the experiments which were carried out in that facility.

The research work described in this thesis was supported by the Daniel and Florence Guggenheim Jet Propulsion Center of the California Institute of Technology and by the National Aeronautics and Space Administration, through the Solid Propellant Engineering Section of the Jet Propulsion Laboratory, California Institute of Technology.

The author would like to thank the Sloan Foundation and the National Science Foundation for fellowship assistance and the California Institute of Technology for a Graduate Research Assistantship.

ABSTRACT

The flow field around the injection port for secondary injection of a gas normal to a supersonic stream has been studied in a series of wind tunnel experiments. The experiments were conducted at free-stream Mach numbers of 1.38 to 4.54. Gaseous nitrogen, argon, and helium were injected through a circular hole or a transverse slot with sonic flow at the injection orifice. Data are presented which include static pressure distributions on the wall in the region of the injector, shock shapes, and injectant mass fraction, total pressure, and velocity profiles downstream of the injector. A scale parameter has been calculated, based on a simple, inviscid model of the flow field. This scale parameter gives a good general correlation of the data. Use of this scale parameter allows the prediction of a simple scaling law for the normal forces on a wall produced by secondary injection. For the case of injection through a slot, this scaling law has been compared with experimental results reported by other workers. This comparison indicates that further work will be necessary to clarify the effect of free-stream Mach number on the flow field. For the case of injection through a hole, the force scaling law is in approximate agreement with existing rocket motor test results.

TABLE OF CONTENTS

I. INTRODUCTION

The description of the flow field set up by the injection of a secondary gas into a supersonic primary flow is a problem of current engineering interest. Flows of this type occur during thrust vector control of rocket motors, during jet reaction attitude control of vehicles moving through the atmosphere, and during fuel injection into a supersonic burner.

In all of these applications, when a gas is injected into the primary flow, a high pressure region is set up on the wall in the neighborhood of the injector. The detailed mechanism which governs the magnitude of the resulting force on the wall is not yet thoroughly understood, but may be crudely described as follows. The injected material acts as an obstruction to the primary flow and, as such, produces a strong shock wave in the primary flow. This shock interacts with the boundary layer on the wall and may cause it to separate. Both the initial shock and the resulting separation tend to produce a region of high pressure near the point of injection. A further pressure change may be produced farther downstream by mixing of the primary and secondary flows. The relative importance of the pressure fields produced by these processes has not been established and, at present, published theoretical work usually emphasizes one or the other of the processes.

The goal of the present study has been to obtain fundamental information concerning the processes of interaction which occur during secondary injection and, in particular, to determine similarity

rules for the important phenomena. The situation chosen for experimental and theoretical study is the sonic injection of a gas through a wall and normal to a primary flow which is uniform and rectilinear outside a wall boundary layer. The work is divided into two sections; the first is concerned with injection through a circular hole, and the second is concerned with injection through a slot. Apart from the obvious distinction that the first case is three-dimensional and the second case is two-dimensional, a second reason for treating these two cases separately is that boundary layer effects were found to be a much more important part of the two-dimensional case than they were in the three-dimensional case. In each part, a model for the interaction region is presented and is compared with experimental data obtained by the author and by other workers.

II. INJECTION THROUGH A CIRCULAR HOLE

Although it is common practice to discuss a two-dimensional case before presenting a three-dimensional one, since the two-dimensional problem is usually much simpler, this discussion will begin with the case of injection through a circular hole. There are two reasons for this. First, because of its relative experimental simplicity and its importance in engineering applications, the circular hole injection experiments were conducted first. Second, the case of injection through a slot is complicated by an important interaction between boundary-layer separation and the inviscid flow field, an effect which is much less prominent in the three-dimensional case.

A. Description of Experiments

A series of experiments were conducted in the 2.5-inch Supersonic Wind Tunnel at the California Institute of Technology. This facility is described in detail in Ref. 1. Some minor modifications to the tunnel have been made since this report was written, particularly in the test-section region.

During these experiments, gaseous nitrogen, argon, and helium were injected through orifices in the test-section side walls. Test section conditions consisted of Mach numbers 2.56 and 1.38 and Reynolds numbers per inch of 1.3×10^5 to 4.3×10^5 at the first Mach number and 4.5×10^5 at the second. At the Mach number of 2.56 and below a Reynolds number per inch of 1.7×10^5, the boundary layer on the test section wall was found to be laminar; above that Reynolds number it was turbulent at the same Mach number. The

tunnel could maintain quasi-steady state flow in the test section at a Mach number of 1.38 for only approximately ten seconds. It was possible to perform experiments only at a single free-stream stagnation pressure and therefore only at a single Reynolds number per inch. This Reynolds number resulted in a turbulent boundary layer in the region of the injection port.

Because of the very short test-time duration at the lower Mach number, surveys of the undisturbed flow in the test section were carried out only at the higher Mach number. Figure 1 shows Mach number profiles which were obtained at two axial stations in the test section for an intermediate Reynolds number which corresponded to a free-stream stagnation pressure of approximately one atmosphere. These measurements were made in a plane equidistant from both of the glass side-walls of the test section and normal to the wall containing the injector. It is believed that these profiles are representative of the uniformity of the flow which existed for all of the tests, although a variation in test-section Mach number of the order of $\pm$ 1 per cent was observed when the nozzle blocks were removed and replaced for the purpose of changing injectors. Examination of schlieren pictures for various values of test-section Reynolds number indicated that the boundary layer thickness exhibited by the profiles of Figure 1, approximately 0.2 in., is the correct order of magnitude for all of the test conditions. The data of Figure 1 were obtained with a probe made from 0.065 in. outside diameter tubing, flattened and ground at one end to a tip which was approximately 0.10 in. wide by 0.006 in. high, with a hole 0.002 in. high. Probe pressure was measured with

a mercury manometer.

The experimental data consisted of test-section flow conditions, schlieren photographs, static pressure distributions on the test section wall in the region of injection, concentration and total pressure measurements in the flow downstream of the injection port, and the injectant total pressure and mass flow rate. The static pressures were measured by mercury manometers, and the concentration measurements were obtained with a total-pressure probe and a Gow-Mac thermal conductivity cell. The total-pressure probe which was used for the concentration and total pressure measurements for injection through a circular hole was a three-pronged probe with tips spaced 0.125 in. apart. The tips were circular, with a 0.031 in. O.D. and a 0.013 in. diameter hole. The total pressure profiles and the velocity profiles which were then obtained from the total pressure, concentration, and other data, are the work of H. Burden, and are reported in Ref. 2.

Figure 2 is a section view of the circular-hole injector which was used for the majority of these experiments. The section is taken in a plane parallel to the test-section flow, the same one in which the Mach number and boundary layer profiles were obtained. It can be seen that static pressure taps were located on the wall as close to the injector as possible. One other injector, having a diameter of 0.114 in. and a configuration quite similar to that shown in Figure 2, was also used, although the nozzle block section in which this injector was installed was not instrumented with static pressure taps. Discharge

coefficients for each of these orifices were determined experimentally, and the injection pressures were corrected for losses caused by friction in the injectant supply tube.

In addition to the experiments at the California Institute of Technology, experiments were conducted in the 20-inch Supersonic Wind Tunnel at the Jet Propulsion Laboratory. These experiments were part of a series which were conducted by M. W. Dowdy and J. F. Newton, Jr.[3]* Gaseous nitrogen was injected through a sonic orifice 0.100 in. in diameter normal to the surface of a sharp-edged flat plate, 7.00 in. to the rear of the leading edge. The surface of the plate in which the injector was located was parallel to the test section flow, and a boundary-layer trip wire was attached near the leading edge of the plate. Tests were conducted at test-section Mach numbers of 4.54, 3.50, 2.61, and 2.01. The highest and the lowest practical tunnel stagnation pressures were utilized at each Mach number except 3.50 in an attempt to study the effect of test-section Reynolds number at a fixed Mach number, but only at Mach 2.61 was it possible to achieve both laminar and turbulent boundary layers, at Reynolds numbers based upon the distance from the injection port to the leading edge of 0.749×10^6 and 1.99×10^6, respectively. At Mach numbers 4.54 and 3.50, the boundary layer on the plate near the injection port was always laminar; and at Mach number 2.01, it was always turbulent.

---

*Numbers in parentheses refer to references listed at the end of the paper.

The experimental data consisted of schlieren and shadowgraph pictures, tunnel and injection conditions, and static pressure measurements on the plate in the injection region. The static pressures were measured by a single transducer and a pressure-switching mechanism. Further details concerning the experimental apparatus and procedure are available in Ref. 3, and a description of the wind tunnel facilities of the Jet Propulsion Laboratory is given in Ref. 4.

B. Description of the Flow Field

A crude picture of the flow field produced by injection through an orifice has been obtained by examination of schlieren and shadowgraph pictures of the interaction region. Figures 3a and 3b are scale drawings of two shadowgraph pictures taken at different free-stream stagnation pressures but at the same ratio of jet stagnation pressure to free-stream stagnation pressure. The free-stream Mach number was 2.61 and the flat plate model was used here. For these examples, the injected material enters, through a circular orifice, with a static pressure much higher than the value in the undisturbed primary flow. The flow is sonic at the injector and expands rapidly through a strong Prandtl-Meyer fan. The interaction of the two streams produces a strong bow wave on the upstream side of the injector, and the shock-induced pressure field turns the injectant so that it moves approximately parallel to the wall.

The bow shock wave - boundary layer interaction produces a region of boundary layer separation upstream of the shock. For the case of a turbulent boundary layer, the example illustrated in Figure 3a, the separated region is short, and the oblique shock produced by

separation is often too weak to be observed. When the boundary layer is laminar, Figure 3b, the separated region is much larger, and the angle between the separated flow and the wall is never more than a few degrees.

Some details of the flow near the injector are shown on the schlieren photographs. One feature which is usually seen, and which is apparently the region of maximum concentration of the injectant, has the appearance of a streamline of the injectant. Determination of the maximum distance between this feature and the wall (see Figure 3) gives a simple visual measure of the penetration of the secondary fluid into the primary flow. Figures 3a and 3b illustrate flow conditions in which the distance of this feature from the wall is much larger than a characteristic boundary layer dimension.

Shadowgraph pictures taken at the higher Mach numbers and correspondingly lower test-section Reynolds numbers showed wavy shocks and jet outlines, which indicated unsteady flow. This unsteady behavior has also been reported by Amick and Hayes.[5]

C. Analytic Model

In investigating the shock patterns produced by secondary injection, one is reminded of shock shapes produced by blunt axisymmetric bodies. This fact suggested that some insight into the scaling laws for secondary injection could be obtained by setting up a simple model for a solid body which would give a shock pattern similar to that produced by the injectant. For the purposes of this simple model, it is assumed: (1) that a sonic jet is injected into a uniform supersonic flow with no

wall boundary layer; (2) that no mixing occurs between the two flows; (3) that the interface between the flows is a quarter sphere followed by an axisymmetric half body; (4) that pressure forces on the sphere can be calculated by use of modified Newtonian flow; and (5) that the injectant expands isentropically to the ambient pressure with the vector parallel to the wall at the downstream face of the sphere. However, note that it is not assumed to completely fill the semicircular cross section of the downstream face of the quarter sphere which forms the "nose" of the equivalent solid body. Thus no continuity equation is used here and the fraction of the cross-sectional area occupied by the injectant flow is not specified, but must be determined.

Assumption (4) is not as restrictive as the derivation of Newtonian flow equations implies. Although the Newtonian approximation is a limiting process in which $M_\infty \to \infty$ and $\gamma_\infty \to 1$, comparison with experiment has shown that the pressure distributions on the upstream sides of blunt bodies are predicted reasonably well by Newtonian flow calculations over a wide range of Mach numbers, and for $\gamma_\infty = 1.4$.[6]

The coordinate system used in the analysis and in the description of the experiments is illustrated in Figure 3. The x-z plane is shown here with the y-axis perpendicular to the page. The origin of the coordinate system has been chosen so that the $y = 0$ plane includes the center of the injector and so that the origin of the coordinate system lies at the intersection of the bow shock wave with the wall.

The purpose of the analytic model is to determine the radius, h_s, of the equivalent solid body as a function of the properties of the

free-stream and of the injectant. This is accomplished by constructing a momentum balance in the x-direction on a control volume whose bounding surfaces are made up of (1) the spherically shaped nose, (2) the side wall lying under the nose, which is the plane z = 0, and (3) the portion of the x - constant plane lying just downstream of the nose. The x-component of the momentum change of the jet is equal to the net x-component of the pressure force on the control volume, all shear stresses being neglected.

Let us consider the flow over the spherical nose. For Newtonian flow calculations, with the modification suggested by Lees [7], the pressure coefficient, $C_p \equiv (P - P_\infty)/\frac{1}{2}\rho_\infty V_\infty^2$, on the surface of the body is given by

$$\frac{C_p}{C_p^*} = \frac{\sin^2\alpha}{\sin^2\alpha^*}$$

where α is the angle between the local tangent to the surface and the undisturbed flow direction, and must lie between 0 and $\pi/2$. Here C_p^* and α^* are evaluated at the nose of the body. Hence, $\alpha^* = \pi/2$ and C_p^* is the pressure coefficient corresponding to the stagnation pressure behind a normal shock, found from the theory of supersonic flow of an ideal gas:

$$C_p^* = \frac{2}{\gamma_\infty M_\infty^2}\left[\left(\frac{\gamma_\infty+1}{2}M_\infty^2\right)^{\frac{\gamma_\infty}{\gamma_\infty-1}}\left(\frac{\gamma_\infty+1}{2\gamma_\infty M_\infty^2-\gamma_\infty+1}\right)^{\frac{1}{\gamma_\infty-1}} - 1\right] \quad (1)$$

In this case, the Newtonian calculation is applicable only to the surface of the quarter sphere. The total axial force on the control

volume was obtained by integrating the pressure force in the x-direction over the spherically-shaped nose of the equivalent body and the portion of the x = constant plane just downstream of the nose. The contribution of this latter surface is just $-\frac{\pi}{2} P_\infty h^2$ which is equal in magnitude but opposite in sign to one of the terms which results from the calculation of the force on the curved surface (see Appendix B for a detailed derivation). The net result is:

$$F_x = \frac{\pi}{8} M_\infty^2 \gamma_\infty C_p^* h^2 P_\infty \tag{2}$$

In order to calculate the net momentum outflow through the control volume, we note that because the jet is injected normal to the wall, the only contribution is the total x-momentum of the injected gas after it has expanded isentropically to the free-stream static pressure. The analysis could easily be extended to the case of injection at an arbitrary angle to the free-stream flow, merely by including the x-component of the momentum of the injected gas at the injection orifice.

The momentum flux of the expanded secondary flow can be simply evaluated. First, the mass flow of injectant is calculated from the assumption that the injector flow is sonic and fills an area which is c times the actual injector area; that is, c is a discharge coefficient for the injector and $(\sqrt{c}\ d)$ is the equivalent diameter of the injector, and hence is the characteristic dimension of the injector. From this assumption it follows that:

$$m_j = cA_j P_{o_j} \left[\left(\frac{\gamma_j}{R_j T_{o_j}} \right) \left(\frac{2}{\gamma_j + 1} \right)^{(\gamma_j + 1)/(\gamma_j - 1)} \right]^{\frac{1}{2}} \tag{3}$$

where (cAj) is the equivalent injector area. The Mach number at the exit of the control volume is given by the expression for isentropic expansion from a stagnation pressure P_{o_j} to a static pressure P_∞. This expression can be solved for the velocity, V_j, and the result is

$$V_j = \left[\left(\frac{2\gamma_j R_j T_{o_j}}{\gamma_j - 1} \right) \left\{ 1 - \left(\frac{P_\infty}{P_{o_j}} \right)^{(\gamma_j - 1)/\gamma_j} \right\} \right]^{\frac{1}{2}} \tag{4}$$

The momentum flux is just $m_j V_j$, and consequently, the force balance is then given by

$$F_x = m_j V_j \tag{5}$$

All the parameters in this equation are known except the radius, h, and therefore, equation (5) can be solved for this parameter. The result is:

$$\frac{h}{d\sqrt{c}} = \left\{ \left(\frac{1}{M_\infty} \right) \left(\frac{P_{o_j}}{P_\infty} \frac{\gamma_j}{\gamma_\infty} \frac{2}{C_p^*} \right)^{\frac{1}{2}} \times \left[\frac{2}{\gamma_j - 1} \left(\frac{2}{\gamma_j + 1} \right)^{(\gamma_j+1)/(\gamma_j-1)} \left(1 - \left(\frac{P_\infty}{P_{o_j}} \right)^{(\gamma_j-1)/\gamma_j} \right) \right]^{1/4} \right\} \tag{6}$$

Note that when the ratio (P_{o_j}/P_∞) is held fixed, the radius decreases with increasing Mach number. However, for rocket work, it is often more convenient to use the stagnation pressure ratio, (P_{o_j}/P_{o_∞}), as the independent variable.

The first two factors of (6) may be rewritten to give:

$$\left\{ \frac{1}{M_\infty} \left(1 + \frac{\gamma_\infty - 1}{2} M_\infty^2 \right)^{(\gamma_\infty)/2(\gamma_\infty - 1)} \left(\frac{P_{o_j}}{P_{o_\infty}} \frac{\gamma_j}{\gamma_\infty} \frac{2}{C_p^*} \right)^{\frac{1}{2}} \right\} \quad (7)$$

It is evident from this form of these terms that the radius increases with the square root of (P_{o_j}/P_{o_∞}) and, in a more complex manner, with M_∞.

The variation of the terms in the square bracket of equation (6) and that of C_p^* with M_∞ or γ_∞ is not very rapid. Hence, the most important variation of the radius is approximately given by:

$$h \propto (d\sqrt{c}) \left(\frac{1}{M_\infty} \right) \left(\sqrt{\frac{P_{o_j}}{P_\infty}} \right) \quad (8)$$

In terms of the mass flow rate of injectant, m_j, equation (8) can be written as

$$h \propto \frac{1}{M_\infty} \sqrt{\frac{m_j}{P_\infty}} \left(R_j T_{o_j} \right)^{1/4} \quad (9)$$

Note that for simplicity, the complex dependence on γ_j and γ_∞ has been omitted here. Equations (8) and (9) are useful as long as $(P_\infty/P_{o_j}) \ll 1$ and $M_\infty > 2$.

Although the derivation used to obtain equation (6) was based on the assumption of a spherical interface between primary and injectant flows, it should be noted that the functional form of equation (6) is not sensitive to the shape of the interface. For example, the derivation has been carried out for elliptical interface shapes with

eccentricities ranging between 0 and 0.98. The equations for h obtained by this calculation had the same functional form given in equation (6) and differed from it by a multiplicative constant which depended on the eccentricity and which only changed by a factor of 2.3 for the range of eccentricities given above.

It is proposed that the calculated radius can be used as a measure of the scale of the disturbance produced by injection. Note that although the expression for h, given in equation (6), contains no adjustable constants, the exact correspondence between values calculated from equation (6) and any measured feature of the flow, such as the penetration height mentioned earlier, is purely fortuitous. However, if the model is correct, it is to be expected that changes in scale of flow features will be proportional to changes in h.

Since the boundary layer has not been considered at all in this analysis, it would be expected that h would have to be larger than a characteristic boundary layer dimension in the immediate vicinity of the jet, i.e., a characteristic thickness of the boundary layer in the region of maximum separation, in order for the analysis to be applicable.

However, there is a difference between the observed flow field and the model which seems to make this limitation somewhat less severe. As the injectant expands just after leaving the orifice, it is initially conical in shape so that the actual obstruction shape as viewed from the front is probably similar to that of a frustrum of a cone with its small end resting on the wall, and capped by a sphere. This shape

would be expected to produce considerably less of an obstacle to the boundary layer than a quarter sphere of the same projected area.

Figures 3a and 3b given typical examples of the change in boundary layer thickness caused by injection. The maximum thickness of the separated boundary layer upstream of the injector was never observed to be more than about twice the thickness of the undisturbed boundary layer at the same distance from the plate, as determined from the photographs.

To provide a basis for comparison, some experiments with solid objects of the same shape as that postulated in the analytic model have been conducted. These objects were attached to the nozzle wall, and schlieren pictures were taken at a test-section Mach number of 2.56. Photographs with the same shock shape were compared. The separation produced with both laminar and turbulent wall boundary layers was always considerably more extensive than that produced by injection, thus supporting the preceding supposition about the applicability of the model.

D. Presentation of Experimental Data

In the following sections, results are given of experiments concerning the flow field geometry, concentration measurements, and static pressure measurements on the wall. The data are presented in terms of space coordinates normalized by the radius, which is calculated from equation (6). This mode of presentation was used to facilitate the verification of the proposed scaling law.

1. Penetration height. - In most of the schlieren photographs

taken with secondary injection of argon and nitrogen into air, a distinct feature appears which looks like the top or outer boundary of the jet. Although this feature, shown in Figure 3, is probably the line of maximum concentration of injectant rather than the jet boundary, it has been selected as being characteristic of the scale of the disturbance produced by the jet, and hence is called the penetration height of the jet. That flow fields for different injection rates should be geometrically similar is, of course, an assumption which must be verified.

Values of the penetration heights determined directly from schlieren photographs made in the CIT facility are shown in Figure 4. Here, penetration heights normalized by the equivalent injector diameter, $(\sqrt{c}\ d)$, are given as a function of the ratio of injectant to primary stream stagnation pressures; data are presented for two Mach numbers. Nitrogen and argon were used as injectants, and experiments were conducted with two injector diameters.

The magnitude of the penetration height was found to depend directly on the equivalent injector diameter and to vary approximately with the square root of the injector - to - primary flow stagnation pressure ratio. No dependence on injector molecular weight or specific heat ratio was noticed when penetration heights for a given total pressure ratio were compared.

The data shown in Figure 4 were obtained with laminar and turbulent boundary layers. It is particularly interesting to note that measured values of the penetration height were not noticeably dependent on the state of the boundary layer, and comparison of Figures 1 and 4

indicates that they were not noticeably dependent upon the boundary layer thickness for values of h which were appreciably less than the boundary layer thickness at $M_\infty = 2.56$.

The data of Figure 4 show that the height increases with increasing Mach number in the primary stream. This is a result of the fact that for a given primary stagnation pressure, the local static pressure decreases rapidly with increasing Mach number.

Theoretical values of the scale parameter are also shown in Figure 4 for both Mach numbers. The agreement between the calculated and measured quantities is good over the whole pressure ratio range studied, and the dependence on specific heat ratio, molecular weight, and Mach number is correctly predicted.

Values of penetration heights were obtained in the JPL facility from shadowgraph photographs for a wide range of Mach number and pressure ratio. Comparison of these data with that obtained in the CIT facility showed that the JPL, flat plate results were about 20 per cent lower than the comparable CIT, nozzle wall data. This systematic difference is probably due to differences in the optical systems. Also, in comparing the data with the results predicted from the model, it should be remembered that the features examined on either schlieren or shadowgraph pictures are not the jet boundaries themselves, and hence that either the calculated scale factors or the measured penetration heights can only be viewed as being proportional to the actual characteristic scale of the flow.

Comparison of the flat plate data and the results of equation

(6) are shown in Figure 5. Here, all of the measured penetration heights are increased by 20 per cent. The agreement between theory and experiment appears to be good, although the experimental data may have a slightly more rapid variation with Mach number than is predicted from equation (6).

Although the good absolute agreement between the prediction of equation (6) and measured values is fortuitous, the fact that the data agree so well in slope and shape over a range of injector diameter, injection pressure, and primary-flow Mach number indicates that the value of the scale factor predicted by equation (6) is a useful measure of the scale of the interaction phenomena and suggests that the proposed model does include the pertinent physical phenomena. The success of this simple model in predicting the penetration heights also indicates that the gross features of the flow field can be characterized by a single dimension which is proportional to h.

2. Shock shapes. - As a further check on the suggestion that h is a characteristic dimension of the flow field, the shapes of the bow shock waves, as seen from the side, were determined from schlieren and shadowgraph pictures from both the flat plate and nozzle wall data. In all cases, the shock coordinates were normalized by values of h calculated from equation (6). In Figure 6, a few typical cases from the nozzle wall data are compared. The shock shapes plotted here cover the maximum range of parameters studied in the CIT Supersonic Wind Tunnel, and are typical of the measurements made of more than 50 schlieren photographs. In addition, the solid line in Figure 6 repre-

sents the average of the data which were obtained from the flat plate experiments at a Mach number of 2.61. These data showed somewhat less scatter than did the nozzle wall data which are plotted here.

It is again evident from study of these data that the normalized coordinates agree well and that the agreement appears to be independent of pressure ratio, specific heat ratio, injector diameter, and the condition of the boundary layer. In addition, the fact that the data from schlieren and shadowgraph pictures agree well substantiates the assertion that the observed differences in penetration height from these sources is a result of the differences between these two flow visualization techniques.

In order to check the influence of molecular weight on the process, some shock shape data were obtained with helium injectant. Unfortunately, schlieren photographs taken with helium did not reveal the penetration distance directly, although the bow shock was easily observed. However, the normalized shock shapes agree as well as the other data when the data are normalized by values of penetration height calculated from equation (6) with experimentally determined values of the flow coefficient, c. Hence it is evident that the characteristic dimension of the interaction is independent of molecular weight.

The data discussed here are shock shapes in the x-z plane. From experiments conducted in the CIT facility at a Mach number of 2.56, Burden[2] has shown that the shock shape is axisymmetric about an axis lying in this plane, and parallel to the wall but displaced a distance h along the z-axis from the wall. Thus, given this axis, the curve in Figure 6 gives a complete description of the shock shape pro-

duced by injection.

In Figure 7 are presented curves which represent averages of shock shape data from the JPL flat plate experiments. This method of data presentation was chosen because the curves lie so close together that it would have been very difficult to visualize the important features had the data points been plotted, but yet their significance is lost if they are not directly compared. The scatter in the data is somewhat less than that shown in Figure 6 except where the curves are dashed, in which case the difficulty in interpreting the photographs caused greater scatter. Some of this difficulty at the higher Mach numbers was caused by the unsteadiness in the flow field previously mentioned. The fact that the curves all approach a single curve for small values of (x/h) indicates that the properly normalized shock shapes near the injector port are nearly identical. Now the shock location near the nose of a blunt body in a supersonic flow is very weakly dependent on Mach number (for Mach numbers larger than about 2.0), but is strongly dependent upon the size of the body. Thus, Figure 7 indicates that the dependence of h upon the free-stream Mach number is correctly predicted by equation (6).

3. Concentration profiles. - A more critical check on the proposed scaling law is given by examination of the flow pattern of the injectant. The mixing of the injectant and primary flows has been examined by making analyses of gas samples drawn from various locations in the flow field. Measurements were taken at Mach number 2.56 in the nozzle-wall injection system with argon and helium in-

jectants. The positions most thoroughly studied lie in the x-z plane, $y \equiv 0$; a few positions for other values of y were also examined.

Data obtained with argon injectant in the $y \equiv 0$ plane are shown in Figures 8a and 8b. Here, the origin of each concentration profile is superimposed at the appropriate position on a plot of the x-z plane which also shows the bow shock wave. In Figure 8a, the region close to the injector is shown on an expanded scale, and the data points are presented in detail to illustrate the reproducibility of the experiments. All coordinates are normalized by calculated values of the scale parameter. The normalized diameter of the probe which was used to make these measurements is shown in Figure 8a for each value of h used in the experiments.

The data of Figure 8 show that near the injector the profile is sharply curved on the lower side of the maximum, but that downstream of $(x/h) \approx 4$, the profile is roughly Gaussian except for a slight wall interference effect. It is obvious that the observed penetration height and calculated scale factor correspond much closer to the line of maximum concentration than to the outer edge of the injectant stream.

Mixing occurs rapidly close to the injector. For $(x/h) \approx 1$, the maximum concentration is less than 0.80; thus, even this close to the injector, the injectant is already substantially mixed with the primary flow. Farther downstream mixing is slower, and at $(x/h) \approx 12$ the concentration maximum is still greater than 25 per cent.

Measurements made on planes other than $y = 0$ are shown in Figure 9 for two values of (x/h). These data and that shown in Figure

8 have been used to obtain the cross plots and concentration profiles shown in Figures 10a and 10b. In Figure 10a, cross plots of concentration versus (y/h) for a number of values of distance above the wall, (z/h), and for two values of (x/h) are shown. Above the concentration maximum, the curves are again roughly Gaussian, but below it they have a definite concentration minimum on the (y/h) = 0 axis. This minimum is present at both (x/h) stations, but is much less marked at (x/h) = 12.

The concentration profile of Figure 10b shows the extent of this minimum more clearly. Here lines of constant concentration in the (y/h) - (z/h) plane are presented. The solid points shown on the figure were obtained by interpolation of the data of Figures 8 and 9. The shapes of the two plots are roughly similar, although the (x/h) dimension appears to be growing slightly more rapidly than the (y/h) dimension.

The kidney-shaped cross section seen in the concentration profiles of Figure 10b suggests that a vortex is shed from either side of the injectant jet. The vortex filaments appear to be roughly parallel to the wall, and with vorticity such that, near the wall, primary gas is swept in toward the centerline of the flow, i.e., toward (y/h) = 0. This type of vortex structure has been observed by other workers for the case of subsonic injection into a subsonic stream.[8] Such vortices may explain the steep gradients in concentration observed at the $(x/h) \approx 2$ position.

The data presented in the last three figures were obtained with

argon injectant. Similar data obtained with helium injectant are shown in Figure 11a. As would be expected, these curves, presented in terms of mass fractions, are not identical with the argon data, since the two situations are not directly comparable. The difference becomes more marked with increasing (x/h). The nature of the difference is more clearly shown in Figure 11b, where the profiles for helium and argon at (x/h) = 12.3 are compared with the concentration values normalized by the maximum value. The curves are similar, but the helium profile is lower than that for argon.

Although the general shapes of the curves shown in Figures 11a and 11b are quite similar, such features as jet width and distance of maximum concentration line from the wall are definitely smaller for the helium case. Hence, in the coordinates used here, the helium jet spreads more slowly than the argon jet.

Argon data are presented in Figure 8 and 10 for stagnation pressure ratios which give a 2.2:1 change in penetration height. The normalized concentration profiles shown in these figures are almost identical over this scale change. The data are also insensitive to the state of the boundary layer, since both laminar and turbulent layers are included. Hence, it is apparent that the scaling rule given by equation (6) is valid for the mixing process, too, when changes in scale by not more than a factor of two are considered; the good agreement of the data suggests that much larger changes could be adequately treated.

4. Velocity and total pressure profiles. - Figures 12 through 16

give velocity, Mach number, and total pressure profiles normalized by the respective free-stream values, for argon injection.[2] A single set of injection and free-stream conditions was maintained, and data are presented for four values of (x/h) between (x/h) = 8 and (x/h) = 15. At each axial station, data are given at the centerline and at two off-axis positions. The argon concentration data of Figures 8 to 10 were used to compute the effective specific heat ratio and molecular weight for each of the velocity, total pressure, and Mach number data points. For the cases where argon concentration data had not been obtained at the particular location, the available concentration data were linearly interpolated or extrapolated. The results of these interpolations or extrapolations are presented as solid lines in Figures 12 through 15. The velocity, total pressure, and Mach number profiles were found to be very insensitive to errors in argon concentration in the range of argon concentration which was encountered, so that the interpolated or extrapolated values appeared to be quite satisfactory. The local total pressure and Mach number were calculated with the assumption that the local static pressure was constant and equal to its value at the wall. Examination of the wall static pressure data of Figure 17 and 18 shows the static pressure to be approximately constant and equal to the undisturbed static pressure for (x/h) greater than 8 and for (y/h) in the range of zero to at least 4.3. Because the wall static pressure was found to be nearly constant in this downstream region, the assumption of constant static pressure in this limited region away from the wall is a reasonable one.

Note that each of the velocity, total pressure, and Mach number profiles exhibit two maxima at most locations, and that these occur at the same values of (z/h). These curves show a minimum near the maximum value of argon concentration. This is reasonable, because the velocity which the argon would attain by expanding isentropically from its stagnation pressure to the free-stream static pressure divided by the free-stream velocity is 0.885 for this set of test conditions. In addition, the turning process results in losses, as indicated by the very large total pressure defect in this region. The velocity profiles do approach the free-stream velocity with increasing (x/h), but there is still a substantial velocity defect at (x/h) = 15, (y/h) = 0 and (y/h) = 0.611. In Figure 14, undisturbed boundary layer profiles are superimposed upon the velocity profiles which were obtained with injection, and it can be seen that the flow near the wall is characteristic of the undisturbed boundary layer at the two off-axis stations, and somewhat less so at the axis.

Figure 16 is a composite plot of argon concentration contours and total pressure contours at (x/h) = 12. The concentration contours are essentially the same as those in Figure 10b for this axial station. It can be seen that the shapes of these contours are somewhat similar, but the kidney-shape is somewhat less pronounced in the case of the total pressure contours. The shape of the total pressure contours is a further indication of the presence of the two vortices which have been mentioned earlier.

5. Wall pressure distribution. - The experimental results

discussed up to this point concern the gross structure of the flow field produced by secondary injection. It has been shown that these features of the flow are approximately independent of the state of the boundary layer and of the boundary layer thickness for values of h which are as small as the boundary layer thickness or somewhat less, and that a simple model of the flow leads to the calculation of a single characteristic dimension which is a satisfactory scaling parameter. In contrast, when examining the flow field near the wall, the state of the boundary layer is very important because of its influence on the interaction between the bow shock and the boundary layer.

For example, when the layer is laminar, the bow shock - boundary layer interaction causes the layer to separate far upstream of the interaction region, and the separation angle is quite small, c. g., Figure 3b. When the layer is turbulent, the separation point is much closer to the interaction region, and the separation angle is much larger (Figure 3a). Hence, it is evident that the static pressure distribution on the wall under the separated regions will be quite different for turbulent and laminar boundary layers.

Static pressure data obtained in the CIT and JPL facilities are shown in Figures 17 through 23. Values of the pressure change produced by injection and normalized by the primary flow static pressure are given as a function of the position coordinates normalized by the calculated scale factor.

Consider first the results for M = 2. 56 shown in Figures 17 and 18. In Figure 17, data are shown for pressures measured along

the x-axis, i.e., along a line parallel to the primary flow and passing through the injector port. In general, the pressure increases rapidly between $-1 \leq (x/h) \leq -\frac{1}{2}$ on the upstream side of the injector port, falls to less than half the ambient around the port, and rises to the ambient value in the region $3 \leq (x/h) \leq 4$. When the boundary layer is laminar, the pressure increases slightly farther upstream of the shock due to separation; the corresponding turbulent separation occurs too close to the injector to be clearly discerned.

Off x-axis data are shown in Figure 18 for conditions corresponding to the turbulent boundary layer data of Figure 17. The data are for cuts along both y = constant and x = constant lines and serve to give a rough picture of the off-axis pressure distribution. As would be expected, pressure extremes are found along the x-axis and die off with distance away from this axis.

A wide range of injector parameters are covered by the data presented in Figures 17 and 18. For example, the change in total pressure ratios used here produces a 6.8:1 variation in the penetration height; data with both laminar and turbulent boundary layers are presented, and helium and nitrogen injectants are used. In view of this wide variation of parameters, the correlation of the data of Figures 17 and 18 by use of the normalization factor, h, is satisfactory.

The pressure distributions obtained at different Mach numbers for the flat plate model are shown in Figure 19 through 23. Again, it was not possible to present all of the data points; each figure includes

one set of data points, and the scatter in the data for which only average curves are given is similar to that of the data which are presented.

At the lowest Mach numbers, the pressure distributions were obtained with turbulent boundary layers, and the data are in good qualitative agreement with the nozzle wall data of Figure 17. A curve representing the average of the CIT data of Figure 17 is given in Figure 20 to facilitate this comparison. One of the differences between the nozzle wall and the flat plate data for the case of turbulent boundary layers was that separation could usually be observed in the flat-plate pressure distribution data. In the cases for which the separation shock was visible in the shadowgraph pictures, the point at which the pressure rise was detected corresponded reasonably well with the intersection of the separation shock with the wall.

Data with laminar boundary layers are shown in Figures 21, 22, and 23 for the higher Mach numbers. These data show a much more pronounced pressure rise far upstream of the injector than the corresponding turbulent data; for example, compare data of Figures 20 and 21 which were obtained at Mach number 2.61 and which have similar scale heights. Downstream of the injector, the data are similar for both boundary layer states. In general, the normalized pressure distributions with either a laminar or a turbulent boundary layer are surprisingly insensitive to Mach number.

In spite of the good general correlation of the pressure data in Figures 19 through 23, some systematic variations with pressure

ratio, or scale, can be noted. In the case of laminar separation, Figures 21 to 23, it can be seen that the separation distance normalized by h decreases as h increases. Considering the assumptions of the analytic model, it is not surprising that it does not account for an effect of shock - boundary layer interaction particularly well. However, in the case of the turbulent boundary-layer data upstream of the injector, the correlation is excellent, and thus it appears that the turbulent separation distance is a linear function of h.

In Figures 19 through 23 it can be seen that the agreement in the data is very good immediately downstream of the injection orifice in the region of minimum pressure, but a systematic difference appears somewhat farther downstream, in the range of (x/h) between 3 and 5. As h, or the injection pressure, increases, the pressure in this region rises more abruptly, until it actually overshoots the free-stream static pressure except at Mach number 4.54. At the lower Mach numbers, this overshoot becomes more pronounced, and its maximum value moves forward, in the normalized coordinates, as the injection pressure is increased. This overshoot occurs considerably downstream of any visible feature in the shadowgraph pictures to which it might be attributed.

This pressure overshoot is probably caused by the reattachment of the injectant jet to the wall. The increase in overshoot pressure with penetration height is explained by the fact that h is increased by increasing the total pressure, P_{o_j}. As h increases, the pressure ratio through which the injectant expands, i.e., P_{o_j}/P_∞,

increases, and the velocity in the jet must increase. Hence, the turning shock must be stronger and the pressures produced by the shock must be higher.

In each set of data at a constant Mach number, it was noted that the centerline pressure distribution corresponding to the lowest injection pressure seemed to be somewhat smeared out compared to the others. The pressure changes were more gradual, but extended over a larger region, again in the normalized coordinates. Although no detailed boundary layer studies have yet been made to confirm this supposition, the schlieren and shadowgraph pictures seem to support the notion that this smearing out of the pressure distribution occurs when the scale of the obstruction is of the same order as a characteristic boundary layer thickness. Since the scaling procedure is based upon a single scaling parameter for the flow field, it seems logical that this simplicity would be modified in a region where the scale factor was of the same order as another important characteristic dimension of the flow.

The correlation of the CIT data in Figure 17 is not as good as that of the JPL data presented in Figure 19 through 23, which appears to be excellent. At least some of the scatter in the CIT results is due to the rather crude pressure instrumentation. The data for one of the higher pressure-ratio runs of the CIT data with a laminar boundary layer exhibits what appears to be the pressure plateau characteristic of laminar separation. This pressure plateau does not show up clearly in all of the CIT laminar boundary-layer data, as can be seen in Figure 17. It is not known whether this is entirely due to inaccuracies

in measurement, or whether the much more pronounced effects of laminar separation exhibited in Figure 21 are primarily a result of actual differences in the shock - boundary layer interaction between the two sets of experiments. In any event, the character of the boundary layer on the tunnel wall in the CIT tunnel would be expected to be different from that in the flat-plate experiments in the JPL tunnel.

Several papers have appeared in the literature which present pressure distributions on flat plates with secondary injection, which are similar to the experiments described in this paper[5, 9, 10, 11]. Data from the paper by Cubbison, Anderson, and Ward[9] was considered to be the most directly comparable to that which has been presented here. Figure 24 presents six pressure distributions in the plane $y = 0$ for two Mach numbers; the data are plotted in the manner of Figures 17 to 23, except that the original pressure coefficient notation was retained. The agreement is seen to be quite good, except in the separation region upstream of the injector at free-stream Mach number 4.84. It should be noted that for the two largest values of h, at $M_\infty = 4.84$, the boundary layer was separated up to the leading edge of the plate, thus precluding any similarity in that region.

E. Discussion and Conclusions

Quantitatively, the results of the shock shape, concentration, and pressure measurements indicate that the scaling parameter, h, is satisfactory for the range of variables which has been investigated, with the previously mentioned restriction that it be about equal to or greater than the separated boundary-layer thickness. The correlation

of the shock and concentration data was excellent, but it appears that the size restriction to the applicability of the scale parameter is more severe for the static pressure distribution on the wall than it is for these other features of the flow. Some lack of similarity in the pressure data was observed in the laminar boundary layer separation region, and at the lower Mach numbers in the reattachment region downstream of the injector. It is apparent that a simple one-parameter scale transformation cannot give a detailed correlation of the pressure data in these regions.

1. Review of flow models. - A number of models have been suggested by other authors which lead to a calculation of a scale height for secondary injection. For example, see Reference 12 to 15. Unfortunately, most of these models are for two-dimensional flow and are not directly applicable. However, it is still possible to compare their approach to the one used in this paper.

One assumption used was that the penetration height is fixed by the area required to pass the mass flow of injectant after it expands isentropically to the local ambient pressure.[12] In our case, this assumption leads to the result that the penetration height depends only on the ambient static pressure and injectant specific heat ratio, and is independent of the momentum of the free stream. These conclusions are not in agreement with the experimental results. A second type of model, e.g. Reference 13, is based on the assumption that the separated boundary layer is tangent to the top of the injectant stream, and that side force is only generated upstream of the injector port.

Our experimental work indicates that such a model is valid only when the scale height is less than the boundary layer thickness.

Furthermore, analysis of the results of Newton and Spaid[16] shows that with gaseous injection, the major portion of the side force is applied downstream of the injector port. They found that there was still a small positive contribution to the side force for $(x/h) > 12$. Although this work was carried out in a conical rocket nozzle, the results should apply at least qualitatively to the present discussion.

Additional information is furnished by analysis of the results of Walker, et al.[17], who worked with a conical nozzle which had injector ports of various diameters located close to the nozzle exit. Their values of specific impulse of side injection, I_s, are given in Figure 25 as a function of the ratio of distance between injector port and nozzle exit to values of the scale parameter calculated from equation (6). In these experiments, the ratio of the distance between the injector and nozzle exit to h varied from about 2.9 to 8.5, and the corresponding specific impulse for secondary injection increased by a factor of about 1.4. These results can also be interpreted as showing the effect of systematically increasing the wall area on which the pressure disturbances act from an area corresponding to $(X/h) = 2.9$ to $(X/h) = 8.5$. For this configuration the contribution to side force is small when $(X/h) > 7$. This result agrees with the analyses of the data of Newton and Spaid,[16] discussed in the previous paragraph, and shows that the downstream contribution to side force is very important.

A third model is that which was proposed by Broadwell.[14]

In this paper, the blast-wave theory was used to obtain a pressure field on a flat plate. The scale of this pressure field was determined by calculating a value for drag produced by injection and equating this to the energy added to the free stream per unit length. This drag is therefore completely analogous to the change in the x-component of momentum of the jet in the present model, equations (3), (4), and (5). A value of drag, then, corresponds to a scale height, so that these two approaches can be compared. In Reference 14 the drag, or energy per unit length, is calculated by assuming first, that the injected material reaches the velocity of the undisturbed free stream, and second, that the effect of adding mass can be taken into account by adding heat to a part of the free-stream flow sufficient to produce the same volume change which would be produced by mass addition. The result of this calculation is as follows:

$$D = m_j V_\infty \left[1 + \frac{2 + (\gamma_\infty - 1) M_\infty^2}{2(\gamma_\infty - 1) M_\infty^2} \frac{\mathfrak{M}_\infty}{\mathfrak{M}_j} \frac{T_{o_j}}{T_{o_\infty}} \right] \qquad (10)$$

In order to compare the effect of these assumptions with the present model, an equation for scale height similar to equation (6) was derived by substituting equation (10) for equation (5) in the present derivation. The resulting equation, analogous to equation (6), gave very nearly the same Mach number dependence as equation (6), but showed a strong dependence upon the molecular weight of the injectant at a constant value of free stream - to - injection pressure ratio. This dependence was not observed. These results indicate that the

scale of the flow field is probably determined by an isentropic expansion of the jet in the immediate vicinity of the injector, rather than by the acceleration and mixing process between the jet and the free-stream material which occurs farther downstream. These results and conclusions are also in accord with the fact that the drag of a slender, blunt-nosed body at high Mach numbers is determined almost entirely by the characteristic nose bluntness dimension.[6]

2. Review of the flow field characteristics. - The concentration and pressure data have now made it possible to add some details to the qualitative description of the flow field which was presented earlier. It has been shown that the jet mixes very rapidly as it leaves the injector, and much more slowly for (x/h) greater than about 4. The jet is approximately parallel to the wall at $(x/h) \approx 3$.

A pair of vortices appear to be shed from the jet near the injector; these accelerate the mixing process and result in a region of low concentration of injectant material in a region immediately downstream of the jet near the wall. The flow is separated just downstream of the injector and appears to reattach to the wall in the region $3 \lesssim (x/h) \lesssim 4$. This reattachment may be accompanied by a compression wave system, increasing in strength with jet - to - free stream stagnation pressure ratio and with decreasing free-stream Mach number.

The character of the boundary layer separation for the case of injection into a turbulent boundary layer is quite different from the separation of a laminar boundary layer. The pressure rise due to turbulent separation extends only slightly upstream of the bow shock,

but the laminar boundary layer separates far upstream. In neither case, however, does the height of the separated boundary layer approach the height of the jet, if the jet height is much greater than the undisturbed boundary layer thickness. This result is quite different from the results obtained in boundary-layer separation studies with a two-dimensional step.[18] Part of this difference seems to be the result of the inherent difference between two- and three-dimensional obstructions; the boundary layer can simply go around the three-dimensional object, but the flow must all go over the top of the two-dimensional one. In addition, there is the previously mentioned effect of the jet shape near the wall which tends to provide clearance for the boundary layer.

F. Applications of the Scaling Law to Scaling of Forces

If the scaling law, as developed earlier in equation (6), can be taken as being a good approximation, then it is easy to predict the variation of the side force generated on an infinite flat surface by the variation of the jet parameters. For many purposes, it is desirable to know the change in force produced on the wall by secondary injection.

The side force contribution from the pressure field resulting from secondary injection from an infinite flat plate can be expressed as:

$$\Delta F = \int_{x=-\infty}^{\infty} \int_{y=-\infty}^{\infty} (P-P_{\infty})\, dx\, dy \qquad (11)$$

Dividing through by $(P_\infty h^2)$ we have:

$$\frac{\Delta F}{P_\infty h^2} = \int_{\frac{x}{h}=-\infty}^{\infty} \int_{\frac{y}{h}=-\infty}^{\infty} \frac{P-P_\infty}{P_\infty} \frac{dx}{h} \frac{dy}{h} \equiv \Phi \qquad (12)$$

The integral of equation (12) is evaluated in the normalized coordinates, and therefore will depend only upon the free-stream Mach number and specific heat ratio. That is,

$$\Phi = \Phi\{M_\infty, \gamma_\infty\}$$

The total side force due to injection, F_s, is the sum of the interaction force, ΔF, and the thrust of the injectant, F_j. The thrust of a sonic jet is given by

$$F_j = P_{o_j} A_j c C_f\{M=1\} \qquad (13)$$

where

$$C_f\{M=1\} = \left(\frac{2}{\gamma_j+1}\right)^{\frac{\gamma_j}{\gamma_j-1}} - \frac{P_\infty}{P_{o_j}} \qquad (14)$$

It is useful to compare the total force due to injection with the thrust which would be produced by the jet alone if it were expanded isentropically in a nozzle to the free-stream static pressure. This quantity will be denoted $F_{j_{max}}$, and is given as follows:

$$F_{j_{max}} = P_{o_j} A_j c \gamma_j \left[\frac{2}{\gamma_j - 1} \left(\frac{2}{\gamma_j+1}\right)^{\frac{\gamma_j+1}{\gamma_j-1}} \left\{ 1 - \left(\frac{P_\infty}{P_{o_j}}\right)^{\frac{\gamma_j-1}{\gamma_j}} \right\} \right]^{\frac{1}{2}} \qquad (15)$$

Combining equations (6), (12), (13), (14), and (15), we have

$$\frac{F_s}{F_{j_{max}}} = \frac{8\bar{\Phi}}{\pi M_\infty^2 \gamma_\infty C_p^*} + \frac{\left(\frac{2}{\gamma_j+1}\right)^{\frac{\gamma_j}{\gamma_j-1}} - \frac{P_\infty}{P_{o_j}}}{\gamma_j\left[\frac{2}{\gamma_j-1}\left(\frac{2}{\gamma_j+1}\right)^{\frac{\gamma_j+1}{\gamma_j-1}}\left\{1-\left(\frac{P_\infty}{P_{o_j}}\right)^{\frac{\gamma_j-1}{\gamma_j}}\right\}\right]^{\frac{1}{2}}} \quad (16)$$

and

$$\frac{\Delta F}{F_{j_{max}}} = \frac{8\bar{\Phi}}{\pi M_\infty^2 \gamma_\infty C_p^*} \quad (17)$$

The second term in equation (16) is the ratio $F_j/F_{j_{max}}$, the ratio of the thrust of a sonic jet to the thrust of a jet with optimum expansion.

The usual form for presentation of rocket motor tests has been to give the ratio of side force to axial force as a function of the ratio of secondary to primary mass flow rates. That is,

$$F_s/F_p = f(m_j/m_p)$$

Results from (16) can be compared with rocket motor data by using the expression for $F_{j_{max}}$ written in terms of m_j, as follows:

$$F_{j_{max}} = m_j\left[\frac{2\gamma_j R_j T_{o_j}}{\gamma_j-1}\left\{1-\left(\frac{P_\infty}{P_{o_j}}\right)^{\frac{\gamma_j-1}{\gamma_j}}\right\}\right]^{\frac{1}{2}} \quad (18)$$

Equations (16) and (18) can be used to correlate side force measurements if the dimensionless pressure integral, Φ, is known.

Even when Φ is not known, correlation can be made if $(F_s/F_{j_{max}})$ is held constant, keeping in mind that the first term in equation (16) depends only upon free-stream parameters. This condition implies that valid comparisons can be made when any of the following parameters are changed: injectant molecular weight and total temperature, injector diameter, and primary-stream molecular weight and total temperature. In addition, the dependence of equations (16) and (18) upon P_{o_j} is very weak, particularly if $P_{o_j} \gg P_\infty$. Hence, a change in the ratio (P_{o_j}/P_∞) will only introduce a slight error in scaling.

Subject to these restrictions, it is evident that

$$F_s \propto m_j \sqrt{R_j T_{o_j}}$$

In addition, if changes in axial thrust of the primary flow caused by non-optimum expansion and by secondary injection are neglected, then

$$F_p \propto m_p \sqrt{R_p T_{o_p}}$$

and therefore

$$\frac{F_s}{F_p} \propto \frac{m_j}{m_p}\sqrt{\frac{R_j T_{o_j}}{R_p T_{o_p}}} = \frac{m_j}{m_p}\sqrt{\frac{T_{o_j}/\mathcal{M}_j}{T_{o_p}/\mathcal{M}_p}} \qquad (19)$$

This result indicates that the thrust ratio depends directly on the mass flow rate and on the square root of the ratio of injectant total tem-

perature to molecular weight. The ratio is independent of injector diameter.

The discussion given in the earlier sections of this paper indicates that there are a number of restrictions which must be placed on this scaling procedure. Clearly, the procedure is strictly applicable only if the wall on which the pressure disturbances exist is of sufficient extent that the pressure at its boundaries has returned to the free-stream static pressure. In practice, this means that the boundaries must be at least 10h away from the injector.

In addition to this geometric limitation, it will be useful to summarize again the limitations on the scaling procedure itself. First, it is necessary that the scale height be at least as large as the separated boundary layer thickness.

Second, if the boundary layer is turbulent, scaling appears to be excellent except in the reattachment region. If scaling of a nozzle is carried out by using geometrically similar devices with equal total pressure ratios, (P_{o_j}/P_{o_∞}), then the reattachment phenomena will also be similar and no scaling errors will be introduced. This scaling procedure is that which is most likely to be used in the design of a large rocket nozzle where the boundary layer is almost certainly turbulent.

Third, if the boundary layer is laminar, upstream separation phenomena are more important, and scaling may be less satisfactory. In this case, there is some indication that pressure changes compensate each other;[15] however, no information on such compensation

can be deduced from the present work.

Some direct comparison can be made of the scaling law developed here with experimental rocket engine tests. Even though the flow field in a nozzle is not directly comparable to that treated here, it is felt that the general conclusions drawn from the present work are useful.

Rodriguez[19] and many other experimenters have found that the side force is independent of the injector port area for fixed mass flow and depends linearly on the mass flow of injectant when the primary flow parameters are held fixed. This result agrees with that obtained from equation (19).

Some work has been carried out in which injectants with different total temperatures and different molecular weights were used.[17, 20, 21] The correlation proposed by Lingen[20] and later approximately verified by Chamay and Sederquist[21] agrees exactly with equation (19).

Figure 26 shows data from Reference 20 for gas injection into a rocket nozzle. The parameter (T_{o_j} / T_{o_p}) was changed by a factor of more than 6 for the two cases, and the agreement is excellent, although the data are badly scattered. Figure 27 shows data for nitrogen and hydrogen injection into a rocket nozzle, from Reference 21. The scatter here is much smaller than for Figure 26, but the correlation is not quite so good. It can be seen that the correlation improves with increasing m_j, so that there is about 10 per cent difference between the nitrogen and hydrogen data at the

higher injection rates.

In the previously mentioned paper by Walker, et al., data are reported for injection of different gases into a rocket nozzle. The correlation of these data by the present treatment is presented in Figure 28a. Only data for sonic injection are presented. The choice of h^2 as a correlating parameter was made because it accounts for variations in γ_j and (P_∞/P_{o_j}). It can be seen that the effect of injector diameter is accounted for quite well, but considerable systematic variation remains among data for different gases. It is interesting to note that the correlation is in error by about the same factor over the entire range of h^2, or injection rate, in contrast to the data of Reference 21.

The different treatment proposed by Broadwell[22] gives a somewhat better correlation of the data of Reference 17, particularly at the higher injection rates (see Figure 28b). Figure 28b also includes data for subsonic injection, but does not include the effect of injector port diameter. In another figure of Reference 22, Broadwell shows a correlation of this effect which is as good as that in Figure 28a.

Because of the disagreement between the various sets of experimental data of References 17, 20, and 21, it is difficult to judge the value of the present technique in correlating rocket motor data for different gaseous injectants. Both the technique proposed by Broadwell and that proposed by the author appear to be in approximate agreement with experimental data, although both techniques predict greater

increases in performance with decreasing molecular weight of injectant than are actually realized.

In the case of the technique developed here, the explanation for this discrepancy is believed to be as follows. The assumption of isentropic expansion of the secondary flow appears to be quite satisfactory in the vicinity of the injector. However, it has been demonstrated for gaseous injection into a rocket exhaust that in many configurations, a major portion of the side force is developed quite far downstream of the injector. The concentration and total pressure measurements which have been presented here show that mixing of the injectant with the free stream is quite rapid, and that the speed of the injected gas downstream of the injector is strongly affected by the free stream flow. The effective scale of the obstruction downstream of the injector will then be less than that predicted by equation (6) if the speed of the injectant corresponding to an isentropic expansion to the free-stream static pressure is significantly greater than the speed of the free stream. This effect of mixing will then result in lower performance for a light gas than for a heavy gas when they are compared at the same value of the scale parameter, h, for rocket-nozzle injection configurations for which the side force contribution downstream of the injector is important.

III. INJECTION THROUGH A SLOT

In addition to the experiments on injection through a circular hole into a supersonic stream, a series of experiments were conducted in the 2.5-inch Supersonic Wind Tunnel at the California Institute of Technology in which gaseous nitrogen, helium, and argon were injected through a transverse slot in the test section wall. Injection was normal to the free-stream flow.

A. Description of Experiments

The experiments were conducted at a test-section Mach number of 2.56 and at Reynolds numbers per inch of 1.3×10^5 and 2.5×10^5. The higher Reynolds number resulted in a turbulent boundary layer on the test section wall in the vicinity of the slot injector, and the lower Reynolds number resulted in a laminar boundary layer in the same region.

The slot was 2.00 in. long and 0.006 in. wide, leaving a 0.25 in. section of solid wall between each end of the slot and the test section side wall. This was done to provide clearance for the boundary layer on the side wall, and to avoid the problem of sealing the high-pressure plenum chamber behind the slot against the side walls of the test section. Figure 29 is a section view of the slot injector, in what has been called the x-z plane in the previous section. The injection pressure was measured at a location where the injectant velocity was believed to be very small. A row of static pressure taps was installed along the centerline of this nozzle block, parallel

to the free stream flow, and extending 1.56 in. from the slot in the upstream direction and 2.125 in. in the downstream direction. The four pressure taps in this row nearest the slot passed through the plenum chamber, but are not shown on this figure because including them would have made it unnecessarily complicated. Additional pressure taps were located in rows parallel to the centerline and 0.42 in. to either side. The injectant was introduced into the plenum chamber through two 0.25 in. O. D. tubes, spaced 0.476 in. apart, on either side of the centerline. A perforated baffle was placed between the tube outlets and the slot. This arrangement was chosen in an effort to obtain flow at the slot which was as uniform as possible. The slot configuration shown in the slot detail was chosen so that friction losses would be relatively small, and so that the slot could actually be machined with reasonable assurance of obtaining a uniform cross-section along its length.

Uniformity of the flow produced by the slot was checked by making a total pressure survey along its length. The slot was pressurized with nitrogen, and was allowed to exhaust to the atmosphere. A probe was located 0.01 in. above the slot, and total pressure measurements were obtained which showed the flow to be uniform to within $\pm$ 3.5 per cent in the central region, excluding the last 0.15 in. on each end. The discharge coefficient for the slot was determined as a function of Reynolds number based on the slot width by measuring mass flow rate of nitrogen through the slot with a sharp-edged orifice, in accordance with the applicable supplement to the ASME Power Test

Code.

Essentially the same types of measurements were made for the slot-injection experiments as were made for the hole-injection experiments, with a few exceptions. For this series of experiments, the static pressures were measured with a Statham 0-5 psia pressure transducer, and a Scanivalve pressure-switching mechanism. The probe which was used for the concentration and total pressure measurements was the same one which was used for the boundary layer surveys, and has already been described. The purpose of this configuration was to provide good resolution in the vertical direction, and to provide rapid area increase inside the probe downstream of the tip. When concentration samples were being obtained, a low pressure was maintained inside the probe so that the flow would be sonic at the tip, and so that an attached shock would exist at the probe tip. These conditions were desired so that species of differing molecular weights would not be partly separated before entering the probe by passing through a region of large streamline curvature.

The minimum injection pressures or mass flow rates were determined by the requirement that the flow be sonic at the slot, and the maximum values were the largest at which supersonic flow could be maintained in the wind tunnel test section.

The degree to which the flow field approximated two-dimensionality was checked by examining transverse pressure profiles obtained without injection and with various injection flow rates. These pressure profiles exhibited a maximum deviation from uniformity in

the transverse direction of about ± 3.0 per cent for the highest injection flow rates.

B. Description of the Flow Field

A qualitative understanding of the flow field produced by injection through a slot into a supersonic stream has been obtained by examination of schlieren photographs from experiments in the CIT facility, and has been greatly aided by the work of Buffum, Price, and Slates [23] of the U. S. Naval Ordinance Test Station, China Lake, California. This work consisted in part of detailed optical studies of the flow produced by injection through a slot into a two-dimensional expanding nozzle.

Upstream of the slot the flow field is similar to the flow over a forward-facing step. A sketch of a typical flow field for the case of a turbulent boundary layer is shown in Figure 30a, which is a scale drawing from a schlieren photograph obtained at the CIT facility. For this example, the flow is sonic at the slot, and has a much higher static pressure than that of the primary stream. It expands rapidly through a strong Prandtl-Meyer fan, and is turned by the primary stream so that it eventually moves in a direction approximately parallel to the wall. The flow immediately downstream of the slot is separated from the wall, but it reattaches in a relatively short distance. The obstruction produced by injection causes the boundary layer to separate upstram of the slot, and also results in an oblique shock which intersects the boundary layer approximately at its point of separation. The obstacle which is created by the injected material also

produces a curved bow shock which begins at some point above the wall and in front of the injectant jet, and then joins the separation shock to form a lambda-shock structure. A single shock then continues from this intersection.

The total pressure of the flow which has passed through the lambda-shock structure is different from the total pressure of the flow which has passed through the single shock, so that a slip line is formed which originates from the intersection of the bow shock and the separation shock. This slip line could be seen quite clearly on shadowgraph photographs which were obtained for gaseous injection through a circular hole. Spark schlieren pictures often showed multiple exposures for the separation shock, with only single exposures for other features of the flow, indicating an unsteady separation region. It is probably for this reason that the boundary layer between the separation shock and the jet was not sufficiently well defined on the schlieren pictures to allow the direct measurement of a separation angle. The magnitude of this angle can be estimated by finding the wedge angle required to produce the separation shock angle for the particular free-stream Mach number. Downstream of the bow shock, the flow undergoes an expansion which turns it toward the wall. A recompression shock then turns the flow parallel to the wall.

Figure 30b is a scale drawing of a schlieren picture obtained for injection with a laminar boundary layer. The separation angle for the laminar boundary layer, of the order of 3 to 4 degrees, is much less than that for the turbulent boundary layer, and the separation shock is correspondingly weaker. Because the bow shock and the

separation shock do not intersect for this set of experimental conditions, there is nothing corresponding to the slip line which was observed in the case of the turbulent boundary layer. It is interesting to note that the beginning of the bow shock, as observed from the schlieren photographs, is at the point where the outer edge of the separated laminar boundary layer makes its closest approach to the injectant jet. Immediately downstream of this point, the boundary layer is no longer distinguishable on the photographs. The flow is turned very slightly by the weak separation shock, and more strongly by the bow shock, after which it passes through an expansion region in which it is turned toward the wall, and finally passes through a recompression shock which turns it parallel to the wall.

In view of the substantial qualitative differences between the flow fields which are obtained for injection with a laminar boundary layer and injection with a turbulent boundary layer, it appears that different assumptions may be required in the construction of an analytic model for each case. One of the most important differences here is that in the laminar boundary layer case the bow shock does not appear to become very nearly a normal shock in the vicinity of the jet, as it does in the turbulent boundary layer case, indicating that the obstruction produced by the jet is more nearly covered by the separated laminar boundary layer than it is by the turbulent boundary layer.

C. Analytic Model

It was previously mentioned that the flow for two-dimensional

gaseous secondary injection into a supersonic stream bears some resemblance to the flow over a forward-facing step. With this as a starting point, an analytic model of the flow field has been constructed whose purpose is to calculate an effective step height which can be used as a scale parameter for the entire flow field. The work of Bogdonoff and Kepler[24] and the work of Vas and Bogdonoff[18] concerning supersonic flow with a turbulent boundary layer over a forward-facing step indicate that the separation distance ahead of the step is proportional to the step height if the step height is somewhat greater than the undisturbed boundary layer thickness; therefore, an analysis which is based on an analogy with the flow over a forward-facing step would probably only be useful when the effective obstruction heights were greater than the undisturbed boundary layer thickness.

The analysis is begun with the following assumptions, which are similar to those made in the analysis for injection through a circular hole: (1) that no mixing occurs between the secondary and the primary flows; (2) that the interface between the two flows is a rounded forward-facing step; (3) that the injectant expands isentropically to the free-stream static pressure and is turned parallel to the wall; and (4), that the wall shear can be neglected immediately downstream of the slot. Assumptions (1) and (3) imply that the scale of the flow field is determined by conditions in the immediate vicinity of the slot, rather than in the region far downstream.

The coordinate system which has been used with the analytic model and in the presentation of experimental data is shown on Figure

30. The origin is at the center of the slot, in the plane of the wall. The x-axis is downstream of the slot, along the wall, and the z-axis is normal to the wall.

A momentum balance in the x-direction was constructed for a control volume bounded by the interface between the two flows, the wall, and a plane normal to the x-axis and intersecting it at a point upstream of the attachment of the secondary jet to the wall. Note that because of the existence of this separated region downstream of the slot, the secondary flow through the rear face of the control volume has not been assumed to be a uniform flow over the entire rearward face, so that the effective scale is not determined by the continuity equation. Assumption (4) also seems to be reasonable because of this separated region downstream of the slot.

In the case of the analysis for secondary injection through a circular hole, it was assumed that the boundary layer could be neglected entirely, and that the force exerted by the primary stream on the equivalent solid body could be calculated by modified Newtonian flow theory. In the two-dimensional case, however, the boundary layer cannot flow around the body, but must flow over it, resulting in a viscous-inviscid interaction which is a much more prominent feature of the flow field for the slot than it was in the three-dimensional case. The importance of this viscous-inviscid interaction causes difficulty in the calculation of the x-component of force exerted by the primary stream on the forward-facing portion of the control volume. The following form has been assumed,

$$F_x = C_D q_\infty h \tag{20}$$

where q_∞ is the free-stream dynamic pressure, h is the height of the equivalent step, and C_D is a drag coefficient which is probably a function of the free stream Mach number, M_∞, and the free-stream Reynolds number. In view of the previously mentioned differences between the flowfieldswhich result from injection into a turbulent boundary layer or a laminar boundary layer, it seems likely that C_D would be different for the two cases. The only other term which is included in the momentum balance is the momentum outflow of the secondary jet through the rear face of the control volume, which is calculated exactly as it was in the three-dimensional case. The result is:

$$m_j V_j = cd P_{o_j} \gamma_j \left[\frac{2}{\gamma_j - 1} \left(\frac{2}{\gamma_j + 1} \right)^{\frac{\gamma_j + 1}{\gamma_j - 1}} \left\{ 1 - \left(\frac{P_\infty}{P_{o_j}} \right)^{\frac{\gamma_j - 1}{\gamma_j}} \right\} \right]^{\frac{1}{2}} \tag{21}$$

Here the notation is the same as it was before, except that d refers to the slot width, and the momentum flux is per unit slot length. The momentum balance is

$$F_x = m_j V_j \tag{22}$$

Substituting from equations (20) and (21) and solving, we have

$$\frac{h}{cd} = \frac{2 P_{o_j} \gamma_j}{C_D M_\infty^2 P_\infty \gamma_\infty} \left[\frac{2}{\gamma_j - 1} \left(\frac{2}{\gamma_j + 1} \right)^{\frac{\gamma_j + 1}{\gamma_j - 1}} \left\{ 1 - \left(\frac{P_{o_j}}{P_\infty} \right)^{\frac{\gamma_j - 1}{\gamma_j}} \right\} \right]^{\frac{1}{2}} \tag{23}$$

It is a simple matter to substitute the free-stream stagnation pressure,

P_{o_∞}, for the static pressure, which has the effect only of changing the functional dependence of equation (23) on M_∞ and γ_∞. As in the previous case of injection through a hole, we have the most important variation of the equivalent step height given by,

$$h \propto \frac{dc}{C_D M_\infty^2} \left(\frac{P_{o_j}}{P_\infty} \right) \tag{24}$$

This proportionality can also be written in terms of m_j, the mass flow of the jet per unit length of slot, as follows:

$$h \propto \frac{m_j \sqrt{R_j T_{o_j}}}{C_D M_\infty^2} \tag{25}$$

where R_j is the gas constant for the injected gas and T_{o_j} is its stagnation temperature. Equations (24) and (25) are useful when $P_\infty / P_{o_j} \ll 1$.

A value for C_D remains to be determined. Figure 31 consists of two simplified sketches of the flow field as it is assumed to be for this analysis for the cases of both laminar and turbulent boundary layers. The heavy line represents the shape of the obstacle which is encountered by the inviscid flow. If all of the shocks are relatively weak and the flow deflection angles are small, then the assumptions of linearized supersonic flow are satisfied by the inviscid portion of the flow field, and C_D should be consistent with the Prandtl-Glauert rule, as follows:

$$C_D = \frac{\text{const.}}{\sqrt{M_\infty^2 - 1}} \tag{26}$$

It can be seen from schlieren pictures of the flow fields that the assumptions of linearized supersonic flow are fulfilled to a greater degree of approximation by the laminar boundary layer case than by the turbulent boundary layer case. On the other hand, if both the separation shock and the bow shock are strong, and the ramp formed by the separated boundary layer is such that an abrupt step is still presented to the inviscid flow, modified Newtonian flow theory may give a better value for C_D than that which is given by the linearized theory. This amounts to the assumption that the important contribution to the force on the forward-facing portion of the control volume is determined by the static pressure behind a strong shock in the free stream flow, rather than the boundary layer separation pressure near the wall. A modified Newtonian flow calculation for the drag of a circular cylinder of radius h gives the following result (see Appendix B for a detailed derivation):

$$C_D = \frac{2}{3} C_p^* \tag{27}$$

where C_p^* is the stagnation-point pressure coefficient for the flow of an ideal gas, and is a function of M_∞ and γ_∞. Schlieren pictures of the flow fields indicate that the conditions under which equation (27) is valid are met more closely by the turbulent boundary layer case than by the laminar boundary layer case. The primary difference between equations (26) and (27) is that equation (26) gives a value for C_D which decreases as M_∞ increases above unity, and equation (27) gives a value which increases with M_∞ in the same region, but becomes approximately constant for M_∞ greater than about 2.

Because the experiments in this series were conducted at a single free-stream Mach number, it has not been possible to test either approach, although other published data allow some estimation of Mach number effect.[25, 26] For the purposes of this discussion, however, equation (8) has been used to calculate values of h.

As in the case of the analysis for injection through a circular hole, it is proposed that h be used as a measure of the scale of the disturbance produced by injection. Considering the assumptions which have been made, quantative correspondence between calculated values of h and any measured feature of the flow would appear to be fortuitous.

D. Presentation of Experimental Data

Results of the slot injection experiments are presented in the following sections. As in the case of the circular hole injection experiments, the space coordinates have been normalized by calculated values of the scale factor, h.

The maximum values of h for which supersonic flow could be maintained in the test section was found to be 0.468 cm. If we refer to Figure 1, it can be seen that this value is not greatly larger than the boundary layer thickness. Although it has not been shown that h is equal to an equivalent step height, the schlieren pictures indicated that only for the largest values of h, or of (P_{o_j}/P_{o_∞}), did the obstruction produced by the jet appear to be larger than the undisturbed boundary layer thickness. Because of this experimental limitation, deviations from similarity in these data would be expected to be present, and

these deviations should be functions of the ratio of the two characteristic dimensions of the problem, the jet obstruction height and the boundary layer thickness.

The schlieren pictures which were obtained for the slot injection experiments did not reveal any feature which had the appearance of a penetration height of the jet, as was seen in the pictures for the case of injection through a hole.

1. Wall pressure distribution. - Because it did not seem possible to make a direct comparison of calculated values of h with some feature of the flow field, the scaling procedure had to be verified in a more indirect way.

Figure 32 is a plot of the static pressure along the x-axis, with the pressures being normalized by the free-stream static pressure. The injectant gases are nitrogen and argon, the boundary layer is turbulent, and the values of h which are shown here are the larger ones which were obtained during this series of experiments. The general behavior of the pressure distribution is somewhat similar to that which was obtained along the x-axis for injection through a circular hole, but here the extent of the disturbance is much greater, in terms of the calculated scale factor, than in the previous case. Boundary layer separation upstream of the injector is accompanied by a pressure increase, beginning in the region of (x/h) between -6 and -10. The maximum static pressure which is observed upstream of the injector is very nearly the same as that in Figure 17, for the corresponding three-dimensional case. The pressure minimum downstream of the

injector is not as low, however, as it was in the latter case. The pressure returns to the free-stream static pressure for $(\frac{x}{h})$ between 4 and 6. (In comparing these results with those in Figure 17, it must be remembered that the origin of the coordinates in Figure 17 is the extrapolated intersection of the bow shock with the wall, but in Figure 25 it is the center of the injector.) There is a small tendency for the static pressure to overshoot the free-stream value in the downstream region, and the tendency increases with the ratio (P_{o_j}/P_{o_∞}). It is believed that this is the point at which the jet attaches to the wall and is turned parallel to the wall through a compression wave system, the same as in the three-dimensional case. However, the recompression shock as observed in the schlieren photographs approaches the wall somewhat upstream of this point, at $(\frac{x}{h})$ between 2 and 3 but it is not observed nearer the wall than (z/h) about equal to one.

A comparison of the values of the scale factors corresponding to the data which are presented in Figure 32 with the boundary layer profiles of Figure 1 shows that only the largest of these scale factors is greater than the boundary layer thickness. If the scale factor actually is of the same order of magnitude as an equivalent step height, and some evidence will be presented later which indicates that this is true, then it is not surprising that the scaling law does not work perfectly. The deviation from similarity is a trend toward a smaller scale of the disturbance, measured in units of the scale factor, h, as h increases. This trend is in accord with wall static pressure data which have been obtained for the flow over a forward-facing step, [18,24]

and for the flow over a solid spoiler,[25] when the step or spoiler height is not greater than the thickness of the undisturbed boundary layer, for values of M_∞ ranging from 1.57 to 3.85. Even so, the scaling is reasonably good with a variation in h of about 4.6:1, and the agreement between the nitrogen and the argon data is excellent.

Figure 33 is similar to the previous figure, except that data for the smaller values of h are presented, and data for gaseous nitrogen, helium, and argon injection are presented. The solid line represents an average of data for h greater than 0.2 cm. The trend of decreasing extent of disturbance, in the normalized coordinates, with increasing scale factor is much more pronounced than it was in the previous figure, although the variation in the scale factor for this figure is somewhat greater than in the previous one--about 7.8:1.

The data of Figure 33 constitute important evidence that the lack of explicit molecular weight in the expression for h, equation 23, is correct. The solid points are for each of the three gases with injection conditions chosen to give scale factors near 0.01 cm, and the other data points are a similar set for the scale factor in the range of 0.075 to 0.099 cm. The molecular weight of the gas has been changed by a factor of 10 for each of these sets, and the agreement is very good.

Figure 34 is the same type of plot as the preceding two figures, except that the boundary layer is laminar, and nitrogen gas is the only injectant. The pressure distribution still rises to a maximum immediately upstream of the injectant, falls to a minimum downstream

of the injector, and rises downstream to a value near that of the free stream. However, values of the maximum and minimum are much less extreme than those which were observed with a turbulent boundary layer. For injection through a hole, the pressure distribution along the x-axis was affected by the state of the boundary layer only near the location of boundary layer separation; the maximum pressure which was obtained just upstream of the injector, and the entire pressure distribution along the downstream x-axis was found to be independent of the state of the boundary layer. For injection with a slot, however, the entire flow field is apparently altered. The sketch of Figure 30b indicates the reason that the pressure maximum upstream of the injector is so low in the laminar boundary layer case. The bow shock does not approach the wall very closely, but seems to end at a three-way intersection of the shock, the outer edge of the separated boundary layer, and the jet. As is to be expected, the separation angle of the laminar boundary layer is quite small, so that the pressure rise which is associated with it is correspondingly small. The pressure distribution downstream of the injector indicates that the jet attaches to the wall further downstream than in the case of the turbulent boundary layer.

Experimental difficulties greatly restricted the studies for the laminar boundary layer condition. The range of scale factor presented here is the greatest which could be obtained, because smaller obstruction sizes would have been too small for effective study, and the tunnel would not maintain supersonic flow in the test section with

larger obstruction sizes. Examination of Figure 1 shows that these data are for values of h which are all considerably less than the undisturbed boundary layer thickness, so that it is to be expected that the scaling procedure does not work particularly well.

A second problem which made it impossible to obtain a good check on the scaling procedure was that the laminar boundary layer separation point at the higher injectant flow rates was near the beginning of the curved portion of the nozzle wall downstream of the throat. The location of the separation point was apparently affected by the favorable pressure gradient in this region, thus precluding similarity.

2. Flow field visualization. - It was desired to make another check on the scaling procedure by comparing normalized shock coordinates, although this method of comparison is not as sensitive as that which can be used with other data. Because of the limitation on the maximum scale obtainable, it is not surprising to find that the shock coordinates do not agree well when compared in the normalized coordinates for different injectant to free-stream total pressure ratios. The peak pressure in the separated region for both laminar and turbulent boundary layers depends upon the scale of the obstacle causing the separation if the height of this obstacle is equal to or less than the undisturbed boundary layer thickness.[24] If the pressure behind the separation shock is a function of obstacle height, then the separation shock angle and the boundary layer separation angle will also be functions of obstacle height.

Figure 35, however, is a plot of shock shapes for nearly the same values of the scale parameter, but with different injectant gases, helium and nitrogen. It can be seen that the agreement is quite good in the upstream region where the differences shown between the bow shocks and the separation shocks are within the error in measurement from the photographs, but the recompression shock is definitely higher for helium injection than it is for nitrogen injection. This indicates that the shape of the obstruction produced by the two gases may be different, and that mixing of the injectant and the primary flow may be important.

3. Concentration and total pressure measurements. - Figures 36 to 43 present the results of concentration and total pressure measurements for argon and helium injection which were made downstream of the slot. Figure 36 is an argon concentration profile which was obtained for an intermediate value of h in the region near the injector. This concentration profile, taken together with those of Figure 37, gives information about the mixing of the jet with the free-stream flow as a function of distance from the injector. The bottom scale in Figures 37, 38, 40, and 41 is the dimensionless distance from the center of the injector. The axial station at which each set of concentration and total pressure data were obtained are indicated on this bottom scale, and the position of the recompression shock is indicated for each abcissa. Note that the (z/h) scale of each of these plots is twice that of the (x/h) scale. The total pressure and velocity profiles have been normalized by corresponding undisturbed free-stream quantities.

In calculating the velocity profiles, the variation in gas properties with argon or helium concentration has been accounted for, the stagnation temperature of the free-stream and the injectant gases has been assumed to be constant and equal to room temperature, and the static pressure has been assumed to be constant in a direction normal to the wall between the wall and the recompression shock. For the data of Figure 37, static pressures immediately upstream of the recompression shock were calculated from the flow properties immediately behind the shock and the shock angle. Static pressures at some distance above the recompression shock were calculated by assuming a linear variation in static pressure between the recompression shock and the bow shock. For values of (x/h) greater than about 10, and for the region between the wall and some point part way between the recompression shock and the bow shock these assumptions about the static pressure are believed to be reasonably accurate. They are dubious in the region upstream of the attachment point of the jet, because large vertical pressure gradients are found near the wall for boundary layer flows near separation and reattachment. In the case of Figures 38 to 41, insufficient information were obtained to permit a reasonably accurate correction to the static pressure above the recompression shock, so that the data in this region have not been corrected. This has been indicated on the figures with dotted lines.

Examination of the concentration and velocity profiles indicates that the jet is accelerated and diluted by the primary flow, and this is accompanied by a relatively slow spread of the injectant in the

vertical direction with increasing distance downstream. A comparison of the mass flux of argon at each axial station for the data of Figure 37 was made by numerical computation of appropriate integrals, and the difference between the first and last stations, (x/h) = 6.67 and (x/h) = 30.8, was found to be 1.2 per cent, and the difference between the first and the intermediate station, (x/h) = 14.7, was 15.1 per cent. Considering the precision of the experiments, and the assumptions involved in the calculation of the velocity profile, this agreement is considered to be quite good.

At given values of (x/h) and (z/h), it can be seen that there is a trend toward higher values of velocity for larger values of h. The reason for this is probably some combination of the effect of increasing injectant velocity with increasing injectant stagnation pressure, and smaller thickness of the boundary layer, in the normalized coordinates, with increasing scale factor.

A comparison of the velocity profiles of Figures 38 and 41, for argon and helium injection at similar values of h with a turbulent boundary layer, shows that the velocity profiles at corresponding stations for these two cases are very nearly the same. On the other hand, the concentration profiles show that the mass flux of helium is much less than the mass flux of argon, indicating that the momentum flux of the helium is much less than the momentum flux of the argon at these downstream stations. The wall static pressure distribution and shock shape data for injection conditions similar to these agrees very well, however, particularly in the region upstream of the slot.

This again indicates that the characteristic momentum flux of the jet which determines the scale of these features of the flow should not be evaluated at a point far downstream of the slot, where considerable mixing has occurred, but is actually better approximated by the assumption of an isentropic expansion without mixing.

It should be noted that the flow far downstream of the slot would not be expected to have a wake similar to that which would occur for the flow about a solid object. If the free-stream flow is uniform, then the x-component of momentum flux integrated in any x= constant plane downstream of the jet from the wall to the bow shock will differ from the x-component of momentum flux integrated over a projection of this surface on any other x = constant plane upstream of the disturbance by the shear stress on the wall between the two planes. This fact could be used as a check on the accuracy of the integrated velocity and concentration profiles, if a reasonable estimate of the wall shear could be made.

Figures 42 and 43 are plots of argon concentration vs. (z/h) for nearly constant values of (x/h), but for different injectant and free-stream stagnation pressures. It can be seen that the scaling is not particularly good for the more upstream position, but that it improves as (x/h) is increased. This is in contrast to the case of injection through a circular hole, where the scaling of the concentration data, for a given injectant gas, was very good. The differences for the slot injection case are believed to be partly a result of the small values of h which could be obtained compared to the boundary layer thickness,

and partly a result of a basic difference between the two-dimensional and the three-dimensional situations. In the three-dimensional case, the injectant could penetrate the boundary layer and expand in the free-stream flow, with the boundary layer flowing around it at its narrower base. In the two-dimensional case, the jet always interacts with the entire wall boundary layer. If the obstruction produced by the jet is of the order of the boundary layer thickness or less, the effects of changes in the ratio of these two characteristic lengths becomes important. In terms of the normalized coordinates, as h is increased, the vertical extent of the jet in the downstream region will decrease, because it is mixing with a higher-velocity primary stream. This is the trend which has been observed. It is also to be expected that the concentration profile for injection into a laminar boundary layer will show smaller curvature than a corresponding concentration profile obtained with a turbulent boundary layer, because of the more gradual increase in velocity with distance from the wall which is characteristic of the laminar boundary layer.

E. Scaling Laws for Force on a Wall

If it is assumed that the scaling law as developed in equation 23 is correct, then an expression for the force on a wall can be derived in exactly the same manner that it was in the three-dimensional case. If it is understood that the force terms are now in units of force per unit length of slot, we can write:

$$\Delta F = \int_{-\infty}^{\infty} (P - P_{\infty})\, dx \qquad (28)$$

and define:

$$\frac{\Delta F}{P_\infty h} = \Psi (M_\infty, \gamma_\infty) \tag{29}$$

then by the same algebraic manipulations as in the three-dimensional case, we have:

$$\frac{\Delta F}{F_{j_{max}}} = \frac{3 \Psi}{M_\infty^2 \gamma_\infty C_p^*} \tag{30}$$

All of the results of the earlier analysis follow if $(8 \Phi / \pi)$ is replaced by 3Ψ.

If it is desired to restrict attention to the normal force generated upstream of the slot, we can assume that the calculated value of h is the height of a forward-facing step or equivalent solid spoiler, and follow the procedure recommended for predicting the pressure distribution ahead of such a disturbance which is given in Reference 27. This procedure is to use the best available semi-empirical or empirical equations for the pressure coefficient for the laminar plateau or for the first peak pressure rise for turbulent separation, which are functions of the free-stream Mach number and Reynolds number in the laminar case, and functions of the Mach number in the turbulent case.

For the case of a laminar boundary layer, equations for the separation and plateau pressure coefficient presented by Gadd[28] and Sterrett and Emery,[29] with coefficients resulting from an emperical fit to date of Chapman, et al.,[30] are as follows, for M_∞ between 1 and 3.6:

$$C_{p_{sep}} = 0.93\left[Re_x \left(M_\infty{}^2 - 1\right)\right]^{-1/4} \tag{34}$$

$$C_{p_{plat}} = 1.82\left[Re_x \left(M_\infty{}^2 - 1\right)\right]^{-1/4} \tag{35}$$

where Re_x is the Reynolds number based upon the effective distance from the leading edge of a flat plate. The peak pressure coefficient for a separated turbulent boundary layer ahead of a forward-facing step, for step heights greater than the boundary layer thickness, can be obtained from the following empirical equations:

$$C_{p_{peak}} = \frac{3.2}{8 + \left(M_\infty{}^2 - 1\right)^2}, \tag{36}$$

$$1.5 < M_\infty < 3.5$$

from Love,[31] and

$$C_{p_{peak}} = 0.13 - \frac{1.5}{M_\infty{}^2} + \frac{9.1}{M_\infty{}^3}, \tag{37}$$

$$3.5 \leq M_\infty \leq 6.5$$

from Sterrett and Emery. Using the appropriate pressure rise and the free-stream Mach number, a flow deflection angle can be determined.

If this flow deflection angle is used to construct a ramp from the wall upstream of the step to the top of the step, the separation distance can be approximated by the distance along the wall from the beginning of the ramp to the step. The normal force can then be roughly approximated by the pressure rise given by the previously determined pressure coefficient acting over this separation distance.

With these restrictions and approximations, ΔF becomes

$$\Delta F = C_p' \, q_\infty \, h \cot \delta \tag{31}$$

where C_p' is the appropriate pressure coefficient, as described previously, and δ is the flow deflection angle. The dimensionless incremental force, ψ, becomes

$$\psi = \frac{C_p' \, q_\infty \cot \delta}{P_\infty} \tag{32}$$

Substituting this into equation (30), we have

$$\frac{\Delta F}{F_{j_{max}}} = \frac{3}{2} \frac{C_p'}{C_{p^*}} \cot \delta \tag{33}$$

This method has been used to estimate the pressure distribution for the data of Figure 32, making no correction for any difference between the location of the slot and the location of an equivalent physical obstacle. It can be seen that the incremental force upstream of the slot would be predicted reasonably well. The predicted separation distance is somewhat short, but it definitely indicates that the calculated value of the scale parameter is of the correct order of magnitude.

F. Discussion and Conclusions

Considerable emphasis has thus far been placed upon using experimental results to verify the scaling law. It should be pointed out that the body of data for injection through a slot which has been presented here constitutes a comprehensive description of the flow field, and is a contribution independent of the success of the scaling law. In particular, the concentration, total pressure, and velocity profiles which are presented here are believed to be at present the

only published data of this type for slot injection into a uniform supersonic flow.

Because of experimental limitations, it has not been possible to verify the scaling procedure in as satisfactory a manner as was done for the case of injection through a hole. The dependence of h upon the ratio (P_{o_j}/P_{o_∞}) has been reasonably well verified for the larger values of h by the wall static pressure distribution data, and approximate separation distance calculations indicate that h is of the same order of magnitude as the height of an equivalent physical obstacle. A trend in the direction of a limiting pressure distribution with increasing scale factor was noted in the static pressure data for injection with a laminar boundary layer, but the results are inconclusive. The lack of explicit dependence of the scale factor upon molecular weight of the injectant has been well verified by the static pressure and shock shape data, for the entire flow upstream of the slot, and, at the very least, for some distance downstream of the slot. The effect of molecular weight of the injected gas is seemingly independent of the scale magnitude, or of the boundary layer thickness. The concentration and velocity profiles give reason to believe that mixing is important in the far downstream region, and that this similarity for different gases may not be preserved. Scaling of the concentration profiles applies only to the same injectant gas, because the analytic model predicts the same scale height for different mass fluxes for gases with different molecular weights.

Further work is needed to complete the picture; two-dimension-

al experiments for scale heights much larger than the undisturbed boundary layer thickness are needed. In addition, the effect of the free-stream Mach number predicted by the analytic model has not been verified. The prediction of the free-stream Mach number effect is controlled by the choice of C_D, which was discussed in the section on the analytic model. Experiments will be necessary to evaluate the correctness of this choice.

G. Comparison with Other Published Work

Several papers have been published which are concerned with the flow field for injection through a slot into a uniform supersonic stream,[25, 26, 32] or into an expanding two-dimensional nozzle.[23, 33]

The work of Buffum, et al.,[23] belongs to the latter category. The detailed optical studies which they have presented have been very helpful in obtaining a qualitative understanding of the flow field, but it is not possible to make a useful quantitative comparison with data such as nozzle-wall static pressure distributions to that obtained in this series of experiments because of the different geometry.

Fejer and Josse[33] present side force measurements for cold air to cold air injection through a slot into a two-dimensional expanding nozzle. Their data are presented in part as a magnification factor versus pressure ratio. The magnification factor is defined as the side force divided by the secondary jet momentum, which is evaluated by assuming that the secondary jet expands to the static pressure at the injection station; this is the same way that the momentum of the secondary jet is evaluated in the present analysis.

The pressure ratio is the injectant stagnation pressure divided by the static pressure at the injection station. The curves all show the general behavior of rising rapidly with pressure ratio and then leveling off at an essentially constant value. Many different injector configurations are represented, with different slot widths and injection stations; the pressure at which each curve levels off and the value of the magnification factor at the plateau depend upon the configuration. This plateau behavior for sufficiently large pressure ratio is consistent with equations (16) and (33), which give a value of $(F_s/F_{j_{max}})$ that depends only upon free-stream quantities for sufficiently large values of (P_{o_j}/P_∞).

The work of Strike and Schueler[32] is both experimental and theoretical. Their analysis is similar to that which has been presented here, in that they determine an effective obstacle height, and then calculate a force resulting from increased pressure upstream of the step. The obstacle height calculation is based on that of Vinson, et al.[10]. An objection to this analysis has already been raised in the preceding section, where it was pointed out that it leads to an effective obstacle height which depends only upon the ambient static pressure and the injectant specific heat ratio, and is independent of the momentum of the free stream.

The force is calculated by adding an inviscid interaction term and a viscous interaction term. The inviscid interaction term is computed by calculating a bow shock stand-off distance from the obstacle and assuming that a pressure equal to the pressure behind a

normal shock in the free-stream exists on the wall in the region between the obstacle and the calculated shock stand-off position. The viscous interaction term is computed in essentially the same way as it is in the present treatment.

None of the results of the present investigation, nor the published pressure distributions of Refs. 18, 24, 25, and 26, for flow with injection through slots or flow over forward-facing steps or spoilers show a wall static pressure upstream of the obstacle or of the injector which is the same order as the pressure behind a normal shock in the free-stream flow.

The experimental work of Ref. 32 consisted in part of force measurements for injection through a slot or through one or more holes in a flat plate mounted in a wind tunnel test section. The slots were always much shorter than the plate width, so that a flow which closely approximated two-dimensionality was not produced. For this reason, a meaningful comparison of the present experiments and analysis with these force measurements was not possible.

Heyser and Maurer[25] present data for the flow over solid spoilers mounted on a flat plate, and for the flow with injection through a slot in a flat plate into both subsonic and supersonic free-stream flows. The injectant was air, and the range of free-stream supersonic Mach numbers was 1.57 to 2.80. Pressure distributions were obtained both upstream and downstream of the slot, along the center of the plate, both with and without end plates mounted at each end of the slot. The normal force on the plate ahead of the slot caused by

injection was determined by integrating the pressure distribution. Most of the results of a comparison of the present work with their data can be obtained from Figure 44, a plot of $(F_s/F_{j_{max}})$ vs. (P_{o_j}/P_∞). This is a reproduction of part of Figure 27 in the original paper, with dotted curves added to represent the predictions of the present analysis. The dotted curves have been constructed with the assumption that $C_D = \frac{2}{3} C_p^*$ as mentioned earlier. The large values of normal force at the smaller values of pressure ratio are the result of the non-linearity of separation distance with obstruction height for heights which are not greater than the boundary layer thickness. This conclusion is substantiated by pressure distribution data which are presented in Ref. 25 for both the injection and solid spoiler cases.

The present analysis predicts the correct magnitude of the force ratio for $M_\infty = 2.8$ and for the higher pressure ratios, but it also predicts an increasing $(F_s/F_{j_{max}})$ with decreasing M_∞, which is opposite to the trend of the data, at least at the higher pressure ratios where the assumptions of the analysis are more plausible. If we let

$$C_D = \frac{\text{const.}}{\sqrt{M_\infty^2 - 1}}$$

the trend of the Mach number variation is in the same direction as that shown by the data at the higher pressure ratios, but the variation with Mach number is too rapid. It will be difficult for a theory to account for the details of the behavior of these curves, since curves

for different Mach numbers cross, and the values for $M_\infty = 1.57$ and $M_\infty = 1.83$ are very nearly the same.

Although the data of Figure 44 was obtained with end plates at each end of the slot, a considerable number of pressure distributions were presented in the paper which were obtained without end plates. The separation distances which are presented are all somewhat shorter than those which have been measured in this series of experiments. A figure which is presented to show the effect of the end plates at the various Mach numbers indicates that the separation distances are considerably increased at the lower Mach numbers by the addition of the end plates, but that the separation distances are not strongly affected by their addition at the higher Mach numbers, 2.20 and 2.80, which bracket the Mach number of this investigation. A personal communication from F. Maurer[34] indicated that the experimental conditions for which pressure distribution data are given in Ref. 25 deviated substantially from two-dimensionality for a slot width of 0.1 cm and values of (P_{o_j}/P_∞) greater than 5.

A paper by Romeo and Sterrett[26] presents experimental data for air to air injection through a slot in a flat plate into a Mach 6 supersonic stream. Again, most of the results of the pressure distribution data can be deduced by inspection of normal force data. Figure 45 is a plot of $(\Delta F/F_j)$ vs. (P_{o_j}/P_∞) for various slot widths with a turbulent boundary layer upstream of the slot. These data are for normal forces acting upstream of the slot only and were obtained by integrating pressure distributions. It should be noted that the

trend of greatly enhanced normal force for the smaller pressure ratios which was a feature of the lower Mach number data of Ref. 25 is not in evidence at this Mach number, so that the pressure distribution and force data scale reasonably well with pressure ratio, for the larger slot widths. Because no mention was made of a correction for the discharge coefficient for the slot, the effect of changing the slot width is difficult to interpret, since the mass flow through the slot is not necessarily proportional to the geometrical slot width. Another difficulty in interpreting the data concerns uncertainty about the degree to which the flow approximated two-dimensionality. The flat plate was approximately one-half the width of the test section, no end plates were used, and no evidence was presented to indicate that the flow was in fact two-dimensional, although in the text it was mentioned that pressure measurements were made at locations off the plate centerline. It should be noted that the use of end plates does not automatically result in a two-dimensional flow because of the boundary layers on the end plates, but a comparison of data with and without end plates is useful, particularly if the data show very little change for the two test conditions.

Although the variation of $(\Delta F/F_j)$ with (P_{o_j}/P_∞) given by the data of Figure 45 for the larger slot widths is in reasonable agreement with the present analysis and with the analysis of Ref. 12, the magnitudes of the predicted forces are much too low.

In summary, the data of Ref. 25, 26, and 33 give some evidence that the dependence of the scale factor upon the ratio

(P_{o_j}/P_{o_∞}) is correct, although a more careful test could be made if additional data were available in which the two-dimensional character of the flow were well established, in which the discharge coefficient for the slot were accounted for, and in which the scale of the obstruction were definitely greater than the boundary layer thickness. The importance of the ratio of the scale of the obstruction to the boundary layer thickness has already been discussed in section II. F, which summarized the results of the data which were obtained in the CIT facility. The comparison of the present theory with the data which has been presented in Refs. 25 and 26 indicates that the variation of the scale factor with the free-stream Mach number is not satisfactorily predicted by equation (23). This result suggests that C_D should be a decreasing function of M_∞, but should decrease more slowly than $1/\sqrt{M_\infty^2 - 1}$. An empirical fit could be made to the data of Refs. 25 and 26, but it is doubtful if these two different sets of experiments are really comparable, for reasons which have been previously stated.

A set of experiments are now in progress in the 20-inch Supersonic Wind Tunnel at the Jet Propulsion Laboratory which include gaseous injection through a transverse slot in a flat plate into a supersonic flow. These experiments should provide data which will shed light on some of the uncertainties which have been discussed here.

APPENDIX A

Notation

A_j	injector area
c	discharge coefficient
C_D	drag coefficient
C_p	pressure coefficient, $\{(P - P_\infty)/\frac{1}{2}\rho_\infty V_\infty^2\}$
$C_{p_{sep}}$	pressure coefficient at the wall at the point of boundary layer separation
$C_{p_{plat}}$	plateau pressure coefficient for a separated laminar boundary layer
$C_{p_{peak}}$	first peak pressure coefficient for a separated turbulent boundary layer
C_p'	the appropriate pressure coefficient to be used to estimate normal force on a wall, see equation (31)
d	hole diameter or slot width
D	probe diameter, see Figure 6a
F_i	force on body surface in i direction
F_j	thrust of a sonic injectant jet
F_p	total axial thrust
F_s	total side thrust
h	scale height
I_s	effective specific impulse of injectant, F_s/m_j
K_A	mass fraction of argon
K_{He}	mass fraction of helium
M_i	Mach number
m	mass flow rate

$\mathcal{M}_i$	molecular weight of i^{th} species
P	static pressure
P_o	stagnation pressure
R_i	gas constant for species (i)
Re_L	Reynolds number based on distance between leading edge of plate and injector centerline
T	static temperature
T_o	stagnation temperature
V	velocity
X	axial distance from injector port to nozzle exit
x, y, z	coordinate axes, see Figure 3
α	angle between body surface and free-stream flow, see Appendix B
γ	specific heat ratio
δ	boundary layer separation angle
ΔF	$F_s - F_j$
ϵ	ratio of nozzle area at injection station to nozzle throat area
θ	$\frac{\pi}{2} - \alpha$, see Figure 46
σ	parameter from blast-wave theory, see References 14 and 22
Φ	dimensionless pressure integral, defined in equation (12)
ψ	dimensionless pressure integral, defined in equation (29)

Subscripts refer to:

j and s: injectant stream

∞ and p: primary stream

APPENDIX B

Derivation of Equations (2) and (27)

The relationship for the pressure on an element of surface inclined at an angle α to the flow is

$$\frac{C_p}{C_p^*} = \frac{\sin^2 \alpha}{\sin^2 \alpha^*}$$

where α is defined as follows:

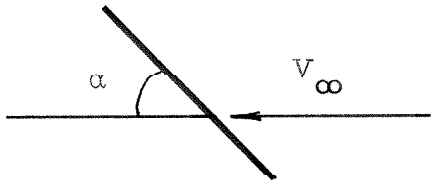

and the other quantities have been defined in the text. For the two-dimensional case, it is desired to calculate the force per unit length on a cylindrical surface of radius h. Reference to Figure 46 a shows that

$$\begin{aligned} dF_{x_1} &= -P \sin \alpha \, dA \\ &= P \sin \alpha \, h \, d\theta \end{aligned} \tag{b-1}$$

where F_{x_1} is the force on the cylindrical surface. But

$$\begin{aligned} P &= P_\infty + C_p \, q_\infty \\ &= P_\infty + C_p^* \, q_\infty \, \frac{\sin^2 \alpha}{\sin^2 \alpha^*} \end{aligned} \tag{b-2}$$

For this case, α^* is evaluated at the nose of the body, therefore

$$\alpha^* = \frac{\pi}{2}$$

We now have

$$dF_{x_1} = (P_\infty \sin \alpha + C_p^* \, q_\infty \sin^3 \alpha) \, h \, d\theta \tag{b-3}$$

From the figure it can be seen that

$$\sin \alpha = \cos \theta \tag{b-4}$$

and

$$F_{x_1} = \int_0^{\frac{\pi}{2}} (P_\infty \cos \theta + C_p^* \, q_\infty \cos^3 \theta) \, h \, d\theta \tag{b-5}$$

$$F_{x_1} = (P_\infty + \frac{2}{3} \, C_p^* \, q_\infty) \, h \tag{b-6}$$

The total force in the x-direction on the control volume also has a contribution from the surface which is normal to the x-axis. This item is just $- P_\infty h$. Therefore,

$$F_x = \frac{2}{3} \, C_p^* \, q_\infty \, h \tag{b-7}$$

If

$$F_x = C_D \, q_\infty \, h, \tag{b-8}$$

then

$$C_D = \frac{2}{3} \, C_p^* \tag{27}$$

Figure 46a also serves as a section in the x-z plane for the three-dimensional case. If we now consider F_x to be a force, rather than a force per unit length, we have for the three-dimensional case, with the aid of Figure 46b,

$$dA = \pi h^2 \sin \theta \, d\theta \tag{b-9}$$

Letting $\sin\alpha = \cos\theta$, and substituting for P, we have

$$F_{x_1} = \int_0^{\frac{\pi}{2}} (P_\infty \sin\theta + C_p^* \, q_\infty \cos^2 \theta \sin\theta) \, \pi \, h^2 \, d\theta \tag{b-10}$$

$$F_{x_1} = \frac{\pi h^2}{2} \left(P_\infty + \frac{1}{2} C_p^* q_\infty\right) \qquad \text{(b-11)}$$

The total x-component of force on the surface of the control volume is obtained by adding the downstream contribution, which is $-\frac{1}{2} \pi h^2 P_\infty$. The result is

$$F_x = \frac{\pi h^2}{4} C_p^* q_\infty \qquad \text{(b-12)}$$

or

$$F_x = \frac{\pi}{8} M_\infty^2 \gamma_\infty C_p^* h^2 P_\infty \qquad (2)$$

If we let

$$F_x = \frac{\pi h^2}{2} C_D q_\infty, \text{ then} \qquad \text{(b-13)}$$

$$C_D = \frac{1}{2} C_p^* \qquad \text{(b-14)}$$

REFERENCES

1. Allan E. Puckett: "Final Report, Model Supersonic Wind Tunnel Project," GALCIT Report No. 40 (1943).

2. H. W. Burden: "Some Effects of Secondary Injection into a Supersonic Flow," A. E. thesis, Graduate Aeronautical Laboratories, California Institute of Technology (June 1964).

3. M. W. Dowdy and J. F. Newton, Jr.: "Investigation of Liquid and Gaseous Secondary Injection Phenomena on a Flat Plate with M = 2.01 to M = 4.54," Jet Propulsion Laboratory Technical Report 32-542 (23 December 1963).

4. Wind Tunnel Staff of the Jet Propulsion Laboratory: "Wind Tunnel Facilities at the Jet Propulsion Laboratory," Jet Propulsion Laboratory Technical Release 34-257 (1 January 1962).

5. J. L. Amick and P. B. Hays: "Interaction Effects of Side Jets Issuing from Flat Plates and Cylinders Aligned with a Supersonic Stream," WADD Technical Report 60-329 (June 1960).

6. G. G. Chernyi: Introduction to Hypersonic Flow, R. F. Probstein, ed. Academic Press, New York (1961).

7. L. Lees: "Hypersonic Flow," Proc. 5th Internatl. Aero. Conf., Los Angeles. Inst. Aero. Sci., New York (1955), pp. 241-276.

8. J. F. Keffer and W. D. Baines: "The Round Turbulent Jet in a Cross-Wind," Journal of Fluid Mechanics, Vol. 15, No. 4 (April 1963), pp. 481-496.

9. R. W. Cubbison, B. H. Anderson, and J. J. Ward: "Surface Pressure Distributions with a Sonic Jet Normal to Adjacent Flat Surfaces at Mach 2.92 to 6.4," NASA TN D-580 (February 1961).

10. J. J. Janos: "Loads Induced on a Flat-Plate Wing by an Air Jet Exhausting Perpendicularly Through the Plate and Normal to a Free-Stream Flow of Mach Number 2.0," NASA TN D-649 (March 1961).

11. W. Lefko: "Loads Induced on a Flat Plate at a Mach Number of 4.5 with a Sonic or Supersonic Jet Exhausting Normal to the Surface," NASA TN D-1935 (July 1963).

12. P. W. Vinson, J. L. Amick, and H. P. Liepmann: "Interaction Effects Produced by Jet Exhausting Laterally Near Base of Ogive-Cylinder Model in Supersonic Main Stream," NASA Memo 12-5-58W (February 1959).

13. J. M. Wu, R. L. Chapkis, and A. Mager: "Approximate Analysis of Thrust Vector Control by Fluid Injection," ARS Journal, Vol. 31, No. 12 (December 1961), pp. 1677-1685.

14. J. E. Broadwell: "An Analysis of the Fluid Mechanics of Secondary Injection for Thrust Vector Control (Revised)," Space Technology Laboratories, Inc., Report No.6120-7744-MU-000 (15 March 1962).

15. C. Ferrari: "Interference Between a Jet Issuing Laterally from a Body and the Enveloping Supersonic Stream," The Johns Hopkins University, Applied Physics Lab., Bumblebee Report No. 286 (April 1959).

16. J. F. Newton, Jr. and F. W. Spaid: "Experiments on the Interaction of Secondary Injectants and Rocket Exhaust for Thrust Vector Control," Jet Propulsion Laboratory Technical Report 32-203 (12 February 1962). (Also ARS Journal, Vol. 32, No. 8 (August 1962), pp. 1203-1211.)

17. R. E. Walker, A. R. Stone, and M. Shandor: "Secondary Gas Injection in a Conical Rocket Nozzle I. Effect of Orifice Diameter and Molecular Weight of Injectant," AIAA Journal, Vol. 1, No. 2 (February 1963), pp. 334-338. (See also Ref. 24 of this paper.)

18. I. E. Vas and S. M. Bogdonoff: "Interaction of a Turbulent Boundary Layer with a Step at M = 3.85," AFOSR TN 55-200 (April 1955).

19. C. J. Rodriguez: "An Experimental Investigation of Jet-Induced Thrust Vector Control Methods," presented at the 17th Annual JANAF - ARPA - NASA Solid Propellant Meeting, Denver, Colorado (23-25 May 1961).

20. A. Lingen: "Jet-Induced Thrust-Vector Control Applied to Nozzles Having Large Expansion Ratios," United Aircraft Corp. Research Dept. Report R-0937-33 (1 March 1957).

21. A. J. Chamay and R. A. Sederquist: "An Experimental Investigation of Shock Vector Control with Gaseous Secondary Injection," ARS Preprint 2216-61 (August 1961).

22. J. E. Broadwell: "Correlation of Rocket Nozzle Gas Injection Data," AIAA Journal, Vol. 1, No. 8 (August 1963), pp. 1911-1913.

23. F. G. Buffum, Jr., E. W. Price, and R. O. Slates: "An Experimental Investigation of the Flow Phenomena Involved in Gaseous Thrust Direction Control Devices," U. S. Naval Ordnance Test Station, China Lake, California, Prepared for the Sixth U. S. Navy Symposium on Aeroballistics, David Taylor Model Basin, Washington, D. C. (31 October - 1 November 1963).

24. S. M. Bogdonoff and C. E. Kepler: "Separation of a Supersonic Turbulent Boundary Layer," Princeton University Report No. 249 (January 1954).

25. A.Heyser and F. Maurer: "Experimentelle Untersuchungen an festen Spoilern und Strahlspoilern bei Machschen Zahlen von 0.6 bis 2.8," Z. Flugwiss., Vol. 10, No. 4-5 (April-May 1962), pp. 110-130. (Also A. Heyser and F. Maurer: Experimental Investigations on Solid Spoilers and Jet Spoilers at Mach Numbers of 0.6 to 2.8, Jet Propulsion Laboratory Translation No. 32 (21 February 1964).)

26. D. J. Romeo and J. R. Sterrett: "Aerodynamic Interaction Effects Ahead of a Sonic Jet Exhausting Perpendicularly from a Flat Plate into a Mach Number 6 Free Stream," NASA TN D-743 (April 1961).

27. L. G. Kaufman II, et al.: "A Review of Hypersonic Flow Separation and Control Characteristics," ASD TDR 62-168 (March 1962).

28. G. E. Gadd: "A Theoretical Investigation of Laminar Separation in Supersonic Flow," JAS, Vol. 24, No. 10 (October 1957).

29. J. R. Sterrett and J. C. Emery: "Extention of Boundary-Layer-Separation Criteria to a Mach Number of 6.5 by Utilizing Flat Plates with Forward-Facing Steps," NASA TN D-618 (December 1960).

30. D. R. Chapman, D. Kuehn, and H. K. Larson: "Investigation of Separated Flows in Supersonic and Transonic Streams with Emphasis on the Effect of Transition," NACA TR 1356 (1958).

31. E. S. Love: "Pressure Rise Associated with Shock-Induced Boundary Layer Separation," NACA TN 3601 (December 1955).

32. W. T. Strike and C. J. Schueler: "Investigation of Interference Effects Produced by Laternal Jets on Surfaces in a Supersonic Stream," AIAA Preprint No. 63-184 (June 1963).

33. A. J. Fejer and J. P. Josse: "An Investigation of Induced Separation of Supersonic Channel Flow," ARL-63-102, Illinois Institute of Technology, Chicago, Illinois (June 1963).

34. Personal communication from F. Maurer (March, 1964).

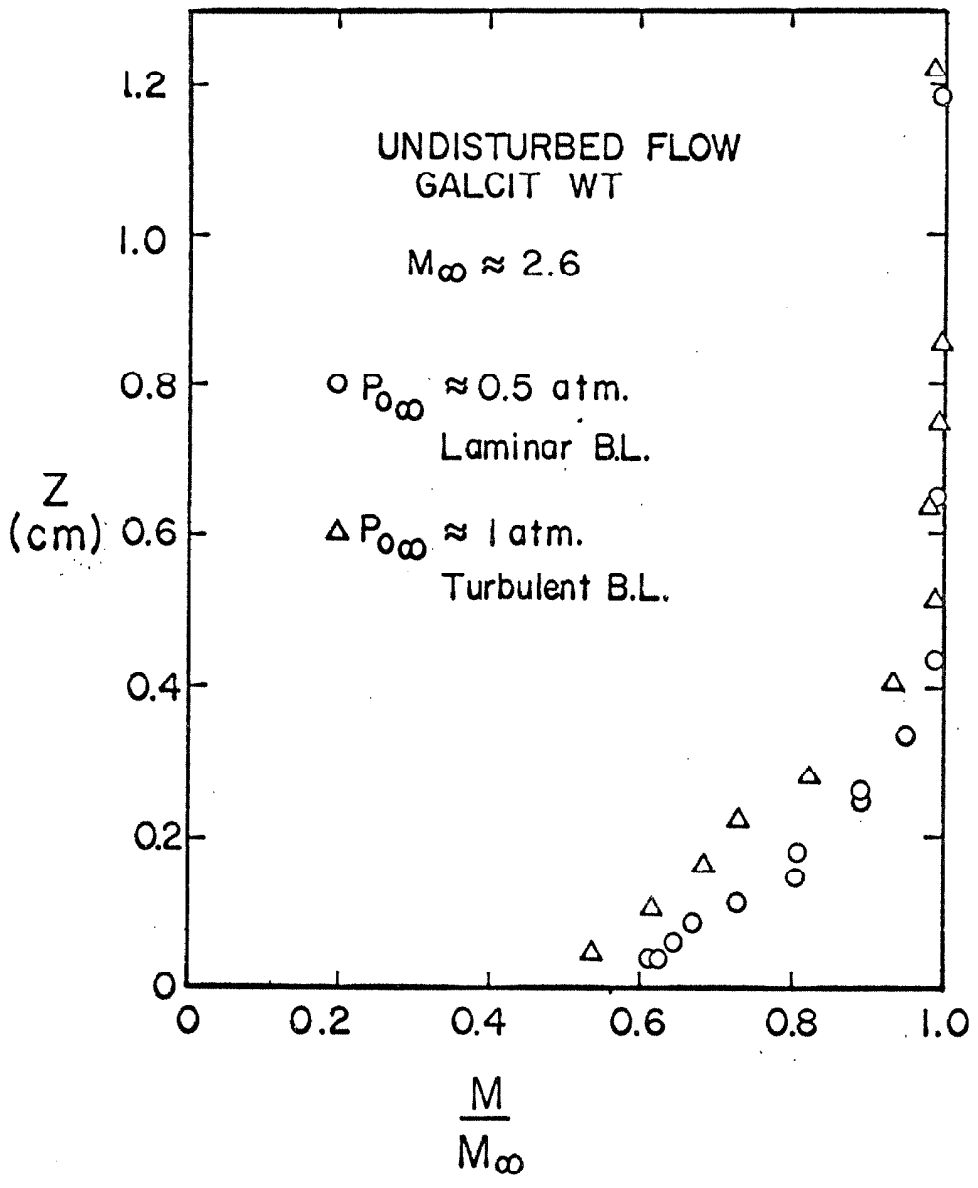

Figure 1. Typical Mach Number Profiles in the Test Section Near the Injector, CIT Supersonic Wind Tunnel

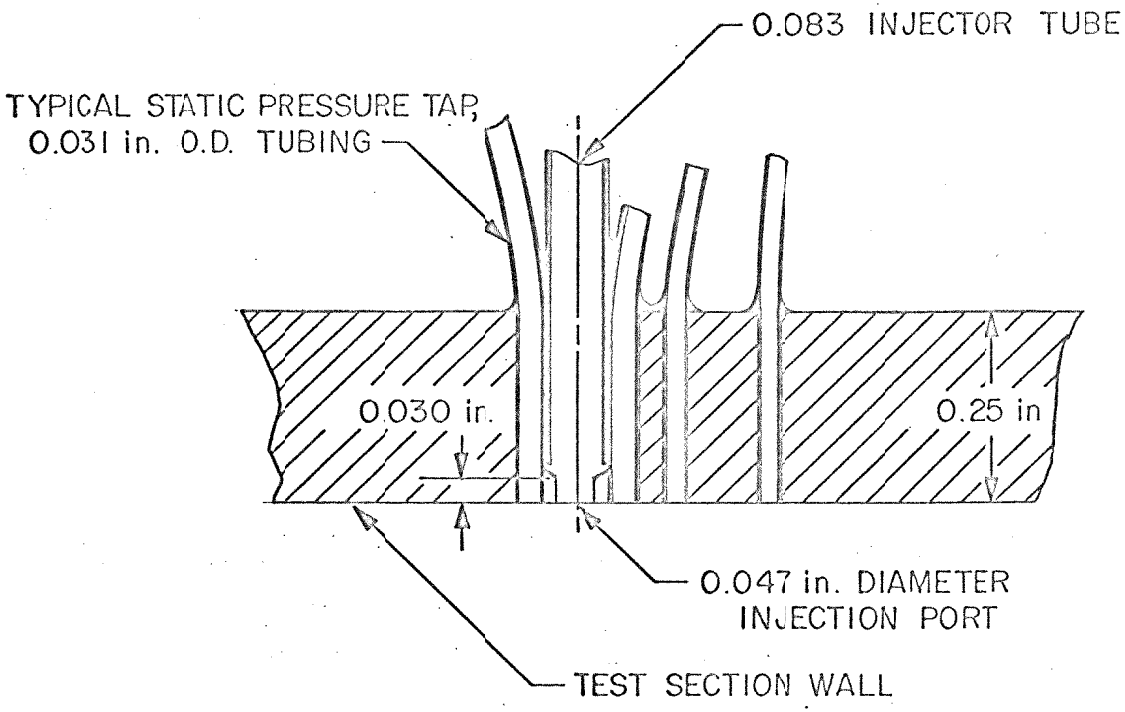

Figure 2. Section View of Circular-Hole Injector

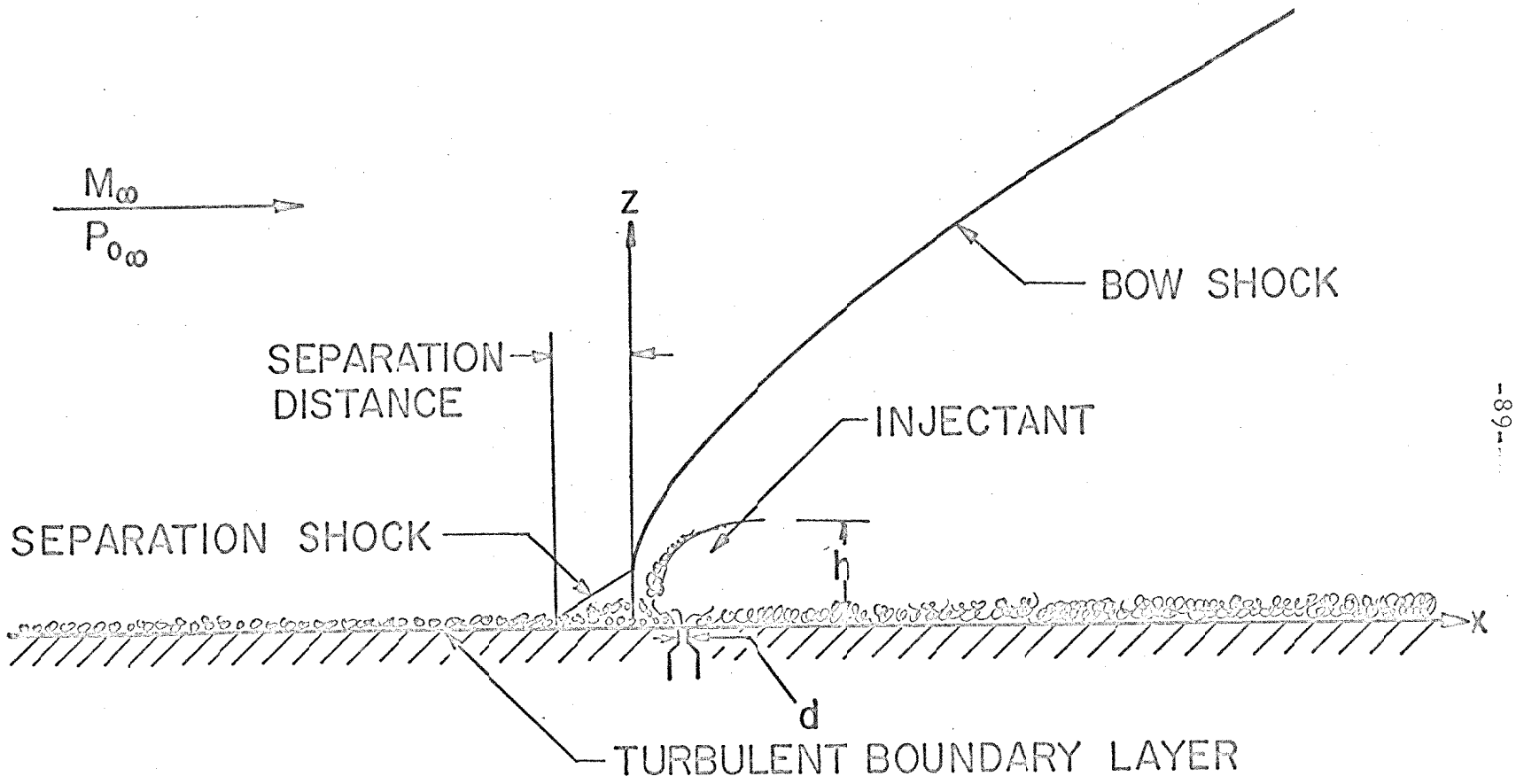

Figure 3a. Sketch of the Flow Field for Hole Injection, Turbulent Boundary Layer

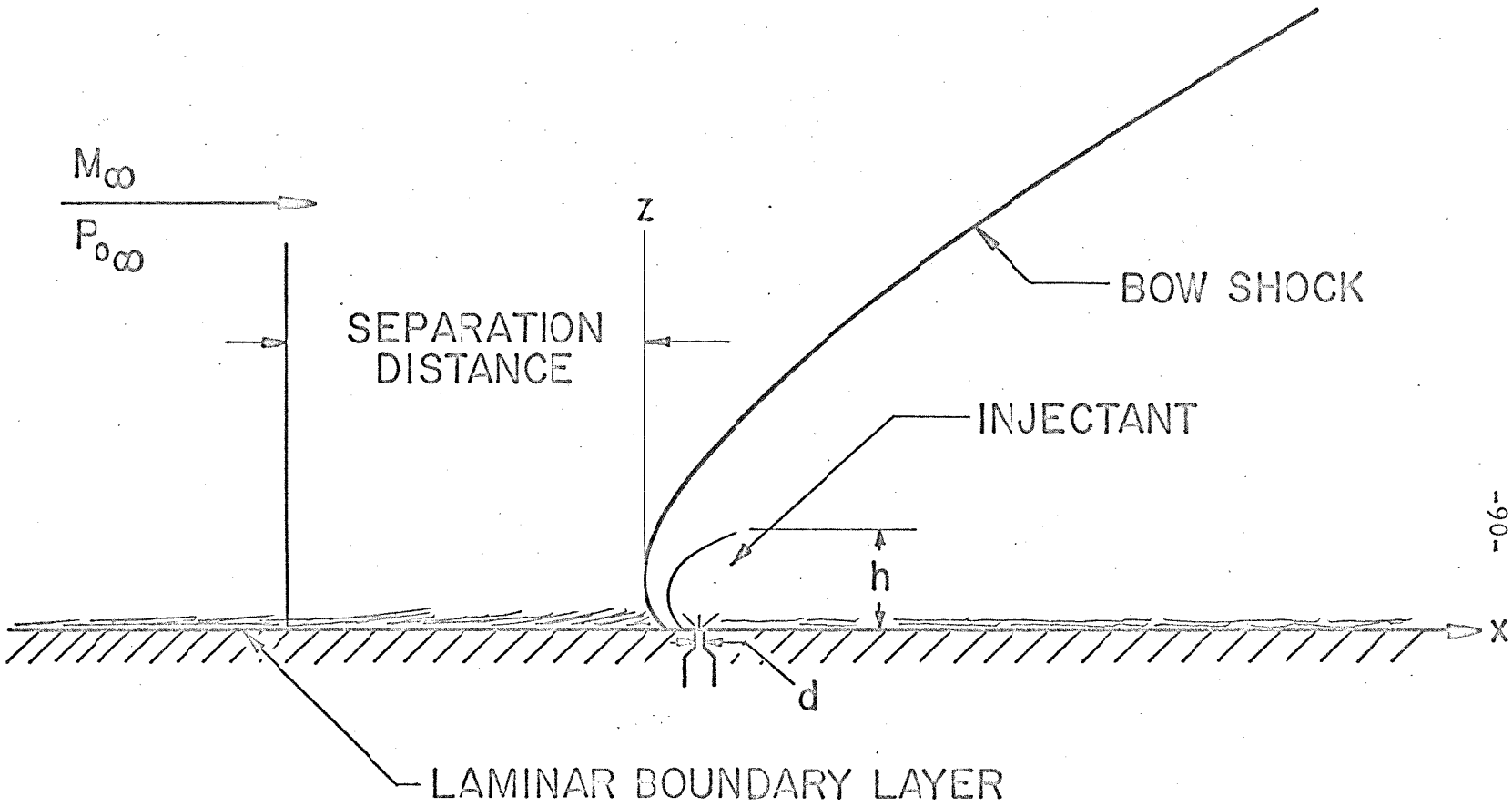

Figure 3b. Sketch of the Flow Field for Hole Injection, Laminary Boundary Layer

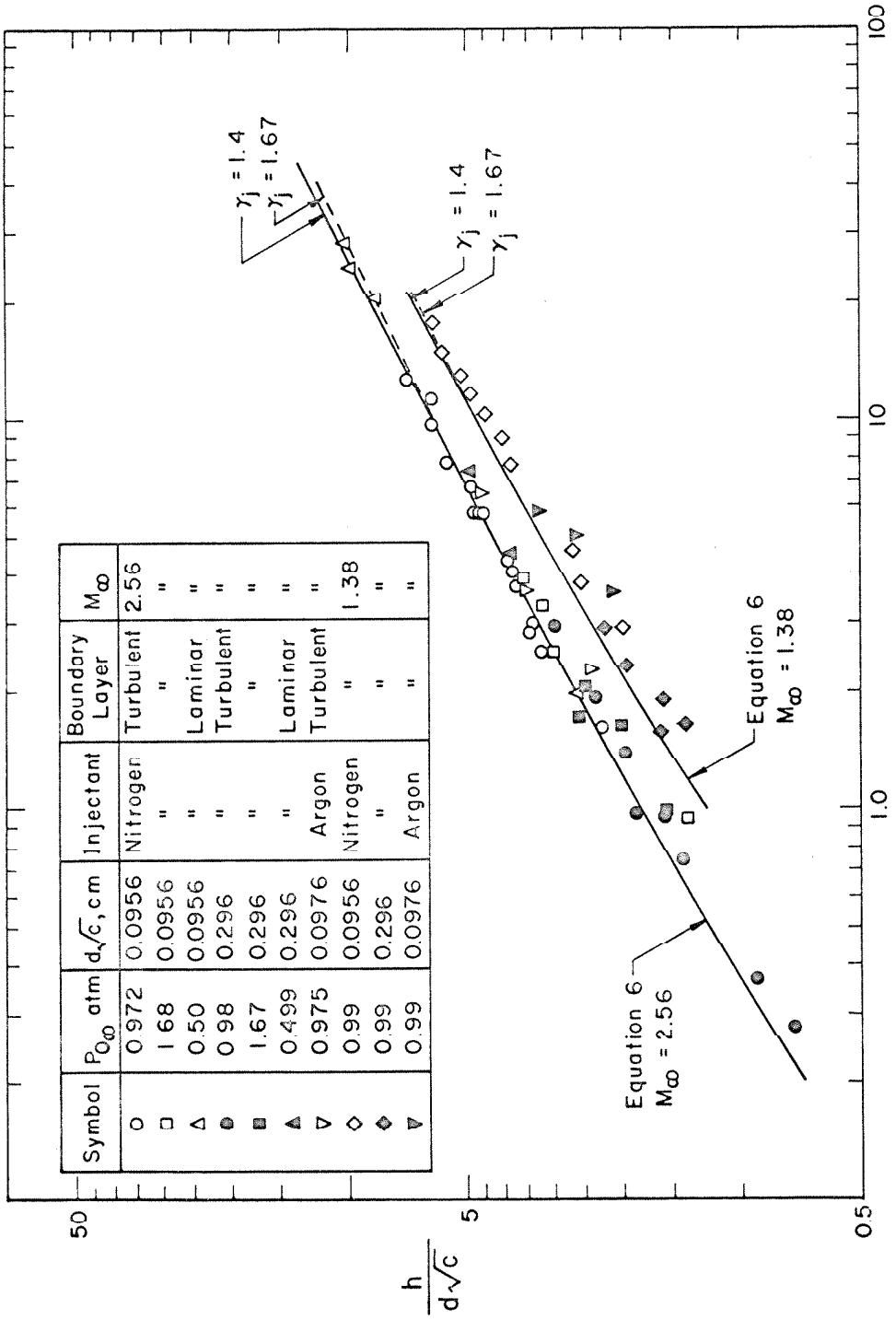

Figure 4. Penetration of Secondary Jet into Primary Flow, Nozzle Wall Data

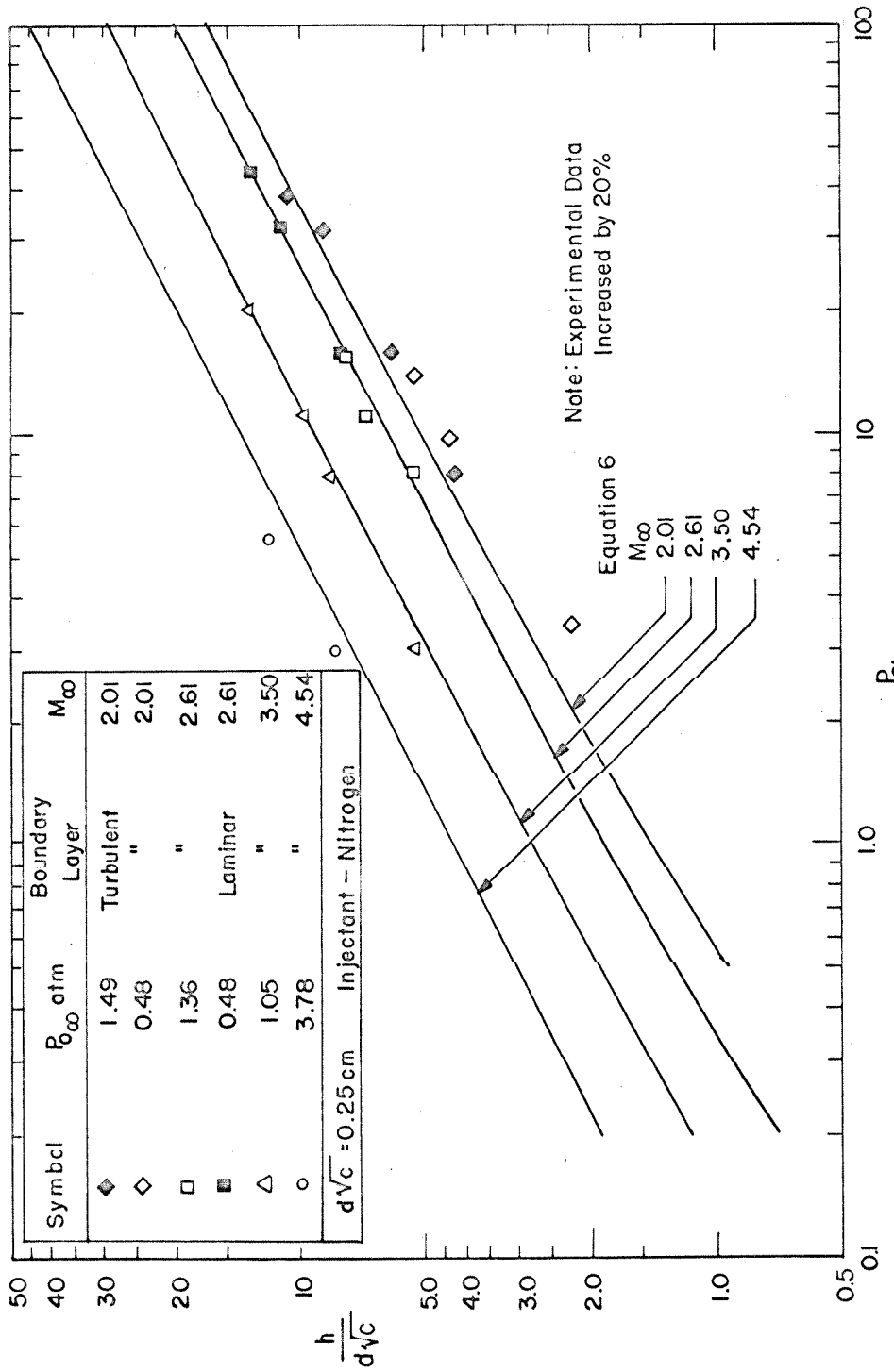

Figure 5. Penetration of Secondary Jet into Primary Flow, Flat Plate Data

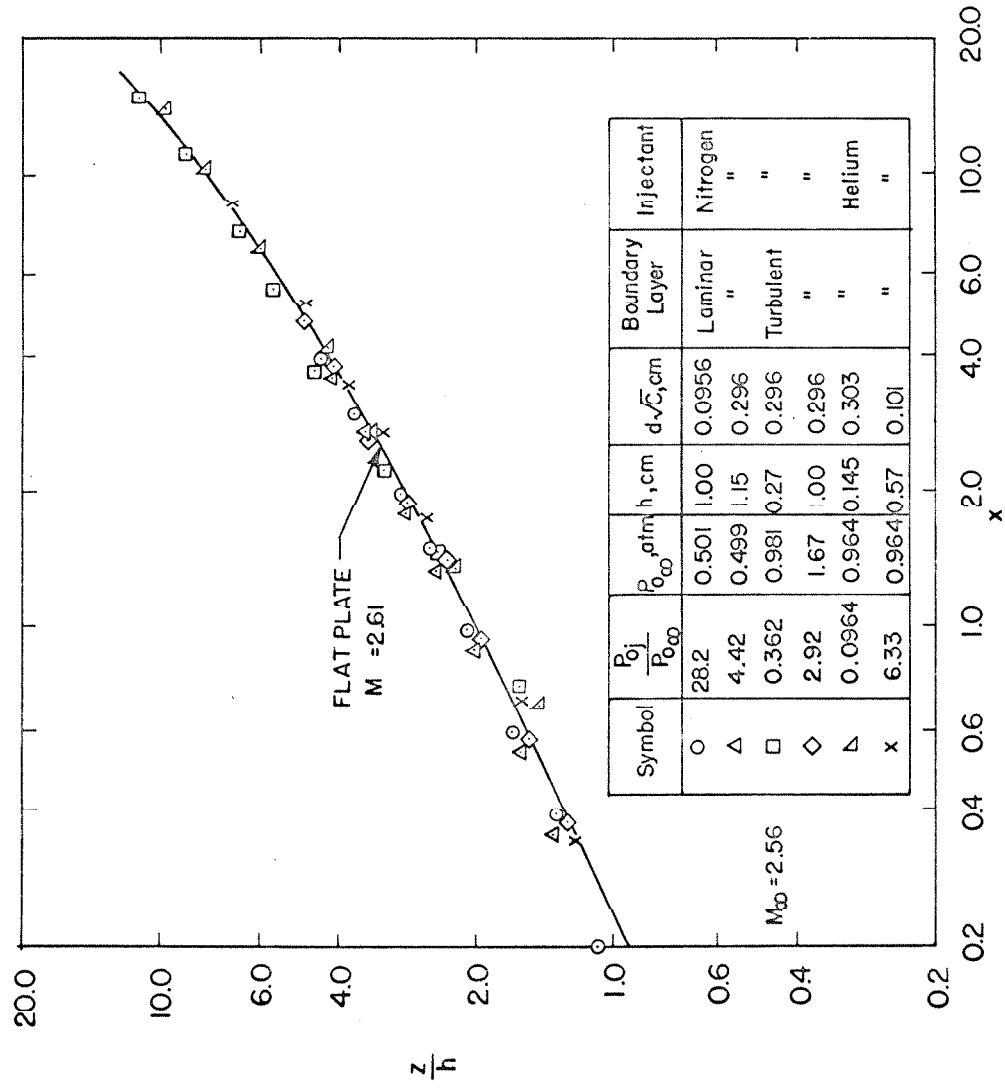

Figure 6. Shock Shapes, Comparison of Nozzle Wall and Flat Plate Results

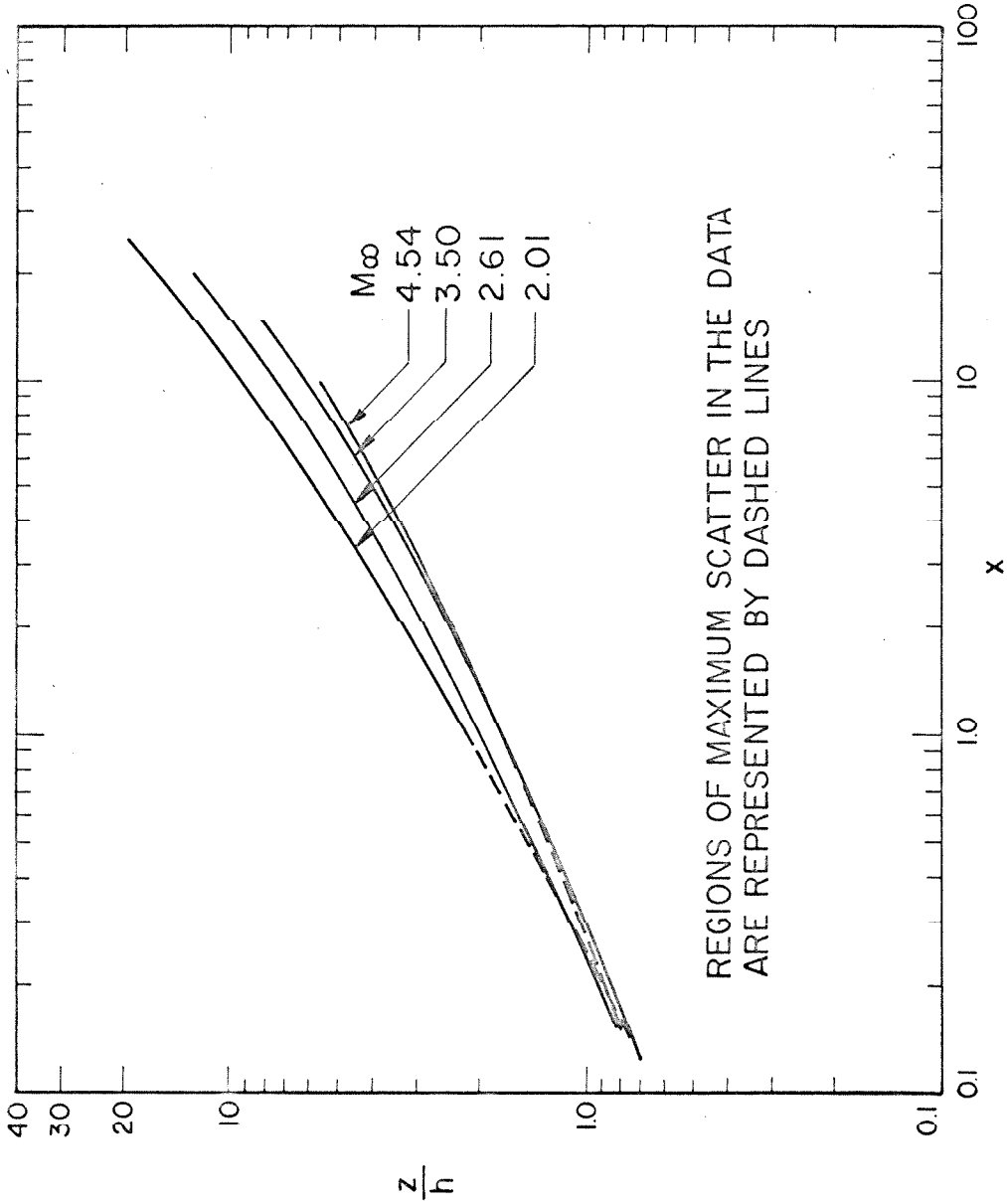

Figure 7. Shock Shapes Showing Mach Number Effect

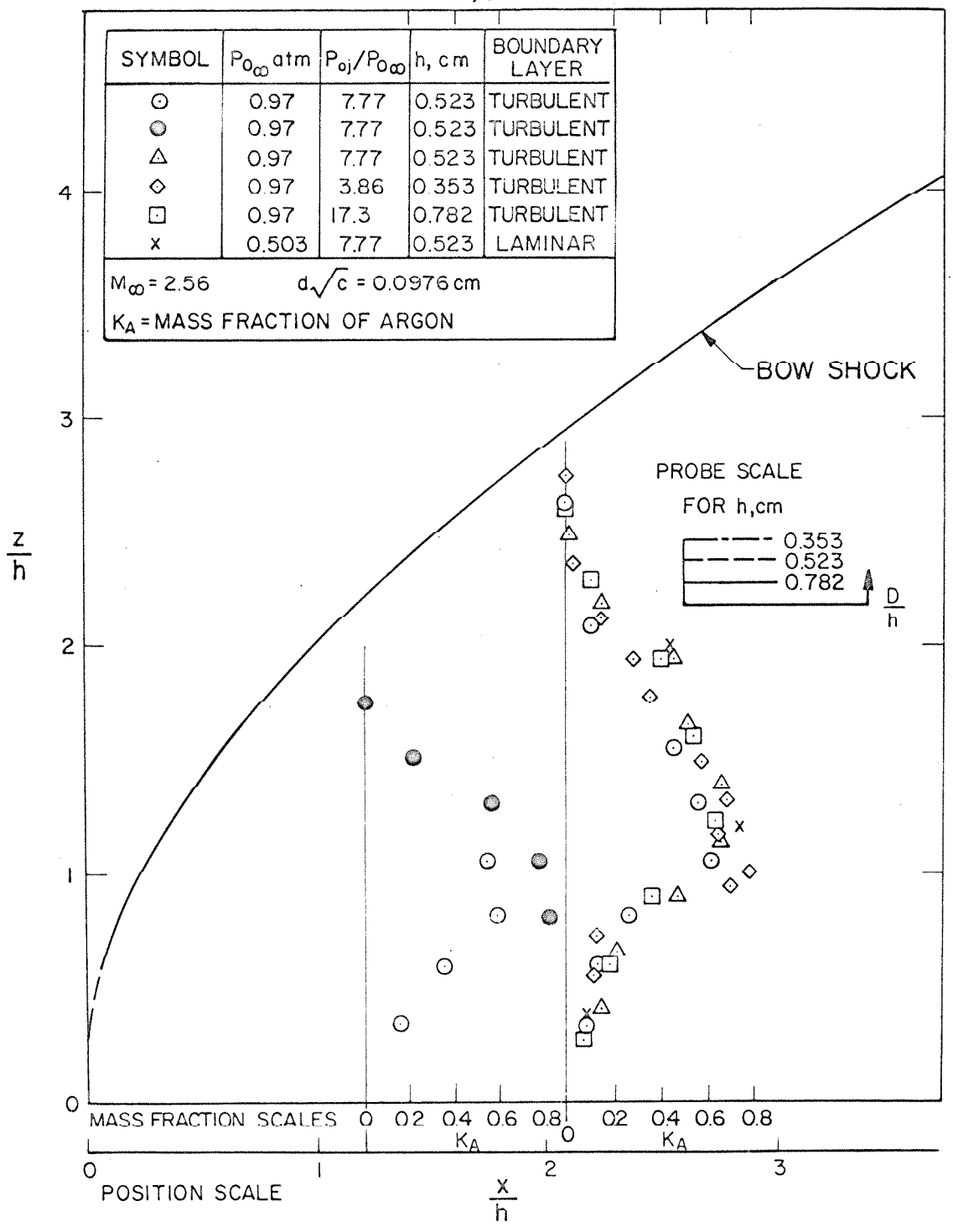

Figure 8a. Concentration Measurements with Argon Injection in the Plane (y/h) = 0, Injector Region

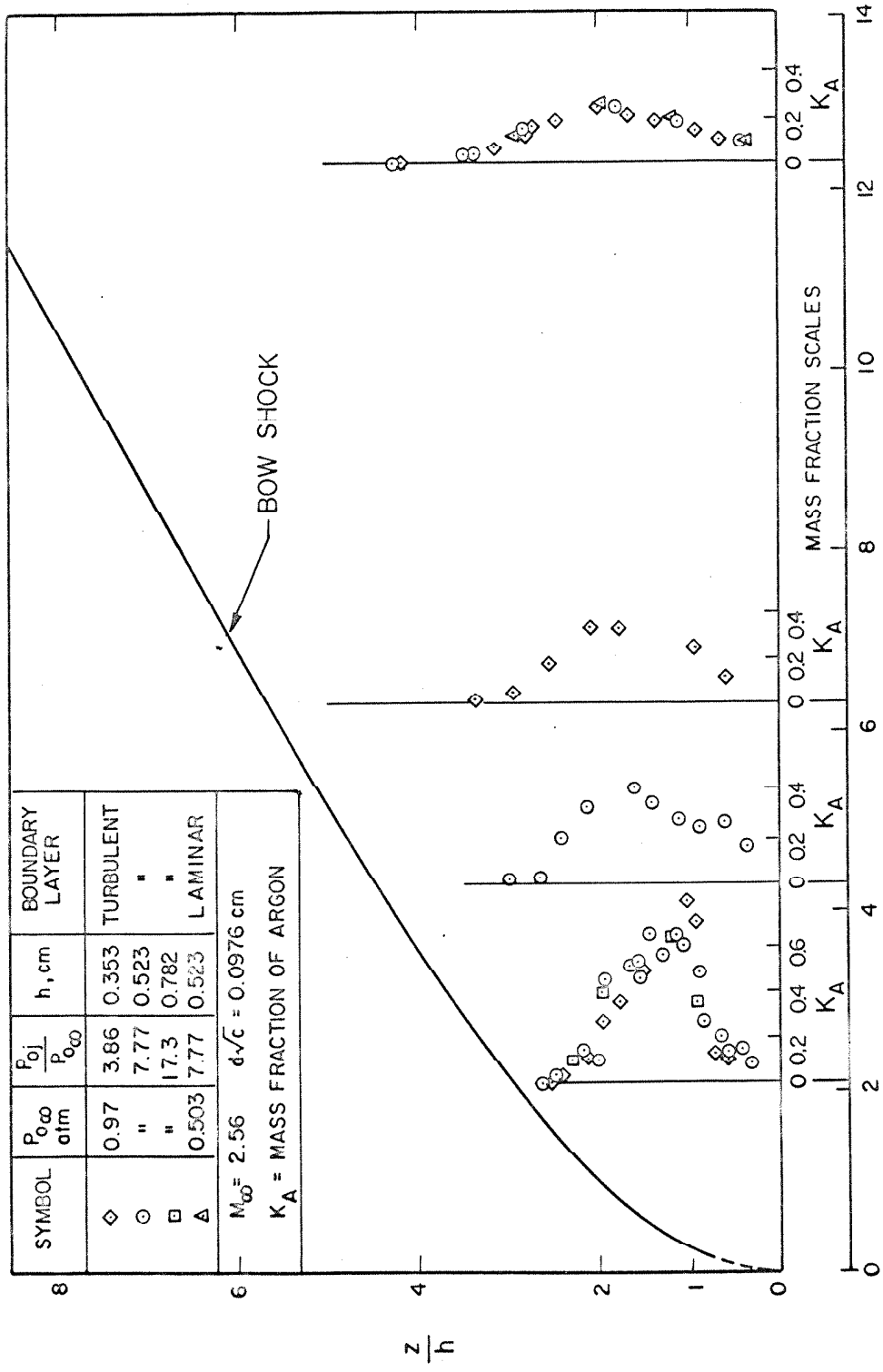

Figure 8b. Concentration Measurements with Argon Injection in the Plane (y/h) = 0, Downstream Region

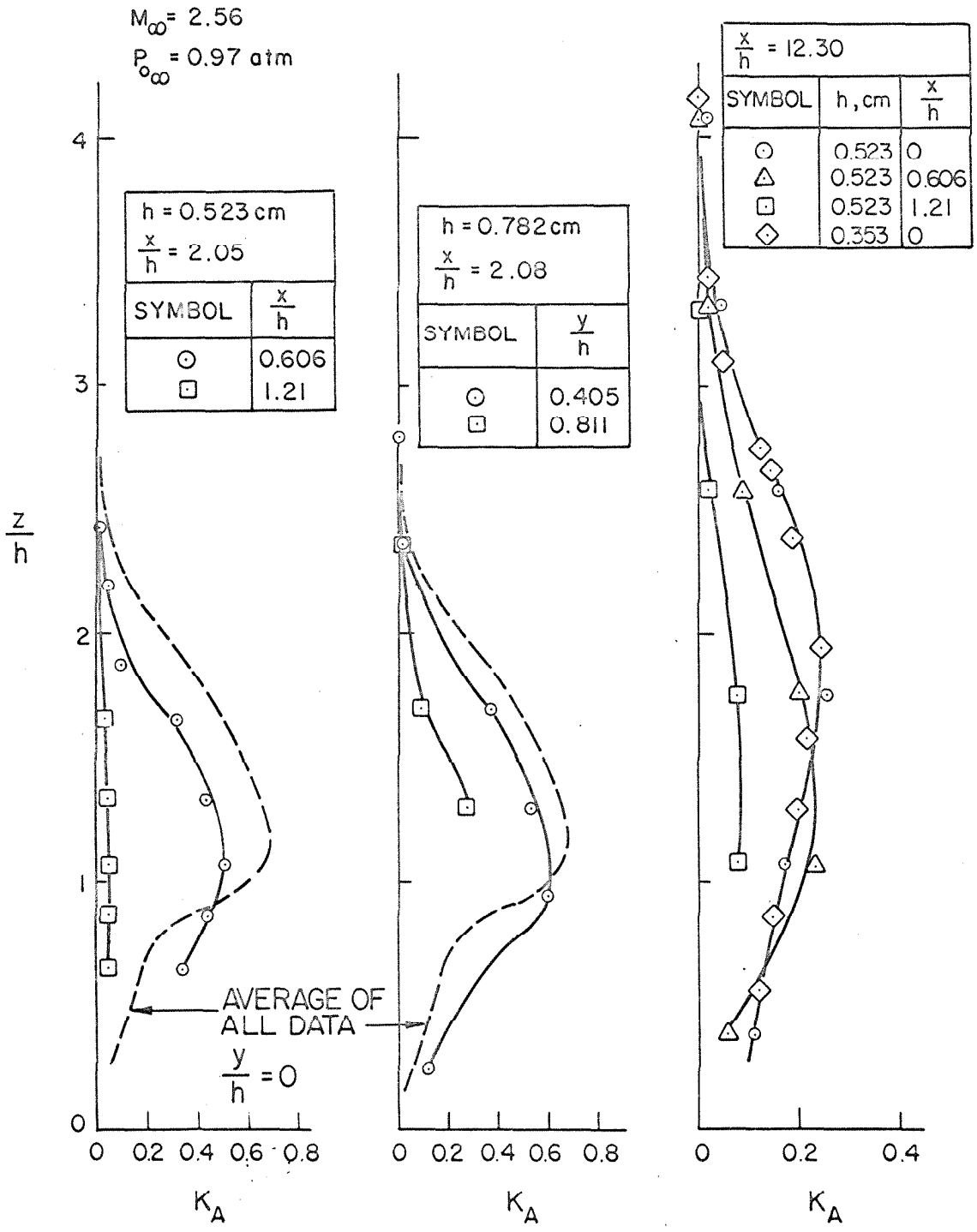

Figure 9. Concentration Profiles in Several Planes, (y/h) = Constant

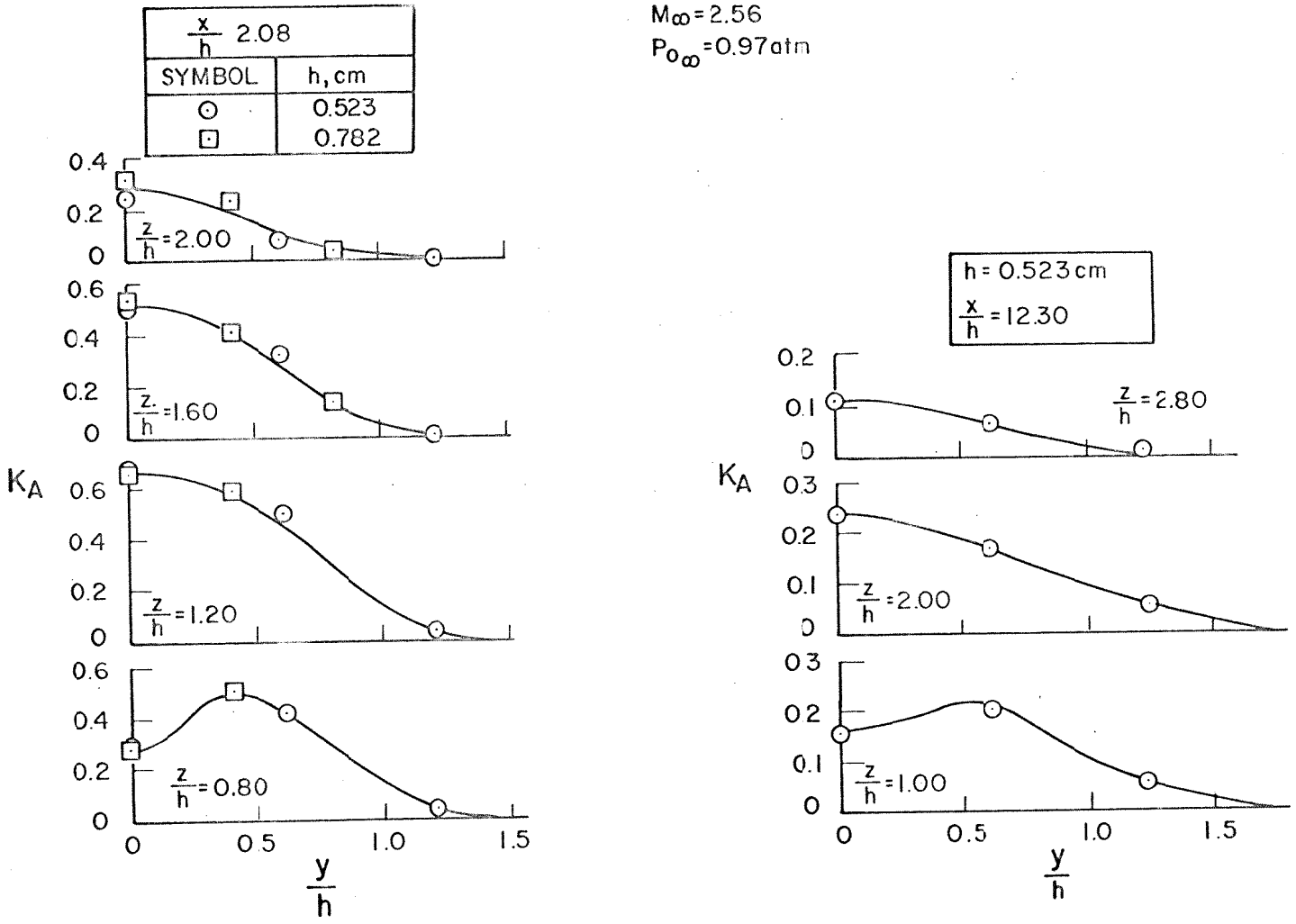

Figure 10a. Crossplots of Argon Concentration Profiles in Planes for which (z/h) = Constant

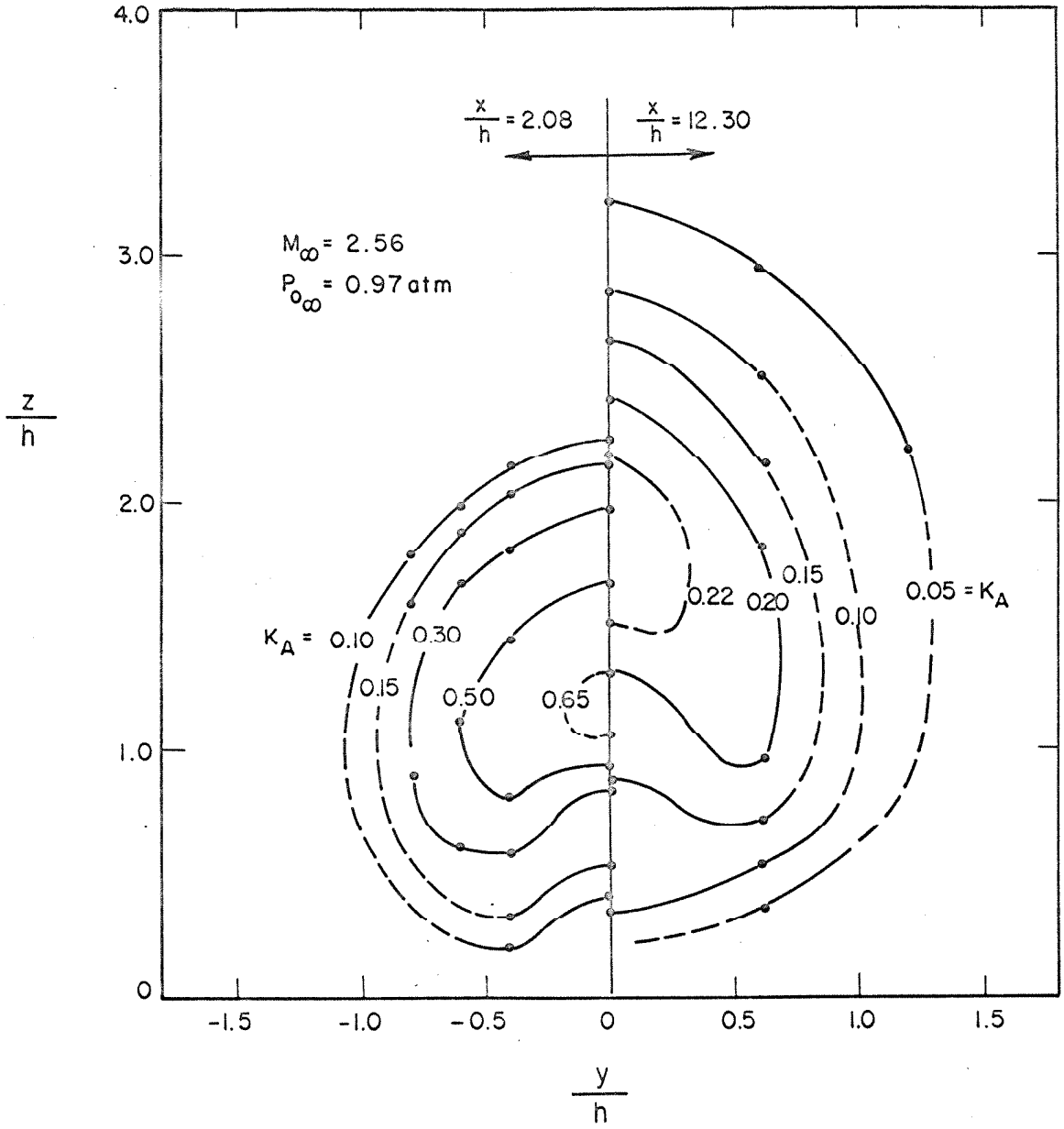

Figure 10b. Concentration Contours in the Planes (x/h) = 2.08 and (x/h) = 12.30

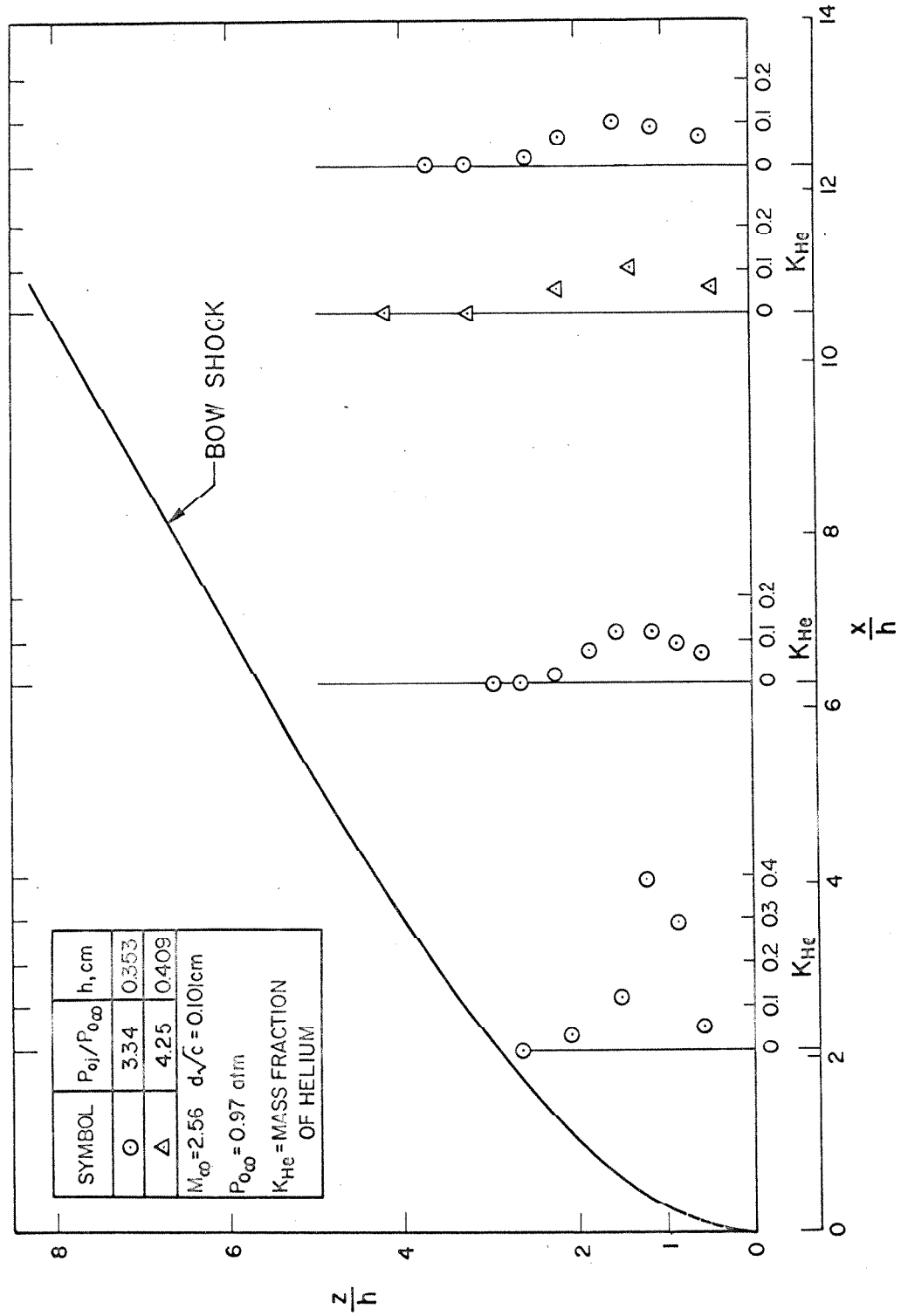

Figure 11a. Concentration Measurements with Helium Injection in the Plane (y/h) = 0

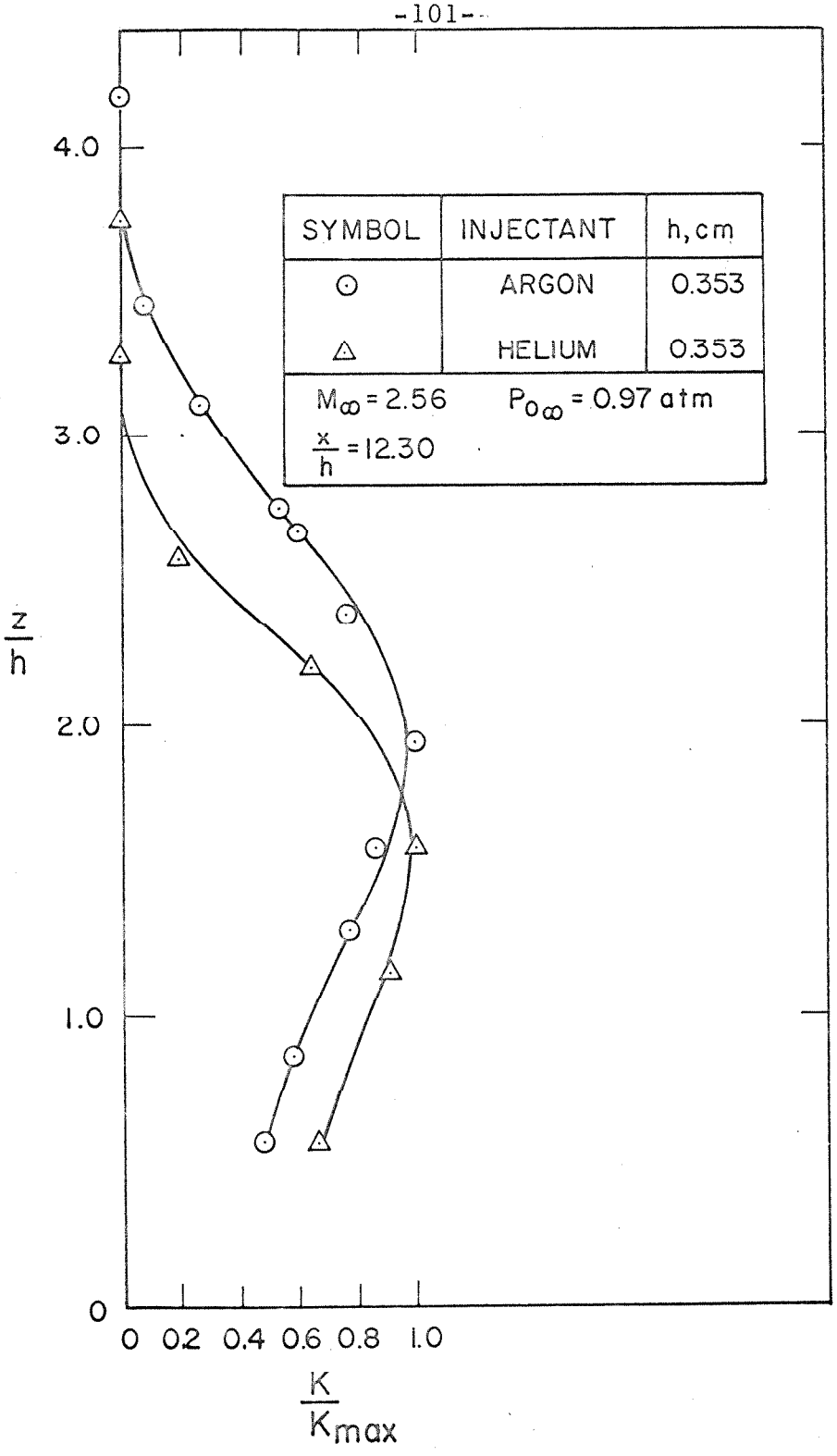

Figure 11b. Comparison of Argon and Helium Concentration Data

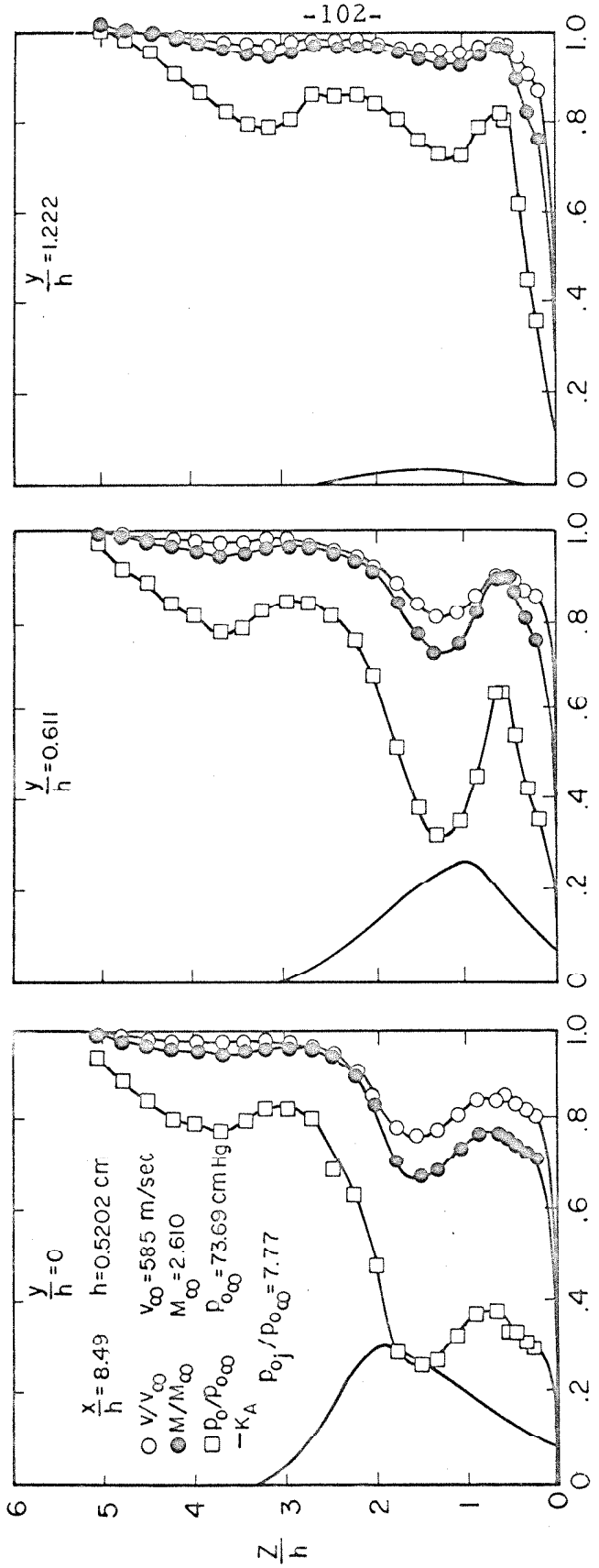

Figure 12. Velocity, Mach Number, and Total Pressure Profiles with Argon Injection for (x/h) = 8.49

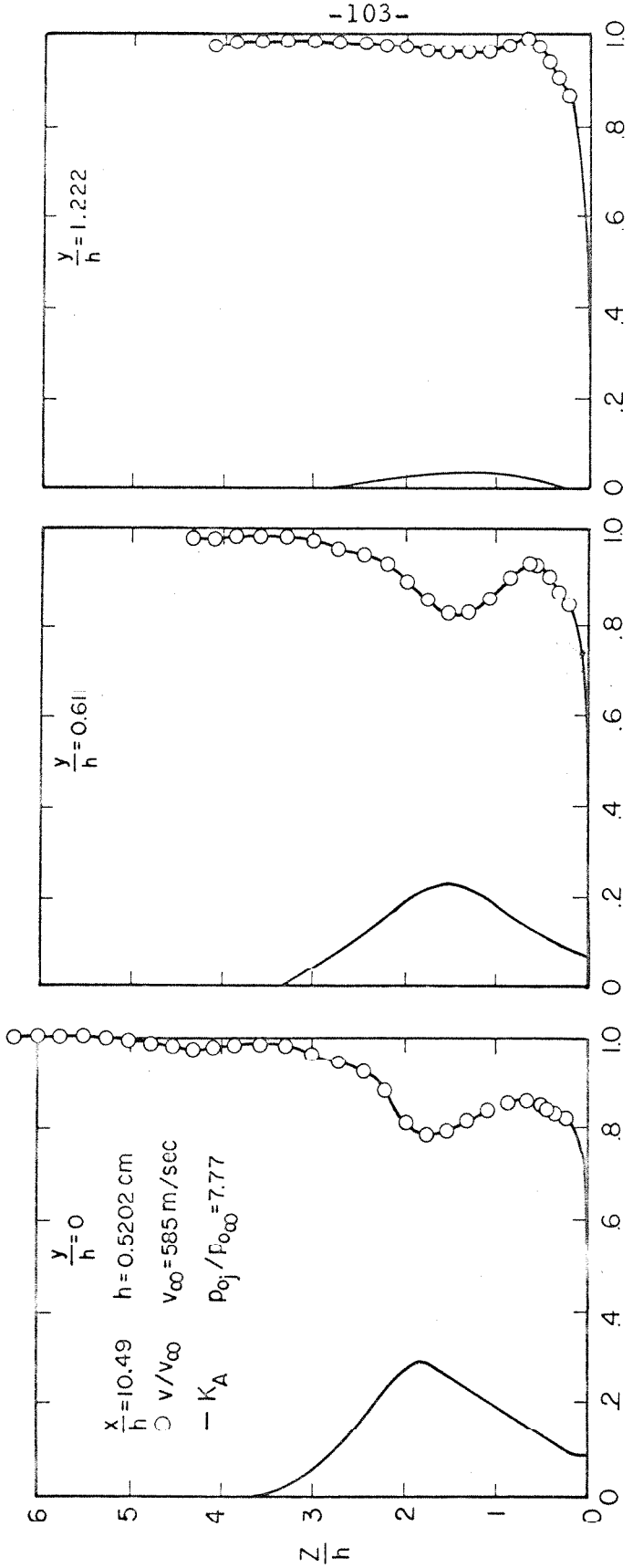

Figure 13. Velocity Profiles with Argon Injection for (x/h) = 10.49

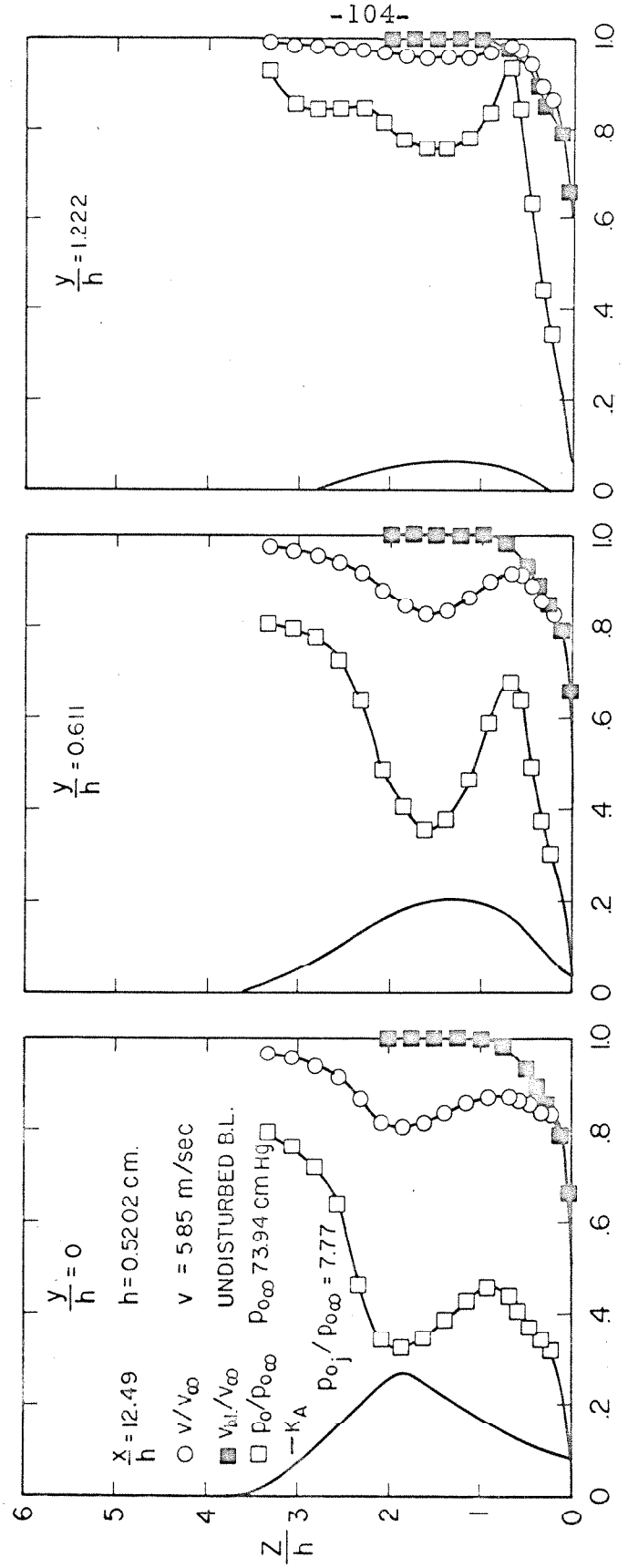

Figure 14. Velocity and Total Pressure Profiles with Argon Injection and Velocity Profiles without Injection for (x/h) = 12.49

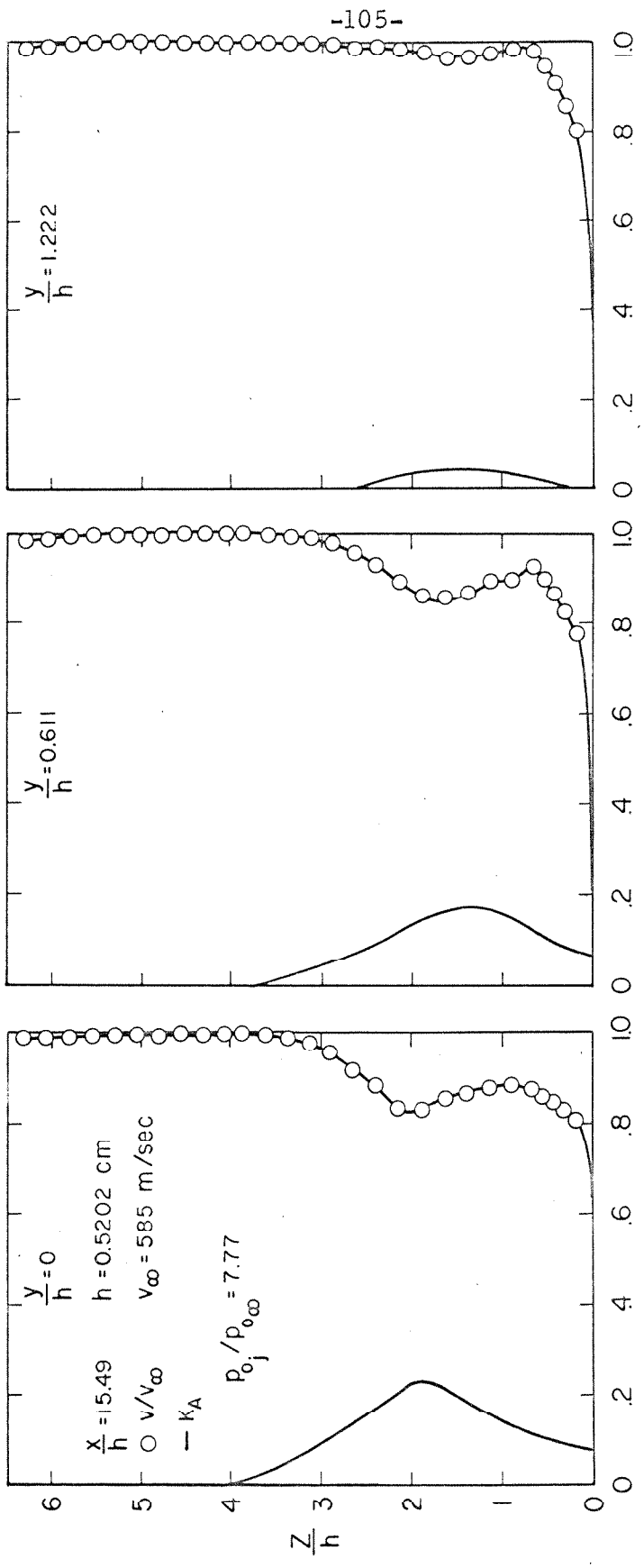

Figure 15. Velocity Profiles with Argon Injection for (x/h) = 15.49

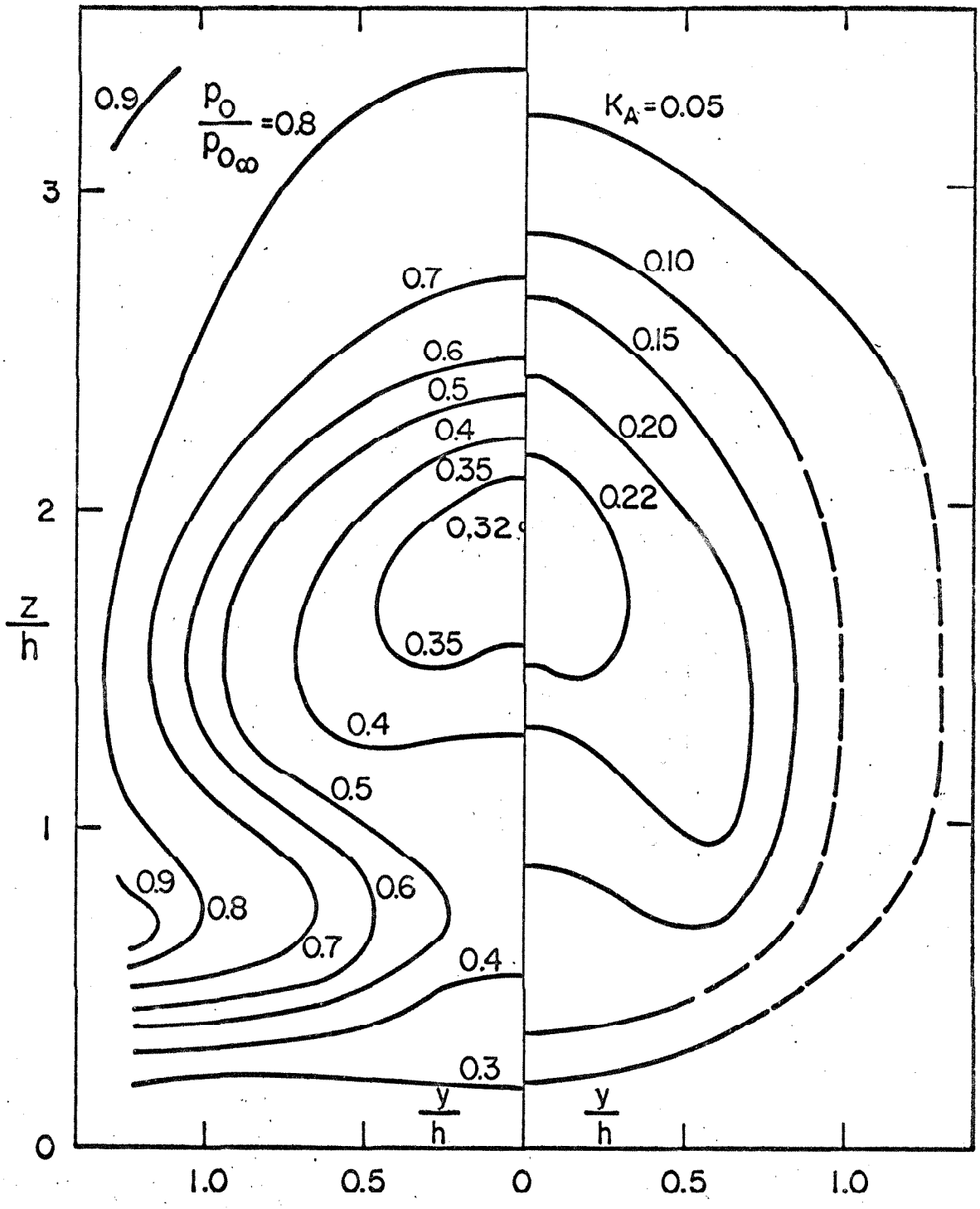

Figure 16. Concentration and Total Pressure Contours with Argon Injection, $M_\infty \approx 2.6$, $P_{o_\infty} \approx 0.974$ atm., $(P_{o_j}/P_{o_\infty}) = 7.77$, $h \approx 0.52$ cm., $(x/h) \approx 12$

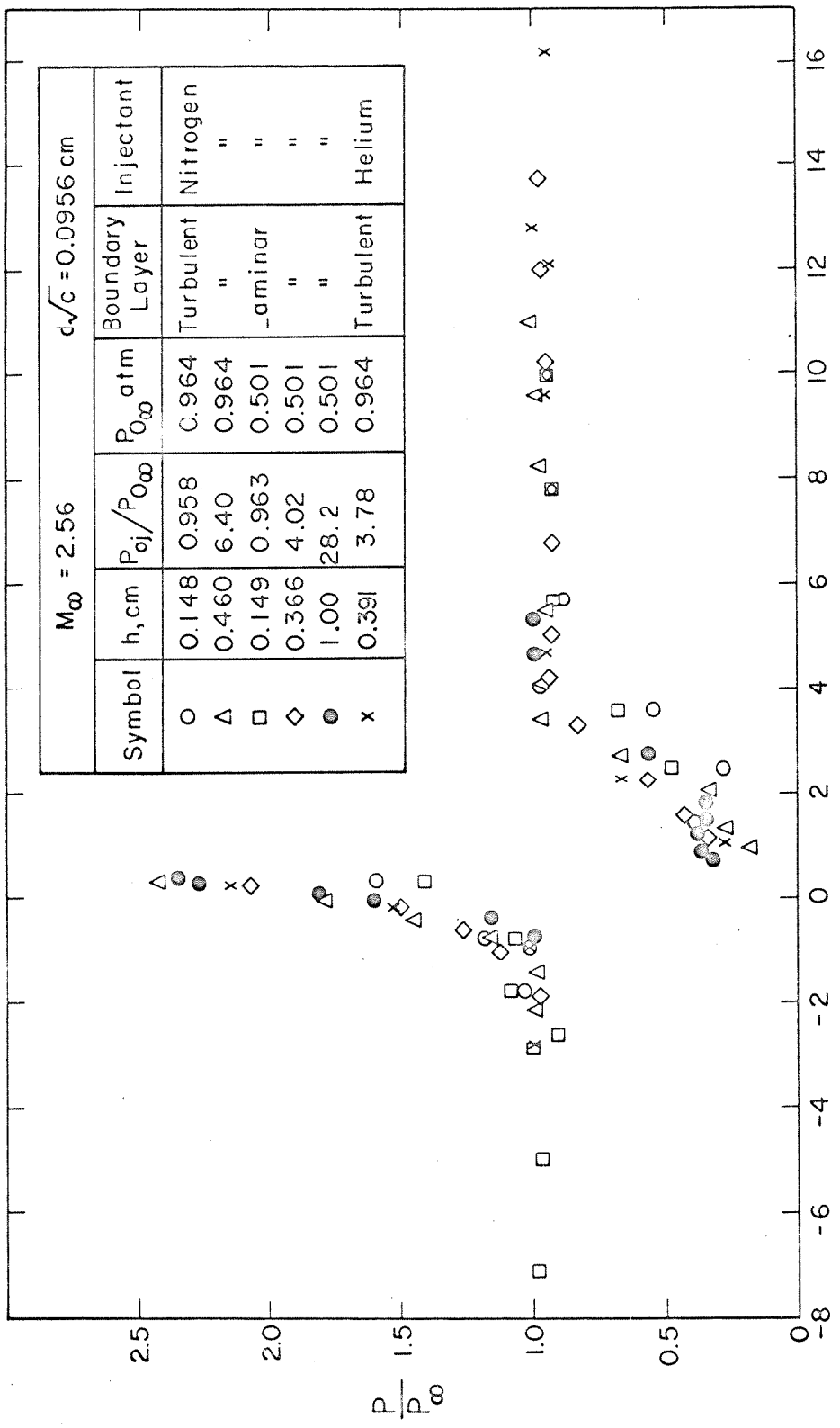

Figure 17. Nozzle-Wall Static Pressure Measurements in the Plane $(y/h) = 0$ at $M_\infty = 2.56$, with Nitrogen and Helium Injectants

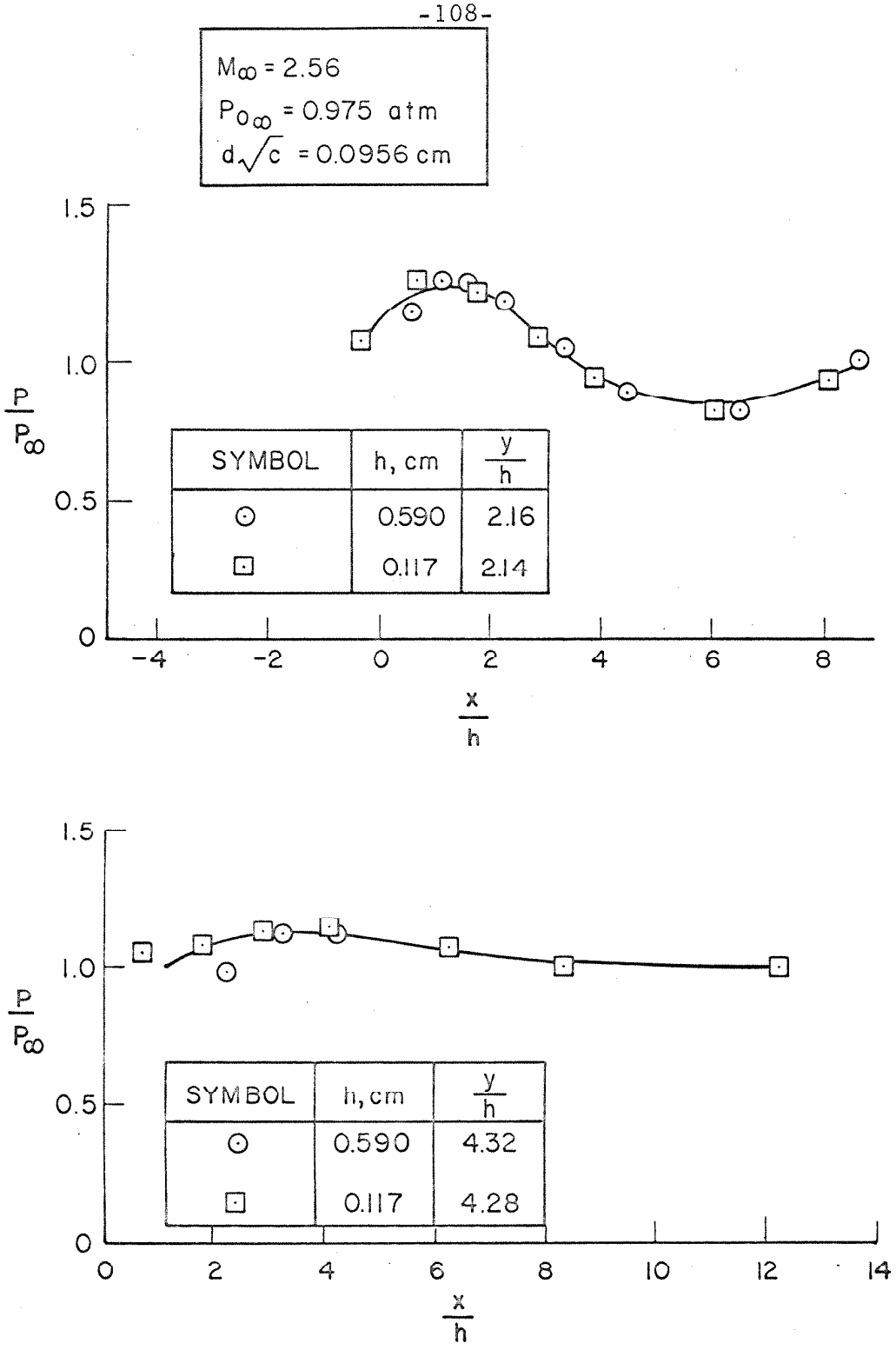

Figure 18a. Nozzle-Wall Static Pressure Measurements in Off-Axis Planes with Nitrogen Injection, (y/h) = Constant

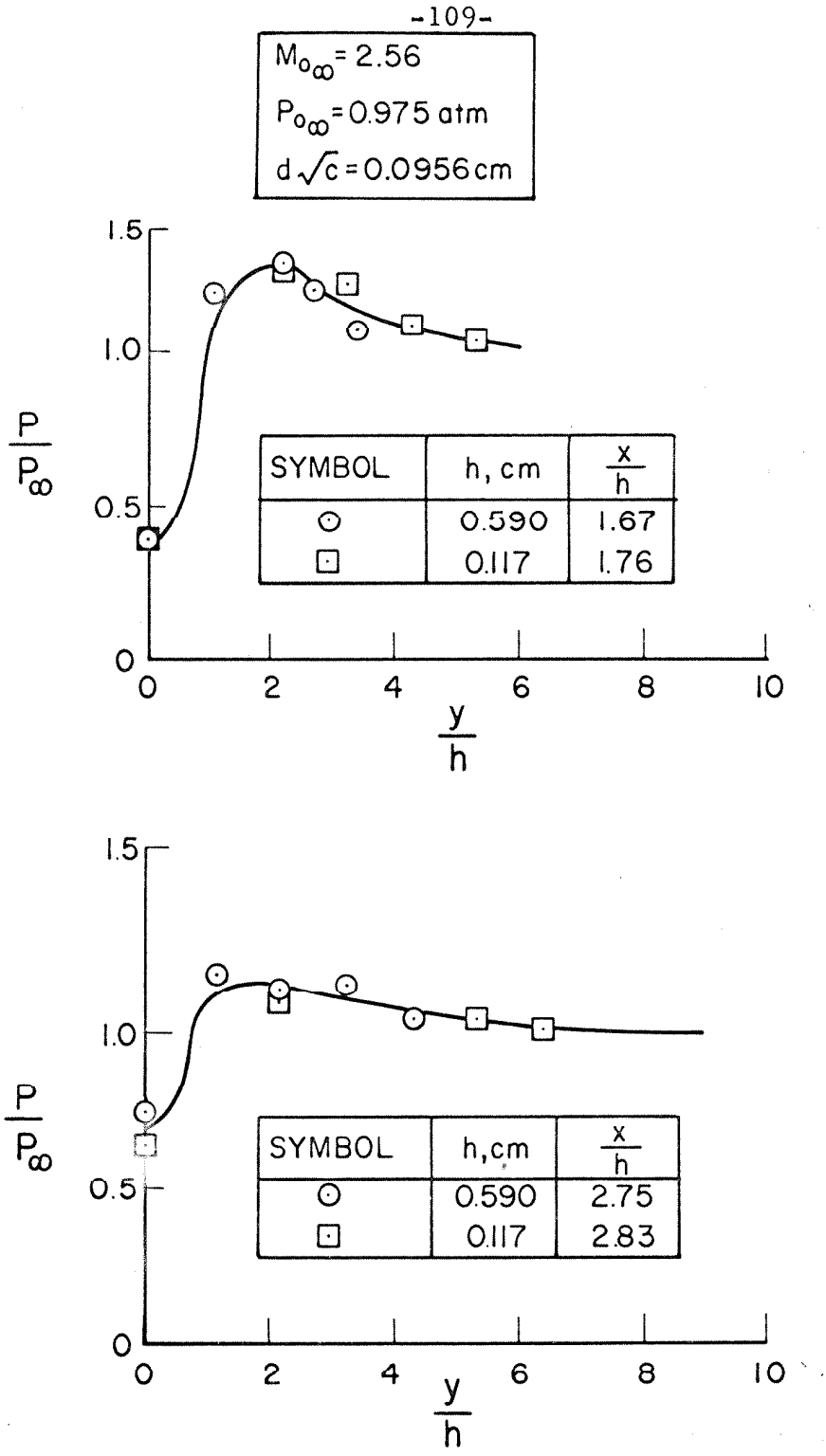

Figure 18b. Nozzle-Wall Static Pressure Measurements in Off-Axis Planes with Nitrogen Injection, (x/h) = Constant

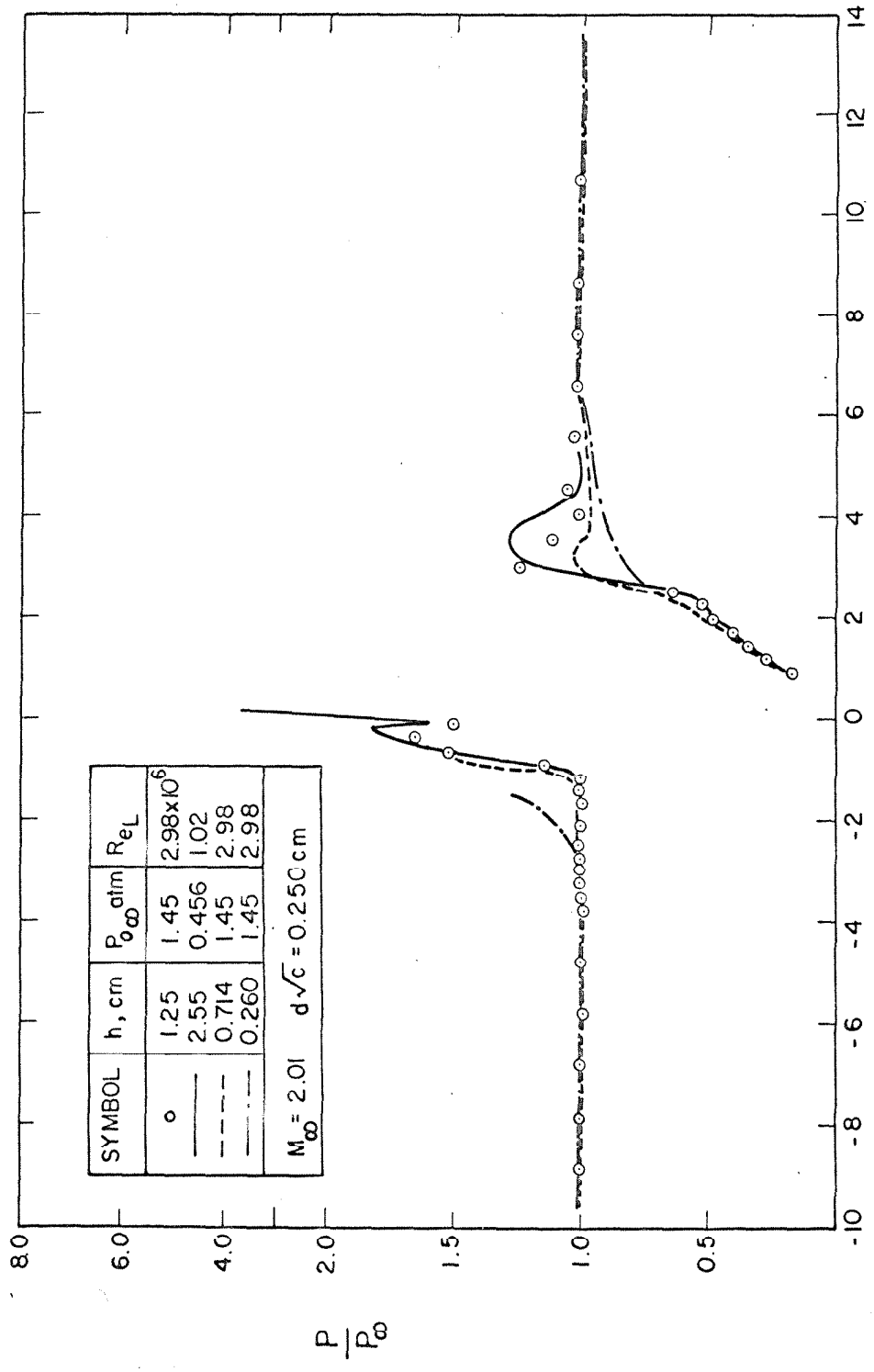

Figure 19. Flat-Plate Static Pressure Measurements in the Plane (y/h) = 0 at M_∞ = 2.01 with Nitrogen Injection. Turbulent Boundary Layer.

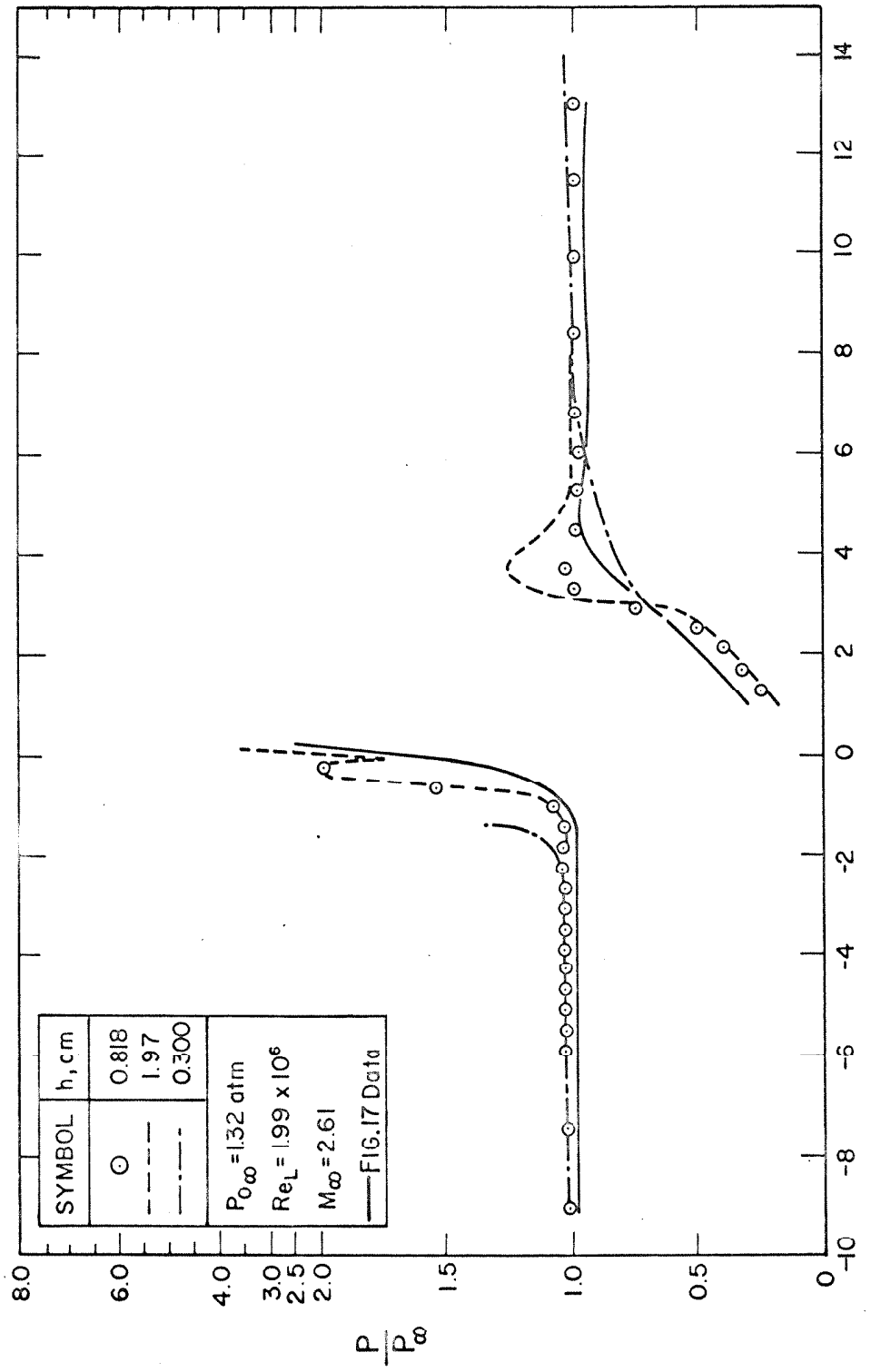

Figure 20. Flat-Plate Static Pressure Measurements in the Plane (y/h) = 0 at M_∞ = 2.61 with Nitrogen Injection, Turbulent Boundary Layer

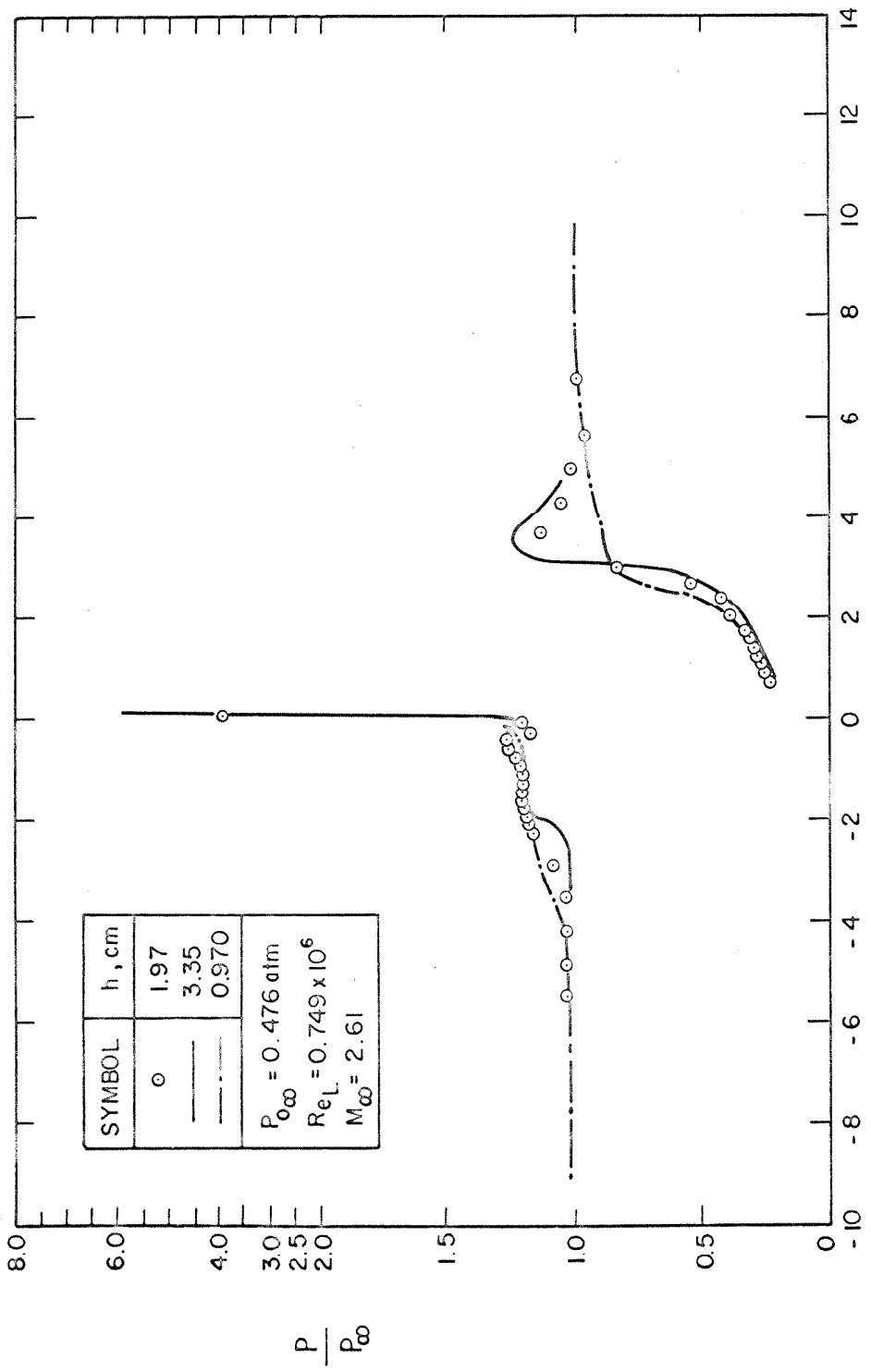

Figure 21. Flat-Plate Static Pressure Measurements in the Plane (y/h) = 0 at M_∞ = 2.61 with Nitrogen Injection. Laminar Boundary Layer

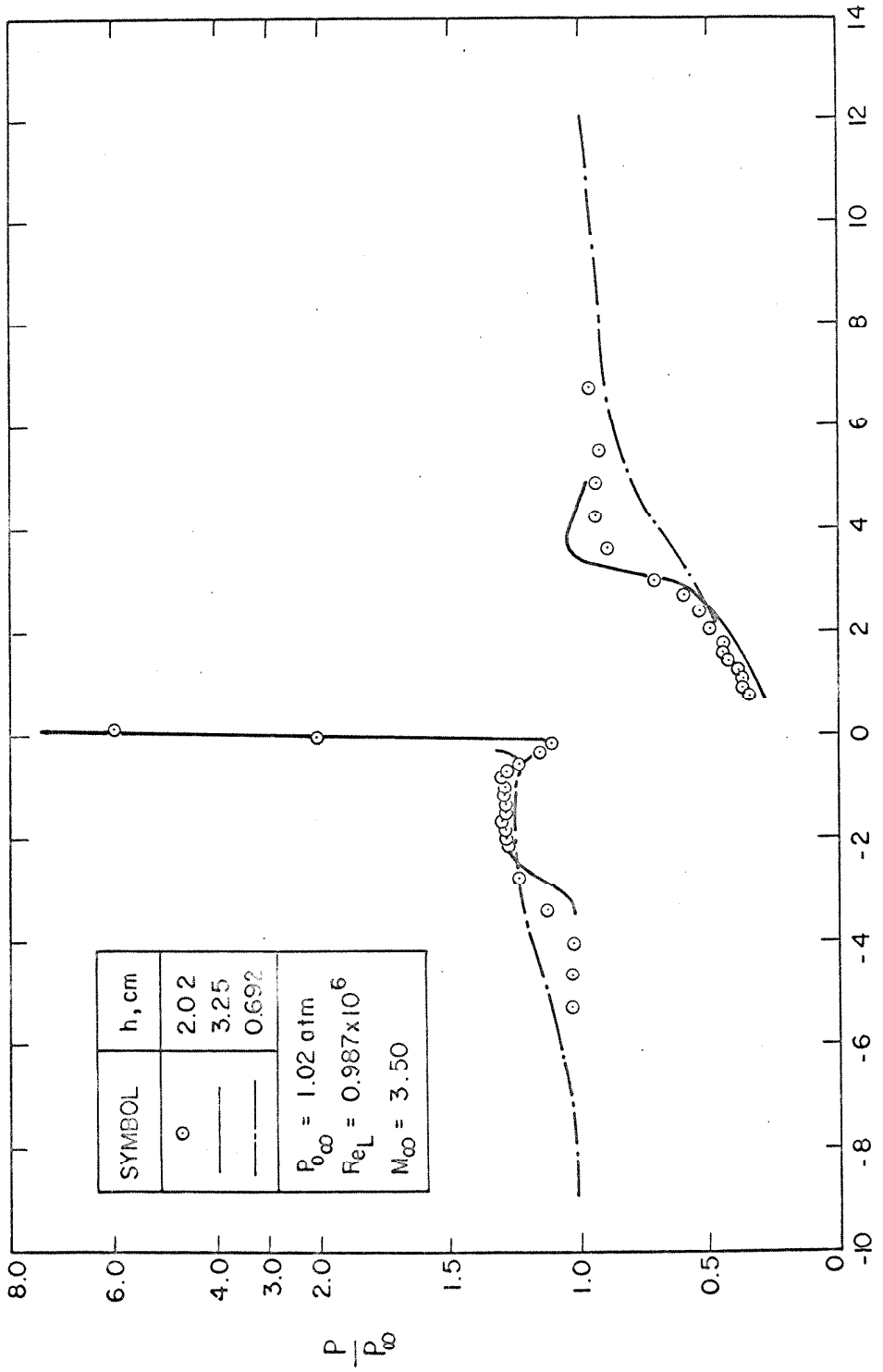

Figure 22. Flat-Plate Static Pressure Measurements in the Plane (y/h) = 0 at M_∞ = 3.50 with Nitrogen Injection. Laminar Boundary Layer

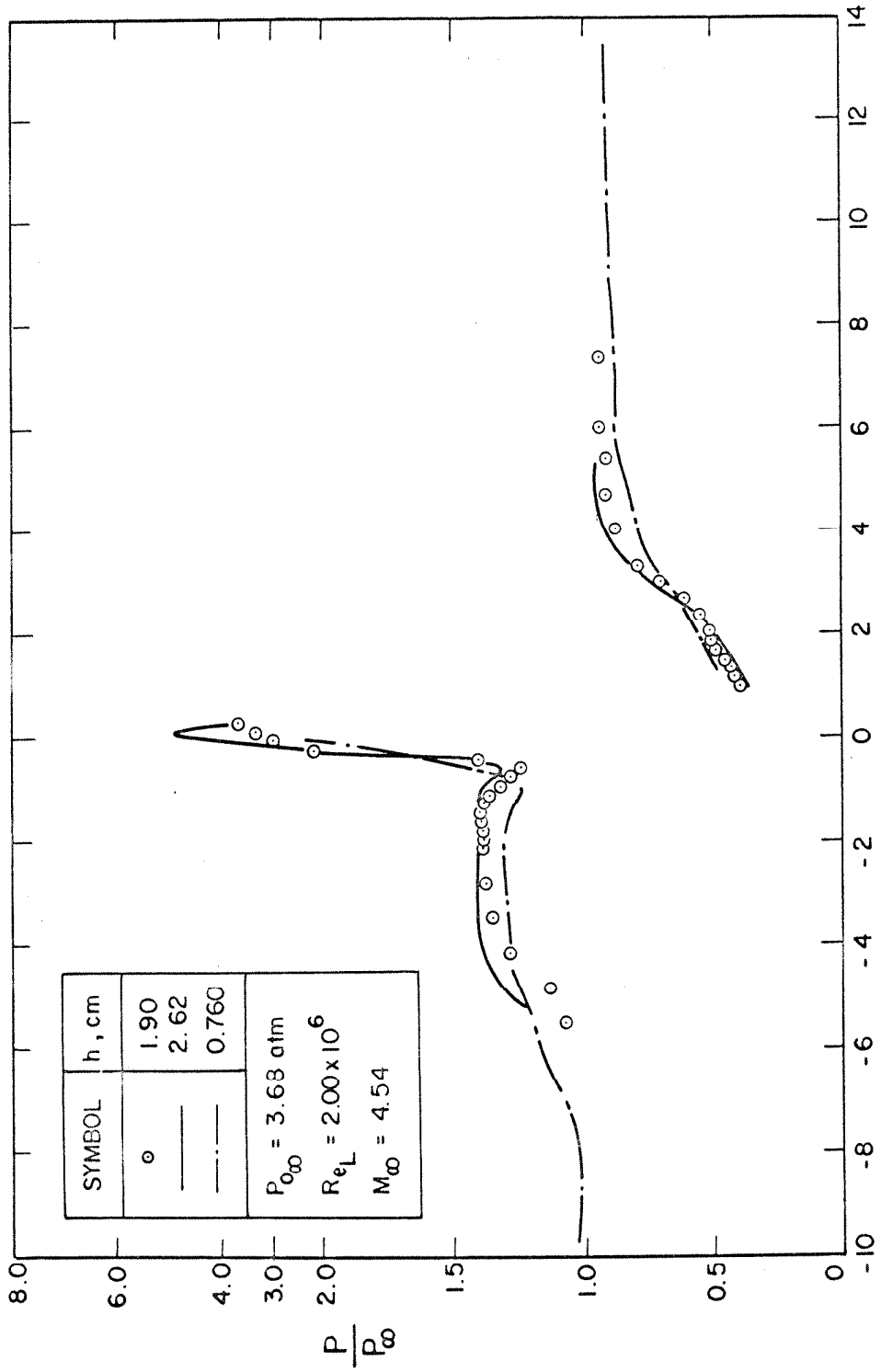

Figure 23. Flat-Plate Static Pressure Measurements in the Plane (y/h) = 0 at M_∞ = 4.54 with Nitrogen Injection. Laminar Boundary Layer

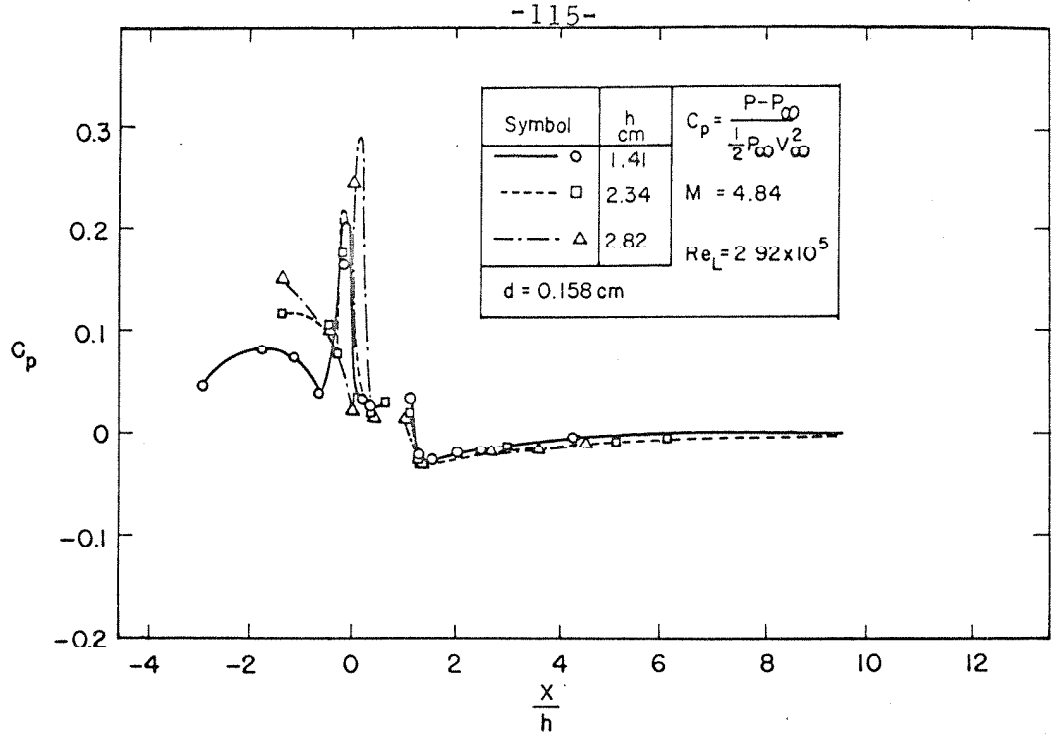

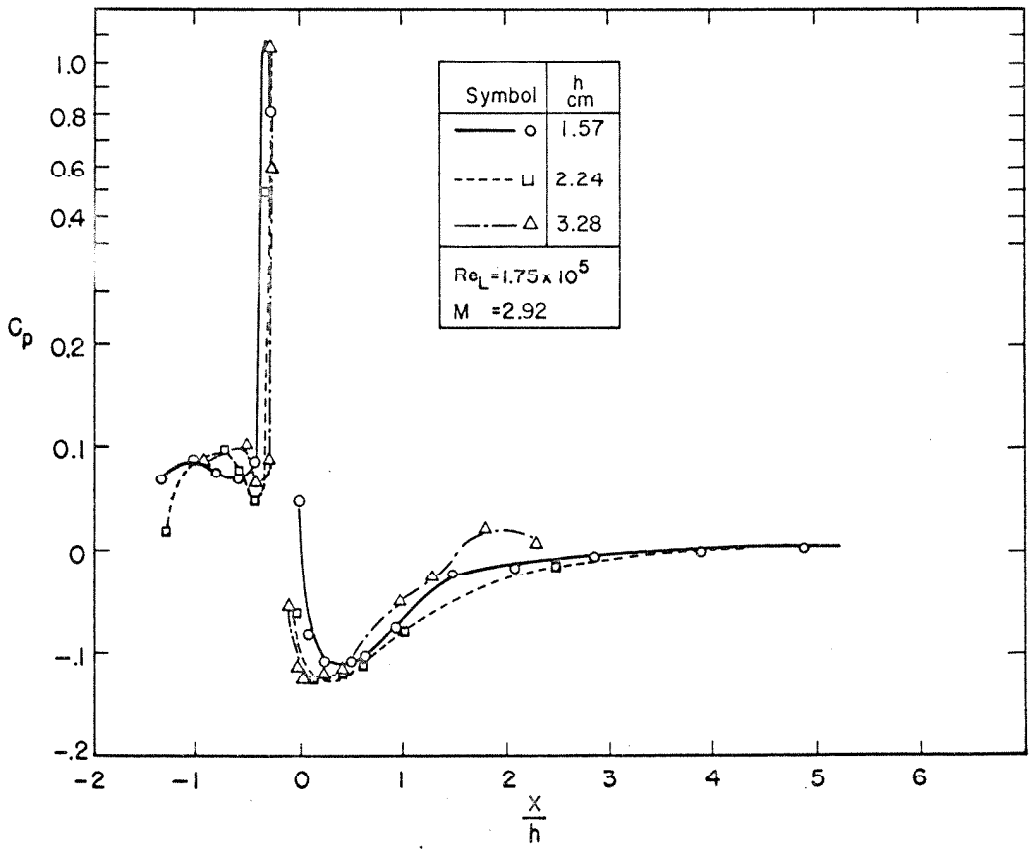

Figures 24. Correlation of Pressure Data from Reference 9

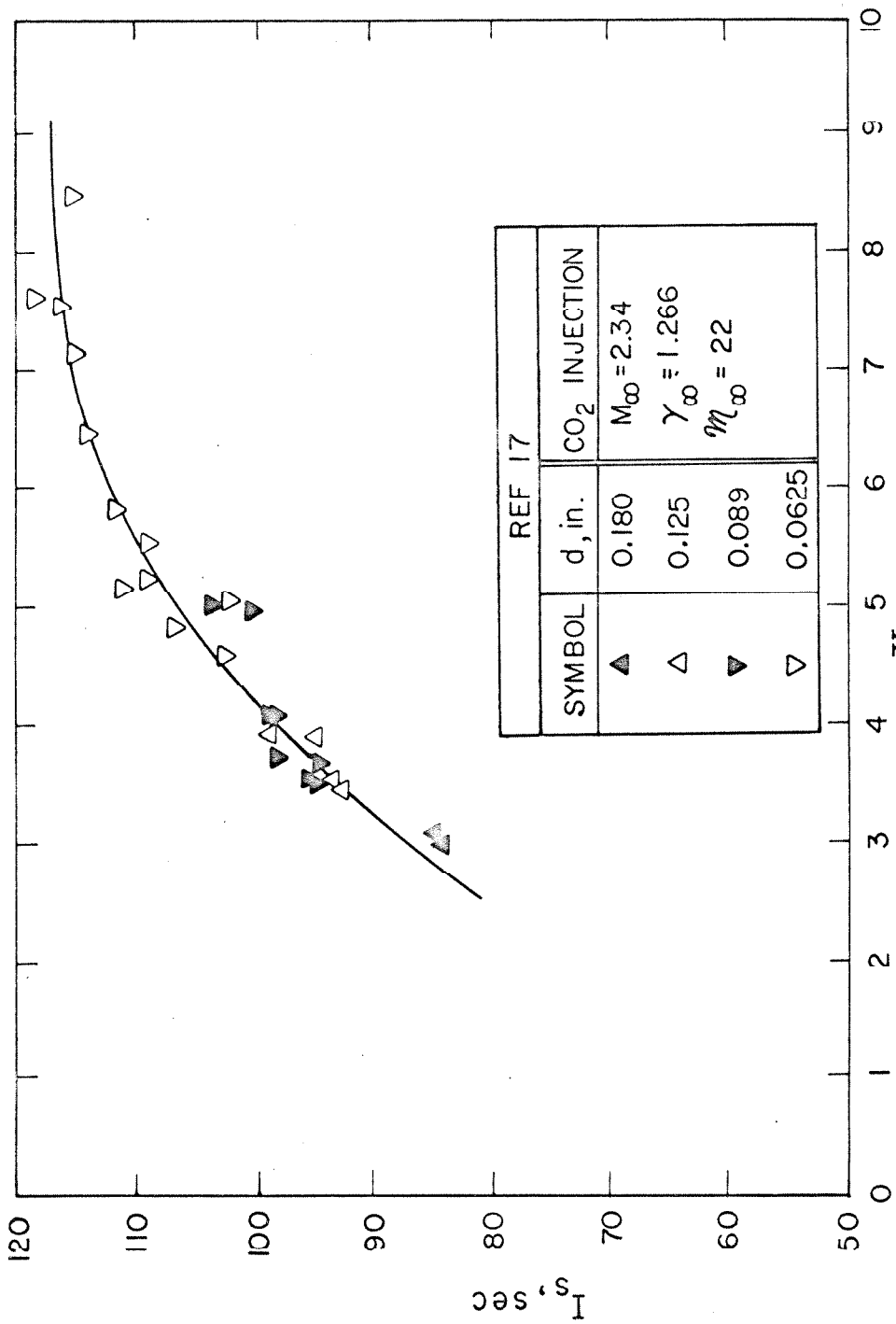

Figure 25. Variation of Side Specific Impulse with Normalized Distance from Injector to Nozzle Exit

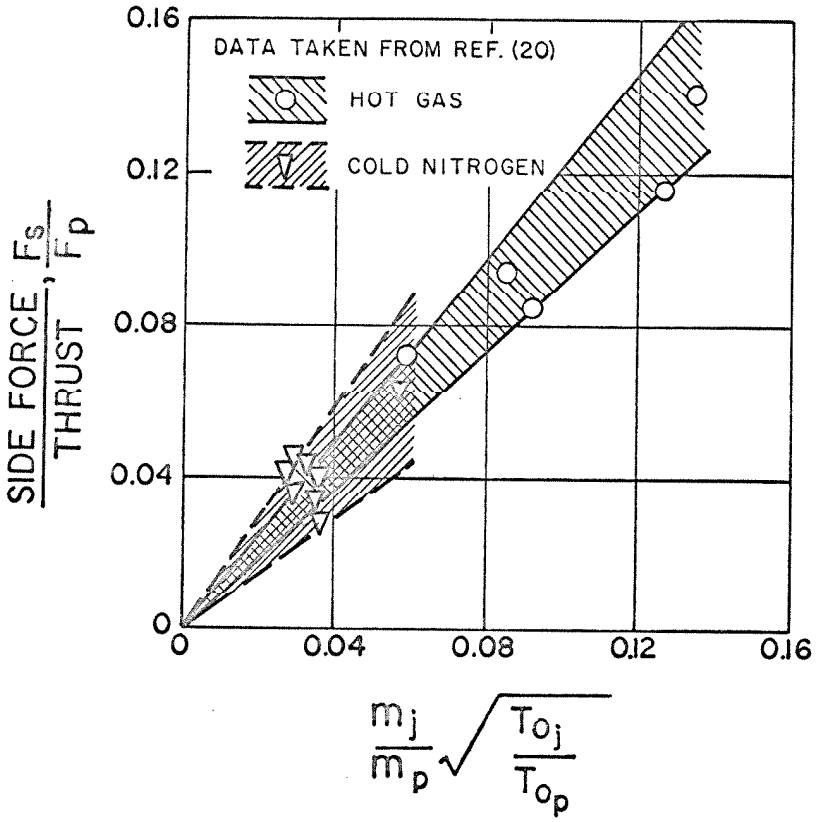

Figure 26. Correlation of Rocket-Motor Thrust Vector-Control Performance for Different Gases and Temperatures (from Reference 20)

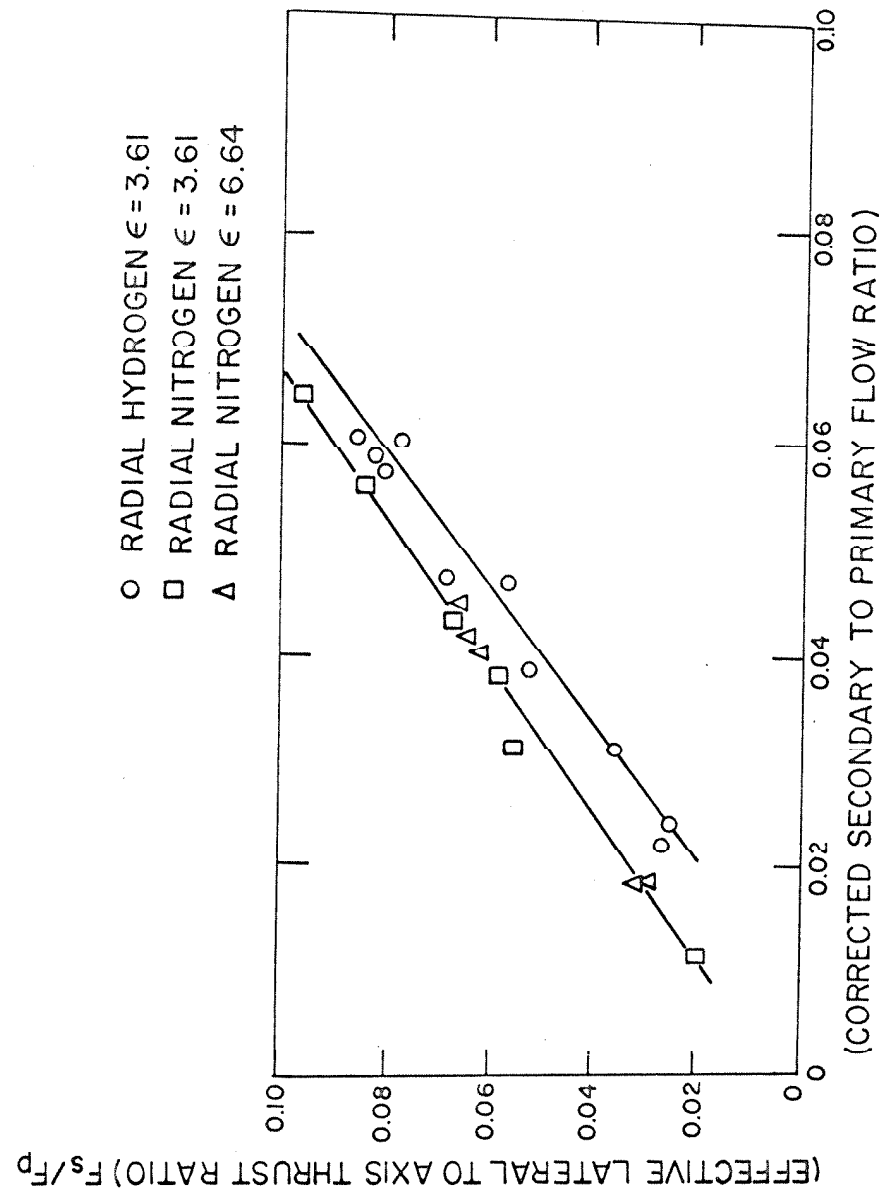

Figure 27. Correlation of Rocket-Motor Thrust Vector-Control Data (from Reference 21)

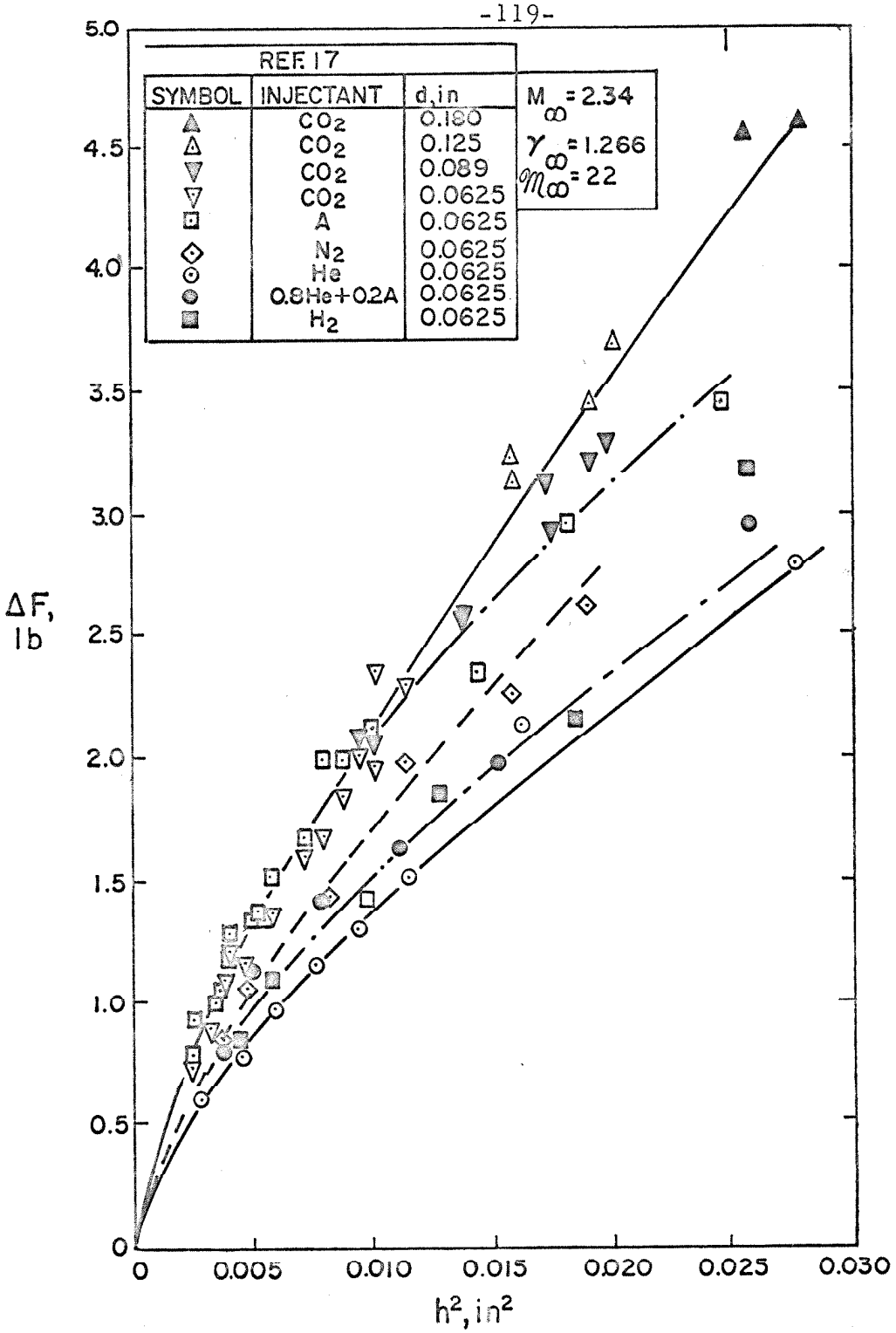

Figure 28a. Correlation of Rocket-Motor Thrust Vector-Control Data (from Reference 17), Present Method

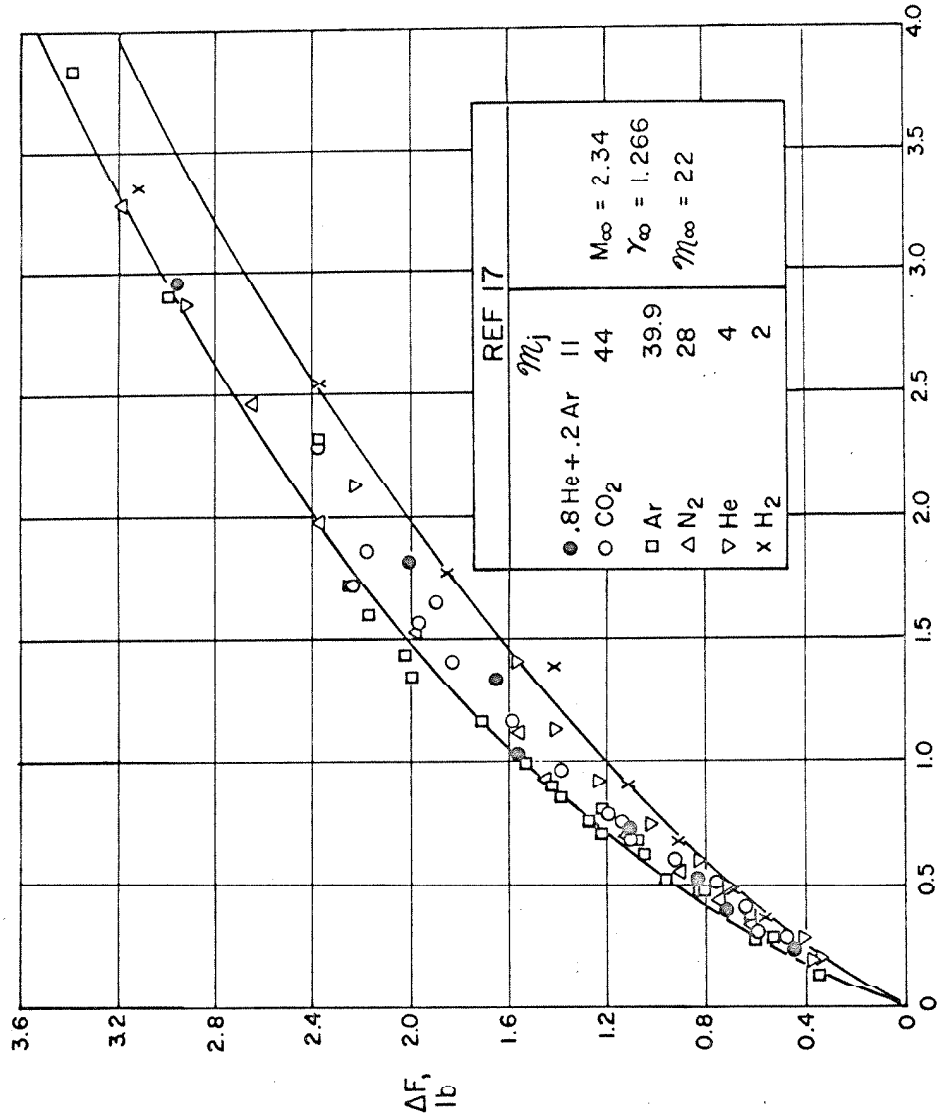

Figure 28b. Correlation of Rocket-Motor Thrust Vector-Control Data (from Reference 22), Method of Brcadwell

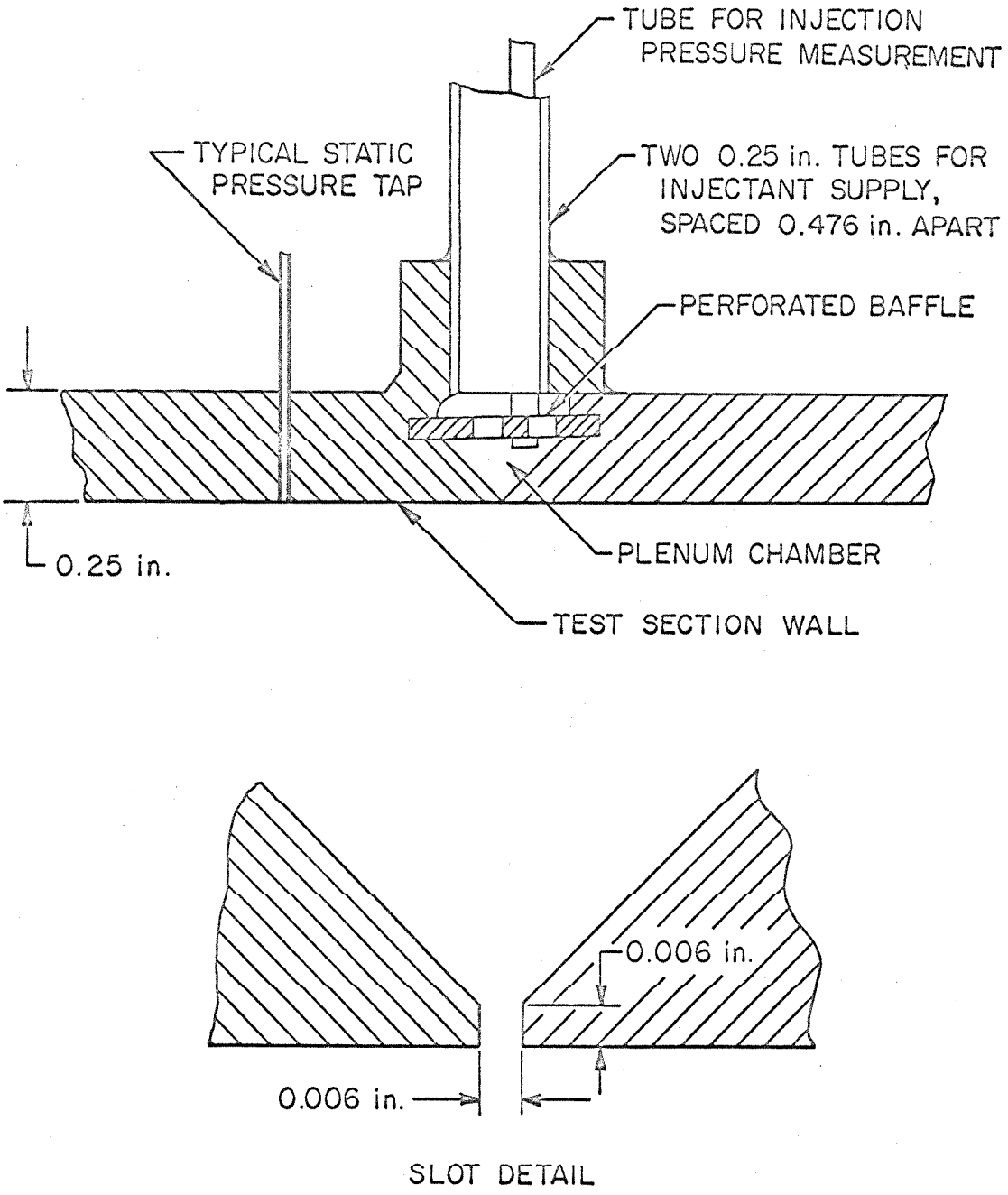

Figure 29. Section View of Slot Injector

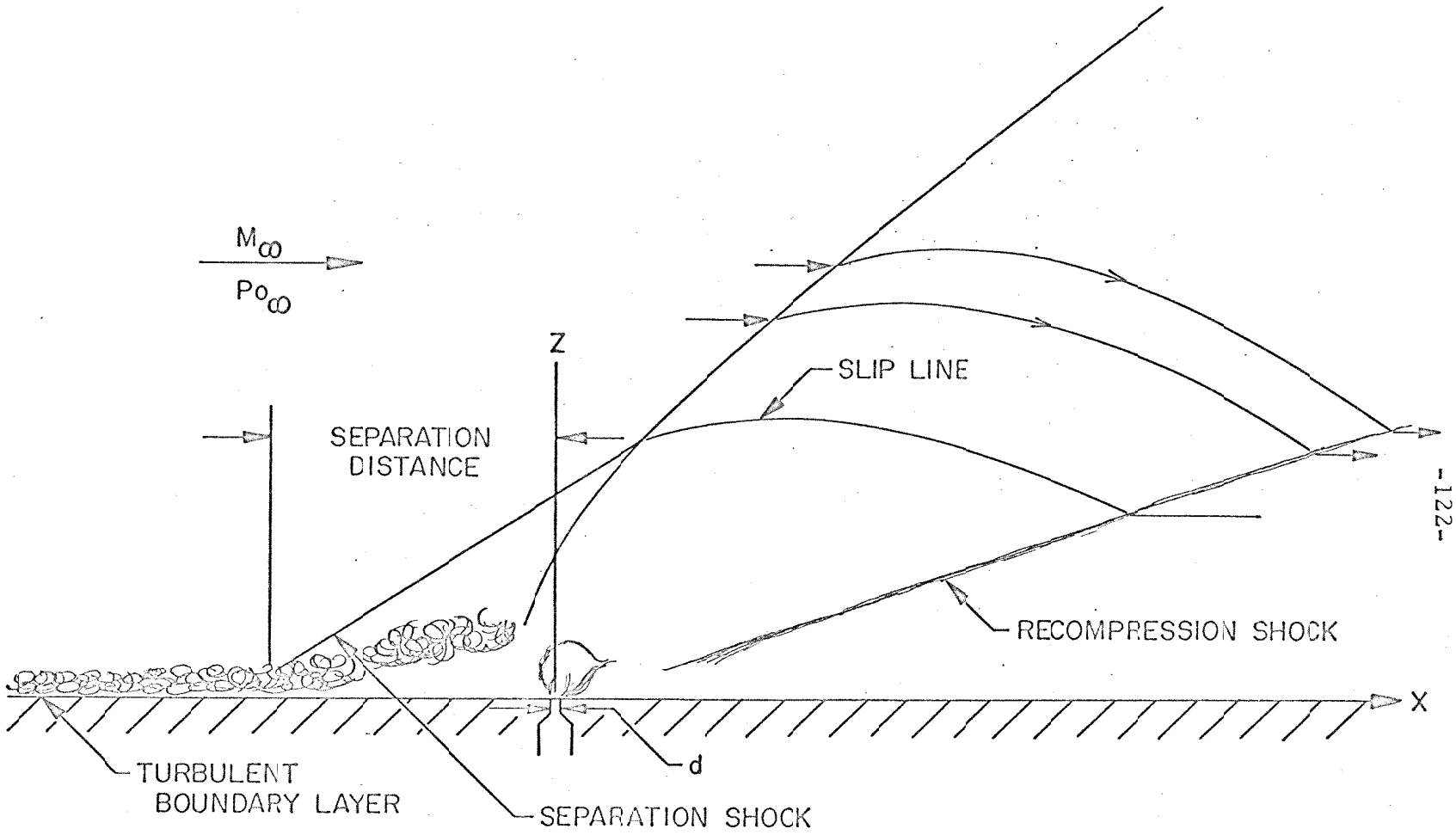

Figure 30a. Sketch of the Flow Field for Slot Injection, Turbulent Boundary Layer

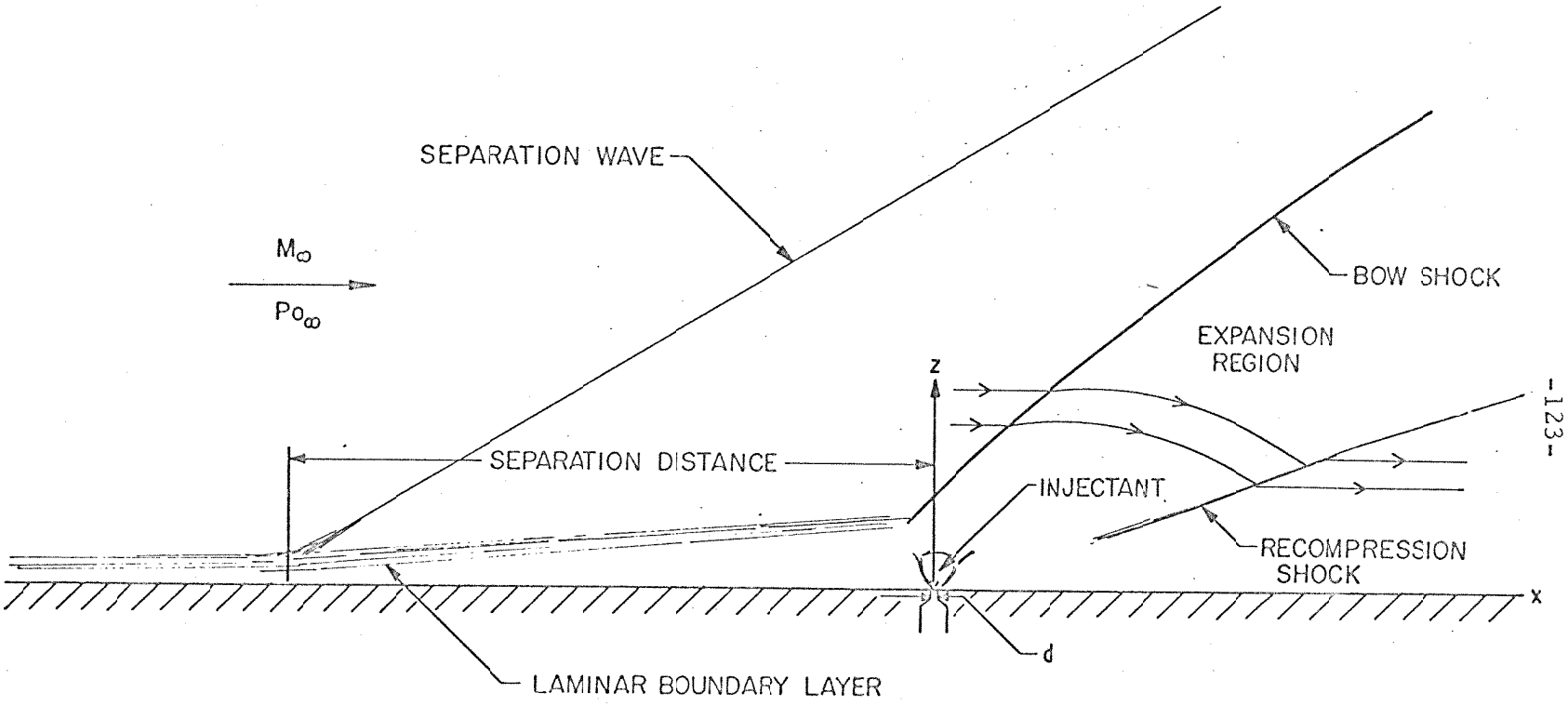

Figure 30b. Sketch of the Flow Field for Slot Injection, Laminar Boundary Layer

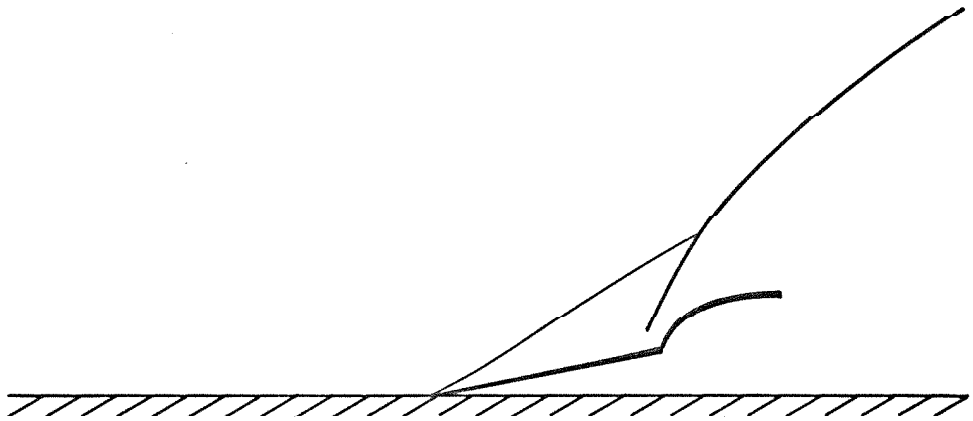

a. TURBULENT BOUNDARY LAYER CASE

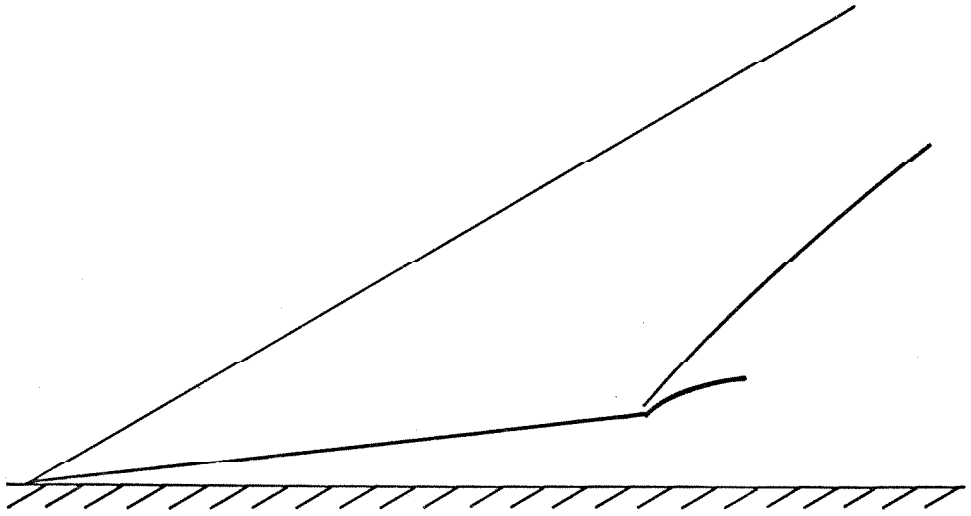

b. LAMINAR BOUNDARY LAYER CASE

Figure 31. The Injectant Obstacle as Seen by the Inviscid Flow Field

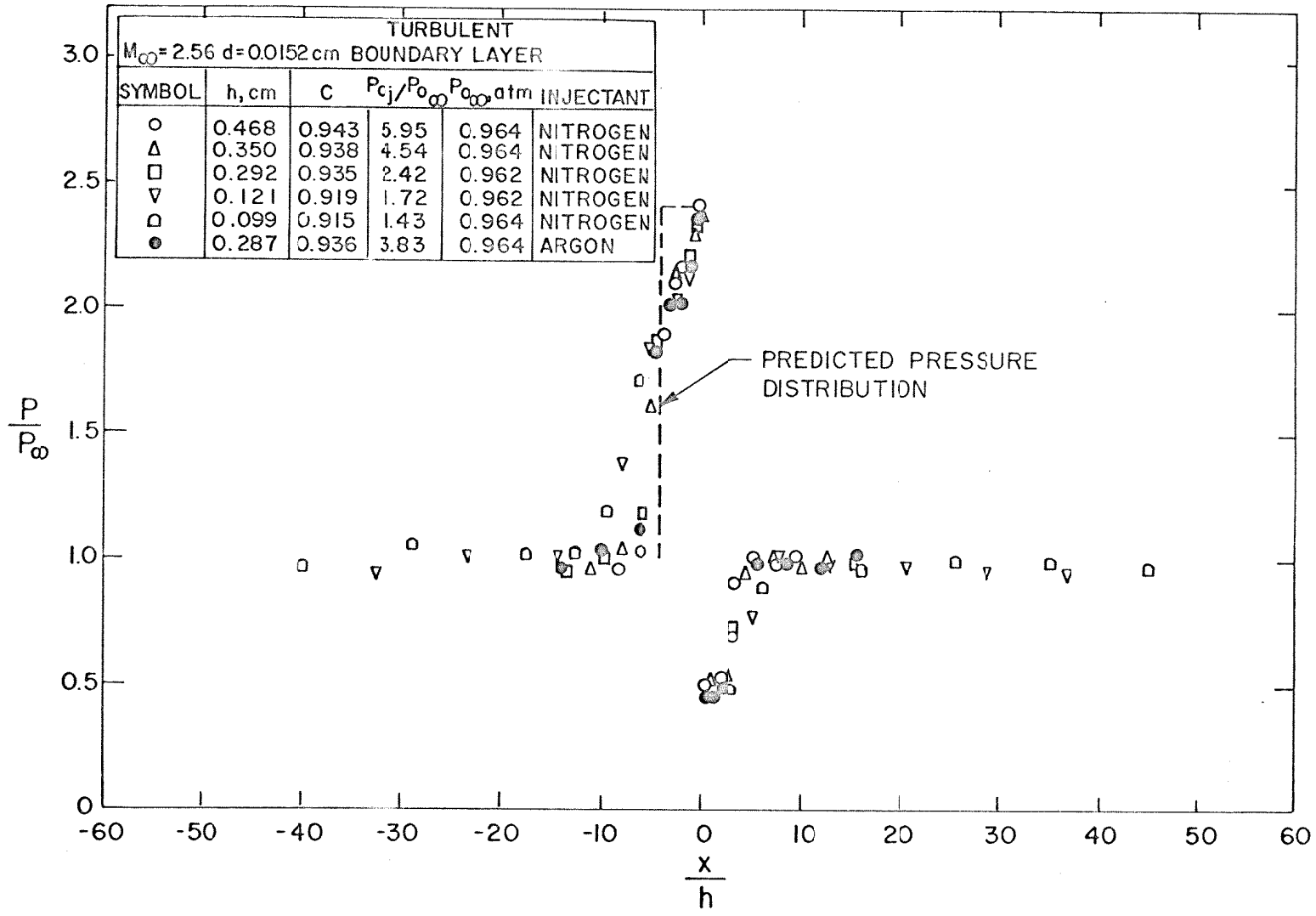

Figure 32. Nozzle-Wall Static Pressure Measurements for Slot Injection. Larger Values of h. Turbulent Boundary Layer

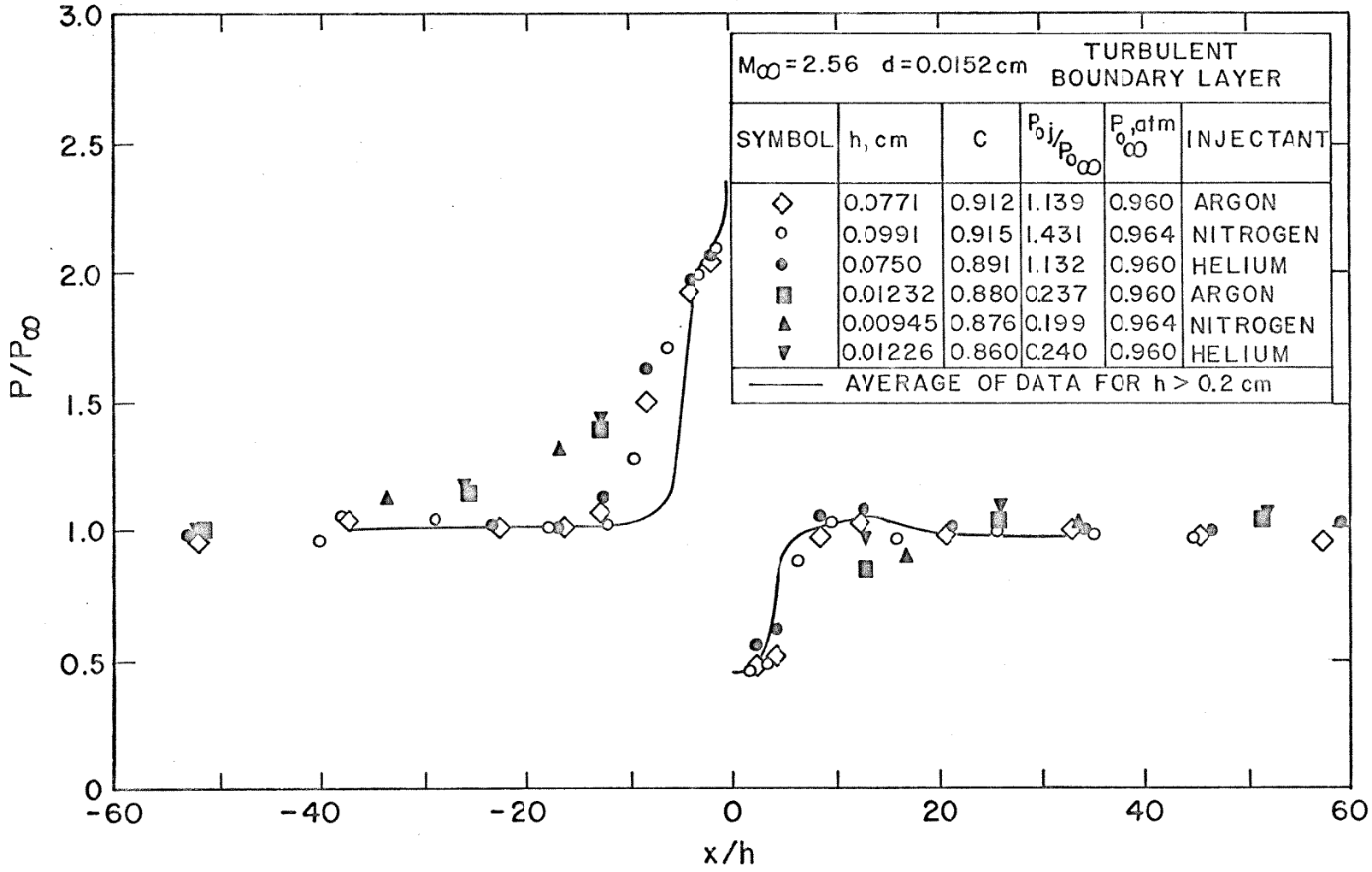

Figure 33. Nozzle-Wall Static Pressure Measurements for Slot Injection. Smaller Values of h. Turbulent Boundary Layer

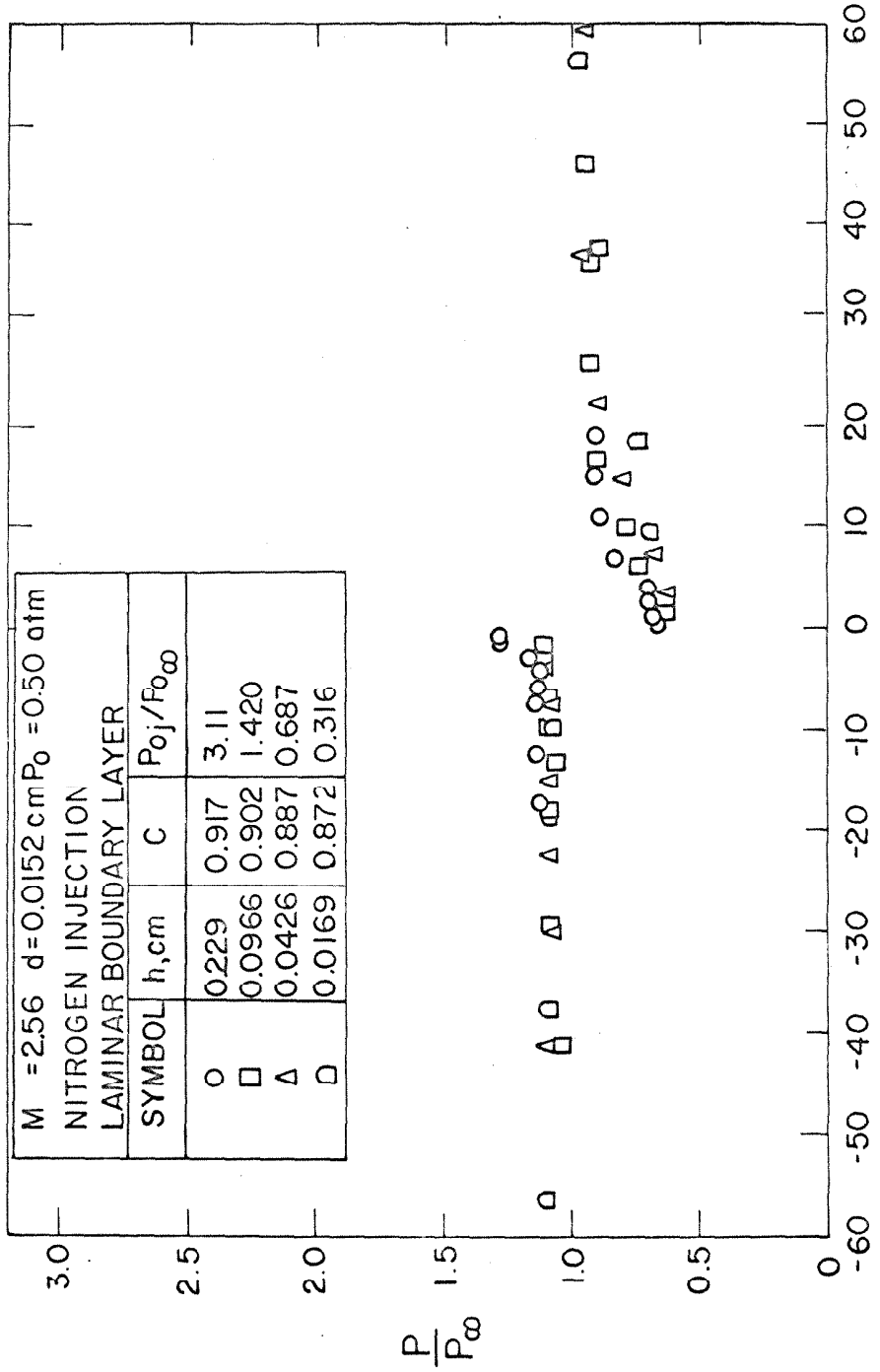

Figure 34. Nozzle-Wall Static Pressure Measurements for Slot Injection. Laminar Boundary Layer

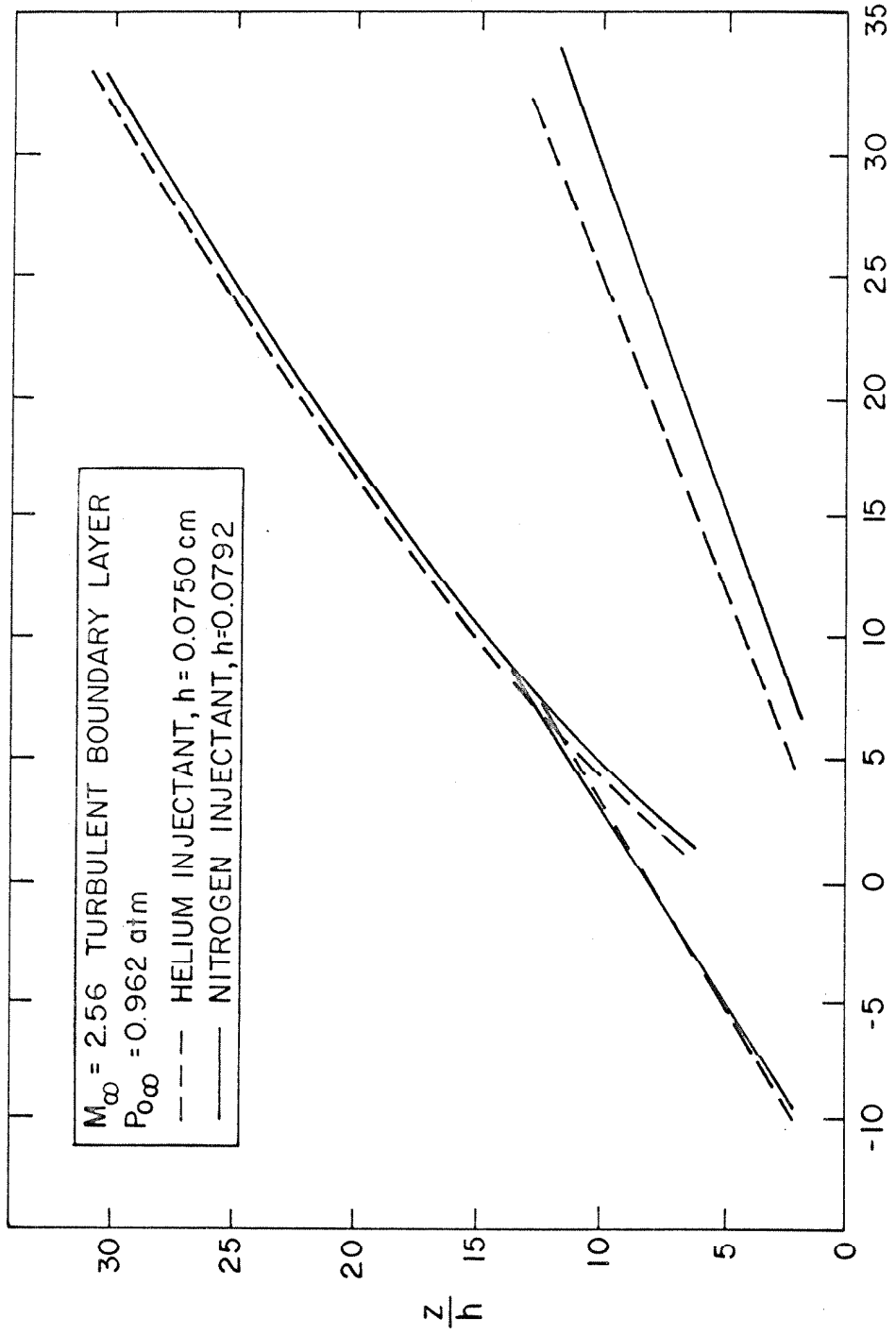

Figure 35. Shock Shape Comparison for Nitrogen and Helium Slot Injection

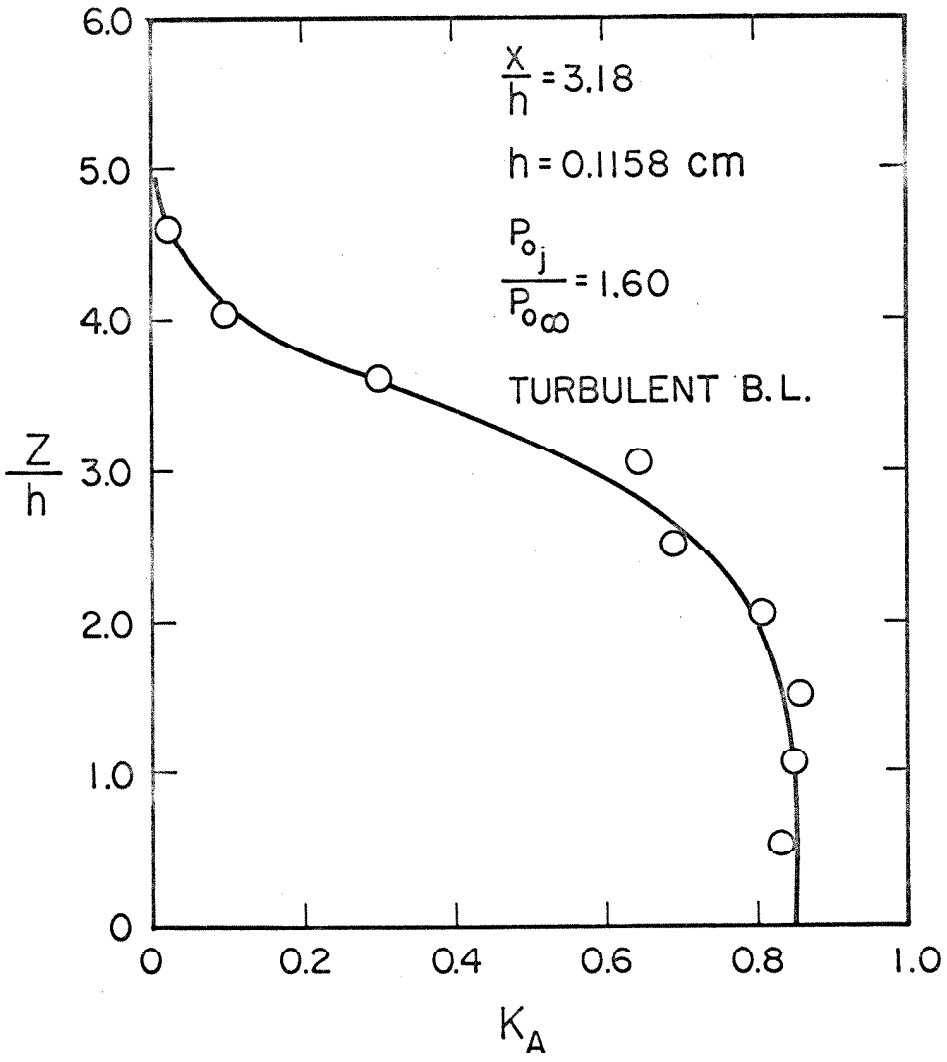

Figure 36. Concentration Measurements with Argon Slot Injection; Injector Region. h = 0.1158 cm. Turbulent Boundary Layer

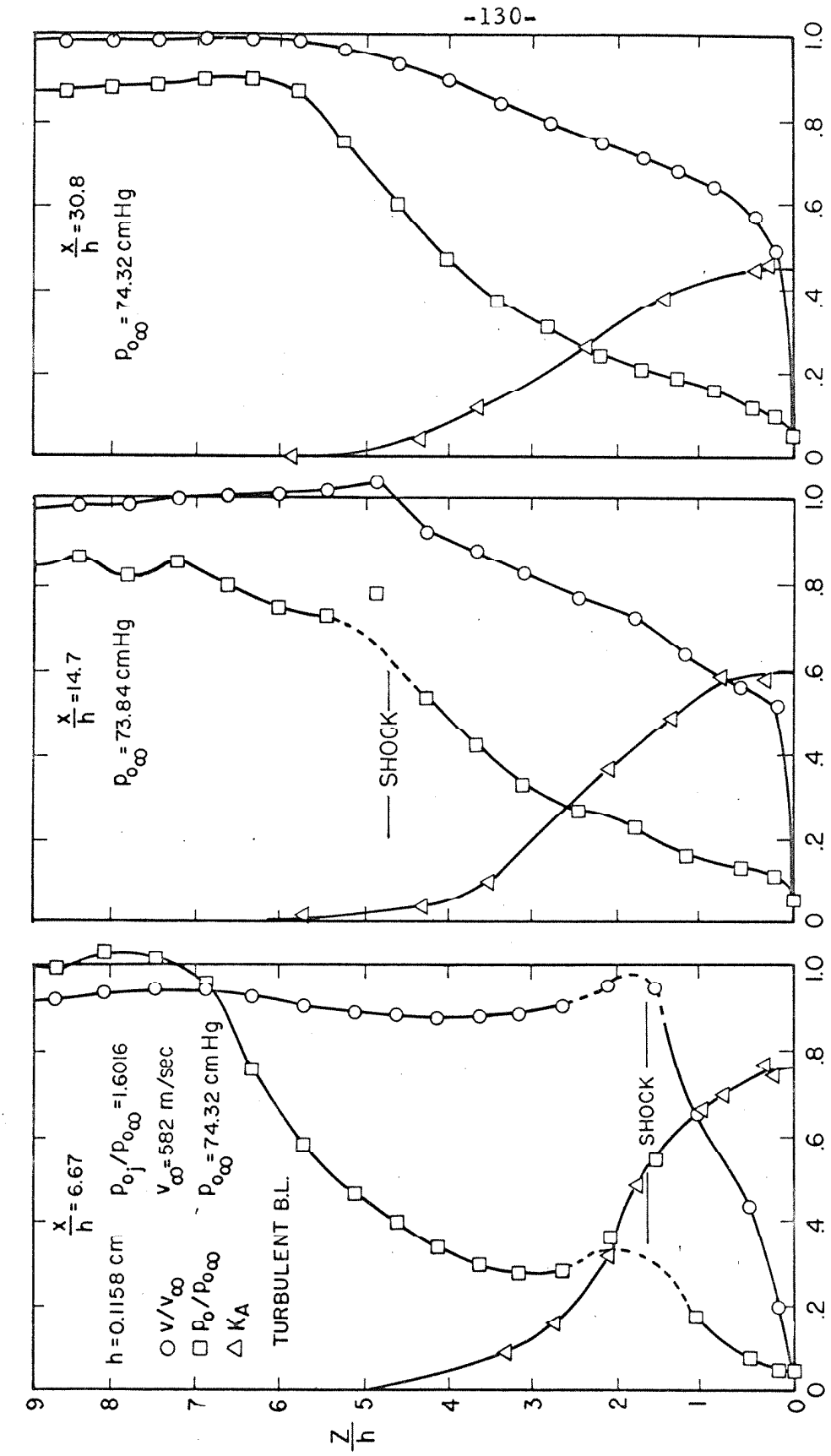

Figure 37, Concentration, Total Pressure, and Velocity Profiles for Argon Injection Through a Slot, h = 0.1158 cm. Turbulent Boundary Layer

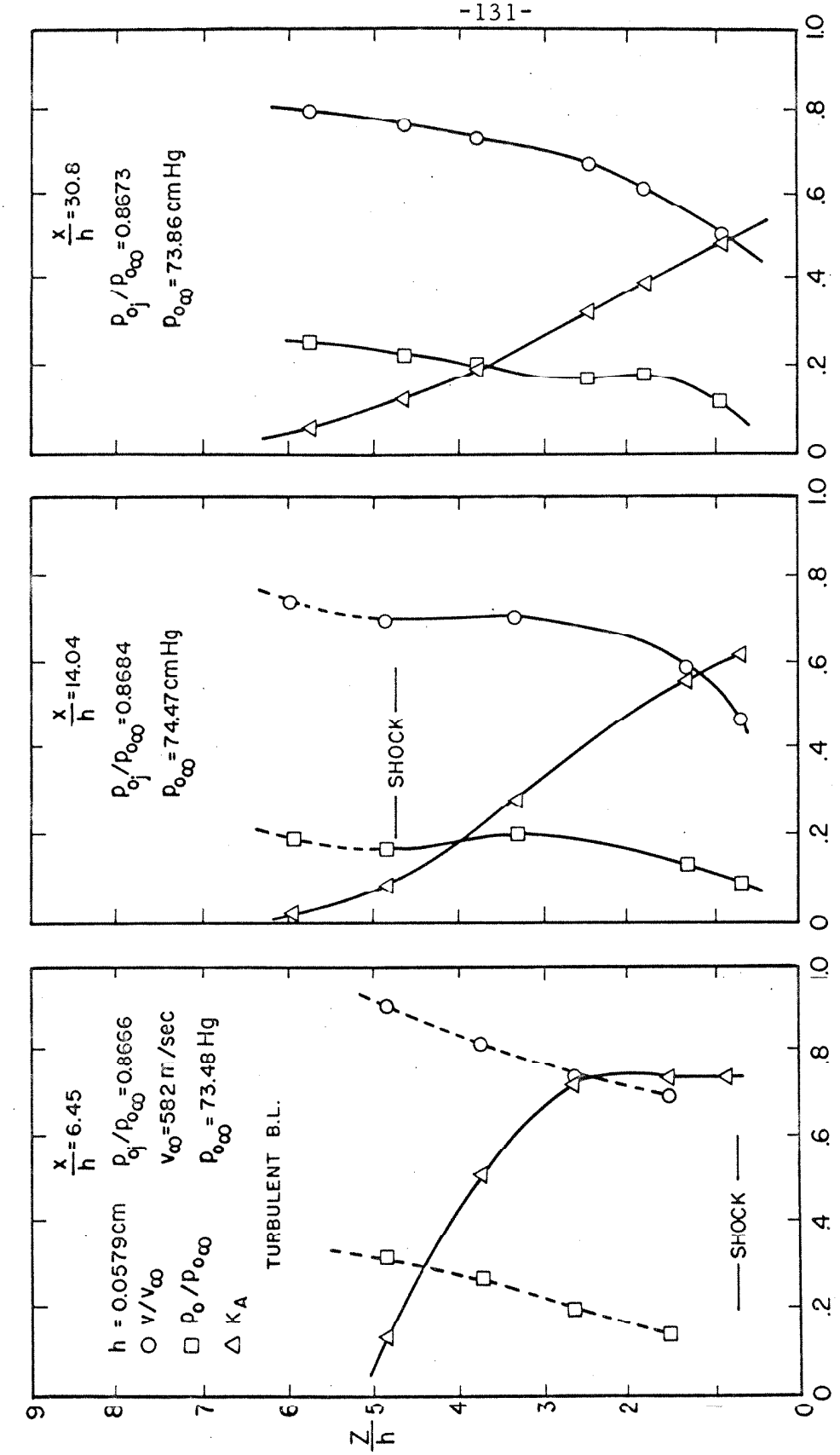

Figure 38. Concentration, Total Pressure, and Velocity Profiles for Argon Injection Through a Slot. h = 0.0579 cm. Turbulent Boundary Layer

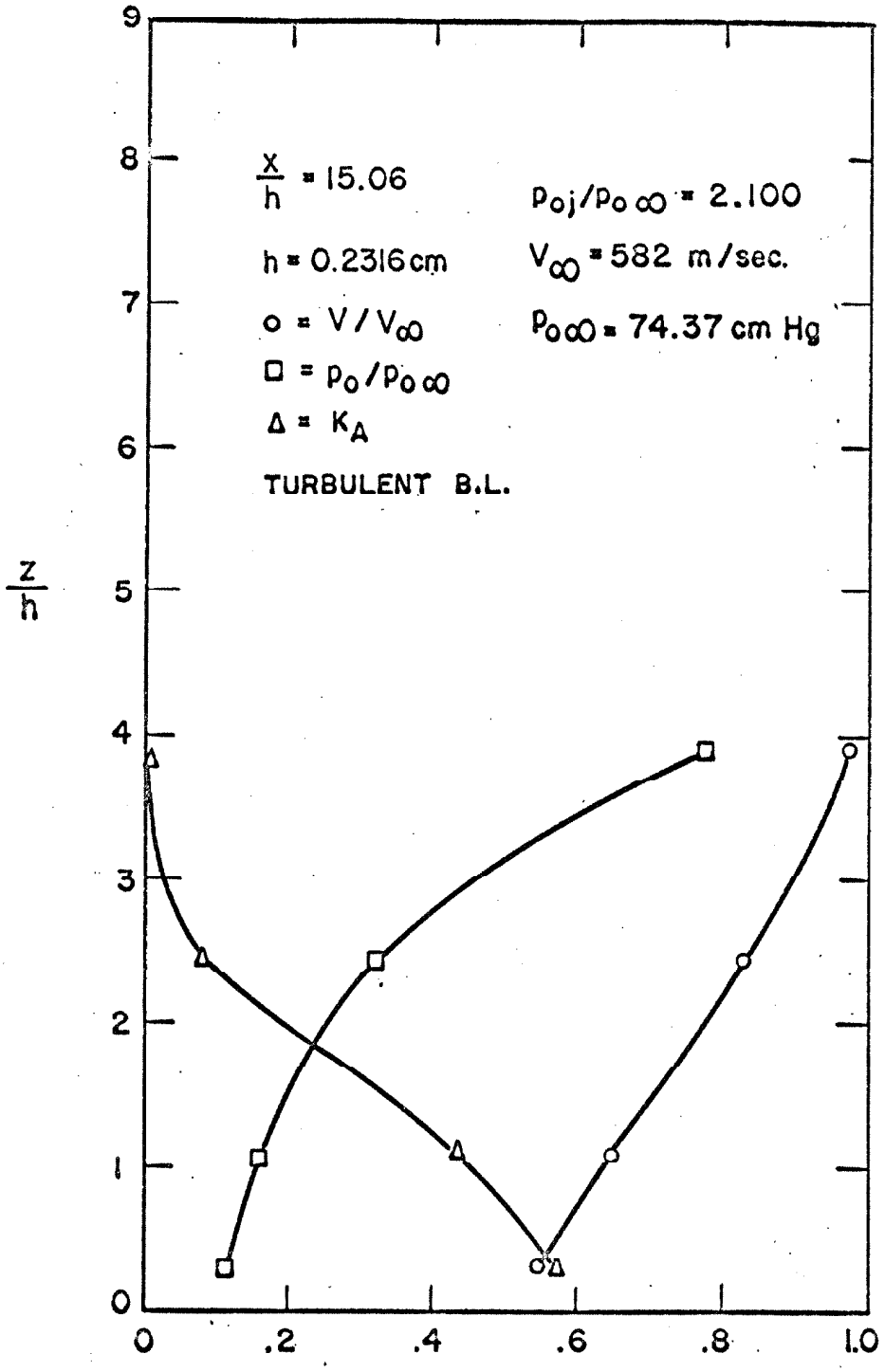

Figure 39. Concentration, Total Pressure, and Velocity Profiles for Argon Injection Through a Slot. h = 0.2316 cm. Turbulent Boundary Layer

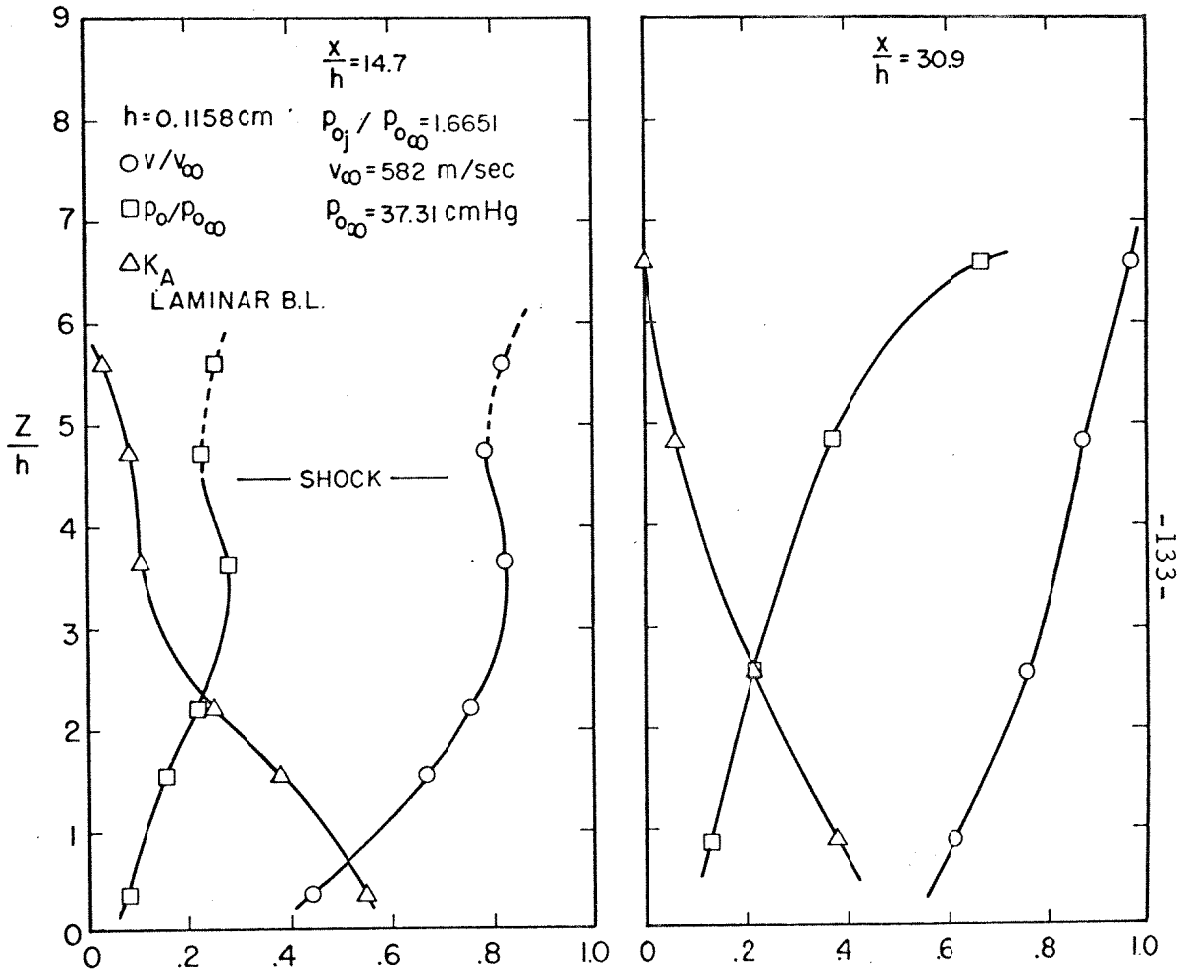

Figure 40. Concentration, Total Pressure, and Velocity Profiles for Argon Injection Through a Slot. h = 0.1158 cm. Laminar Boundary Layer

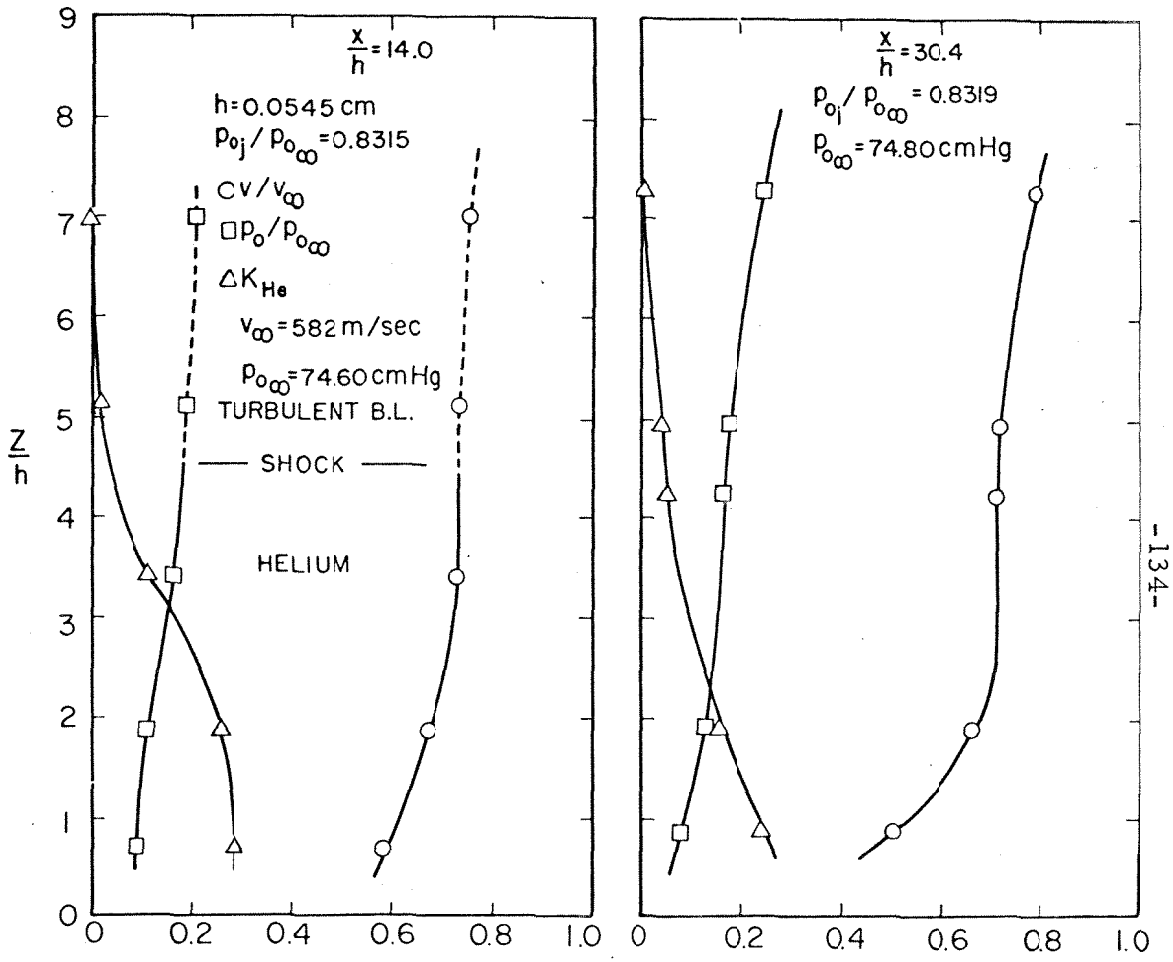

Figure 41. Concentration, Total Pressure, and Velocity Profiles for Helium Injection Through a Slot. h = 0.0545 cm. Turbulent Boundary Layer

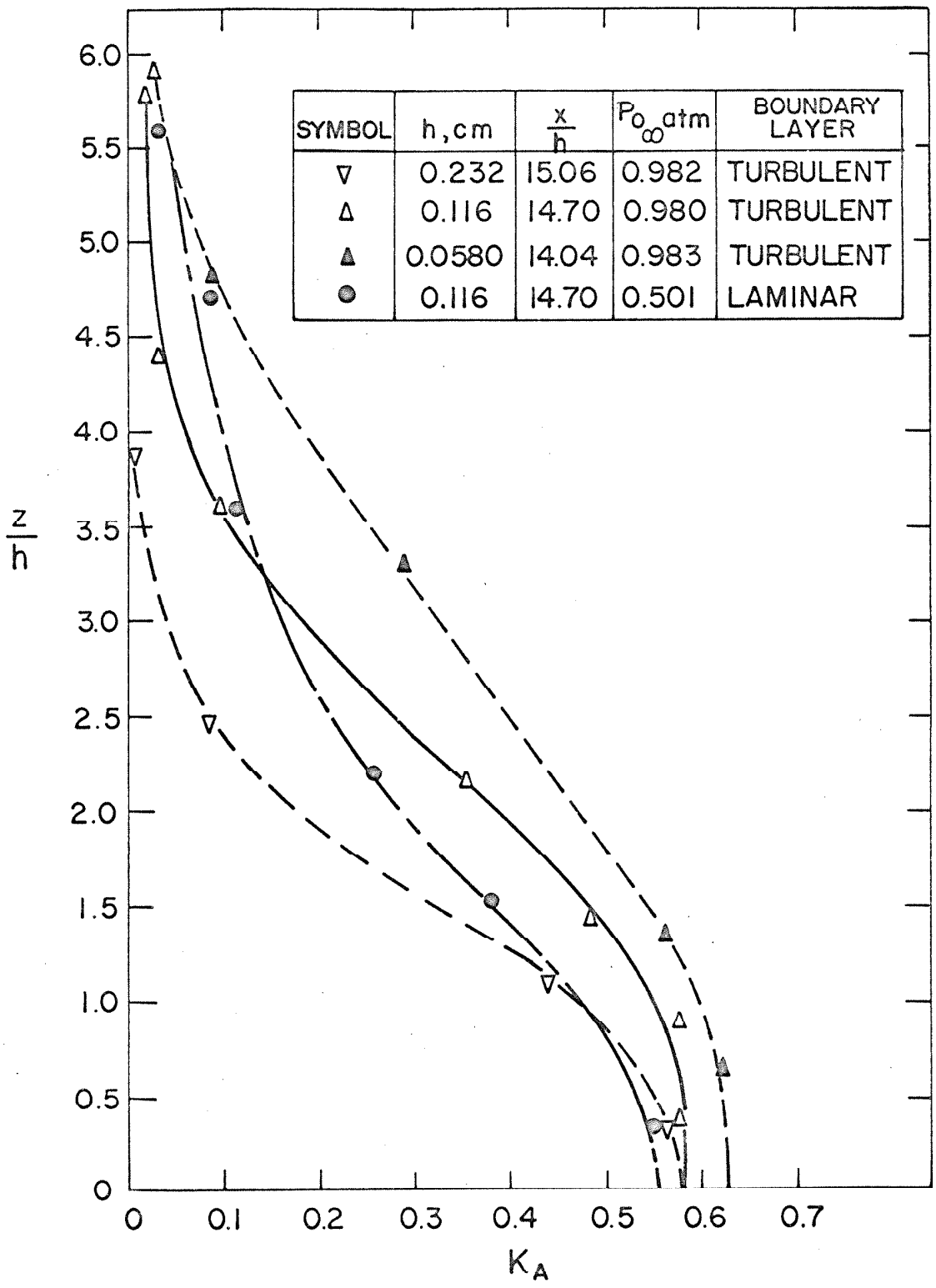

Figure 42. Argon Concentration Profiles for (x/h) ~ 15, Slot Injection

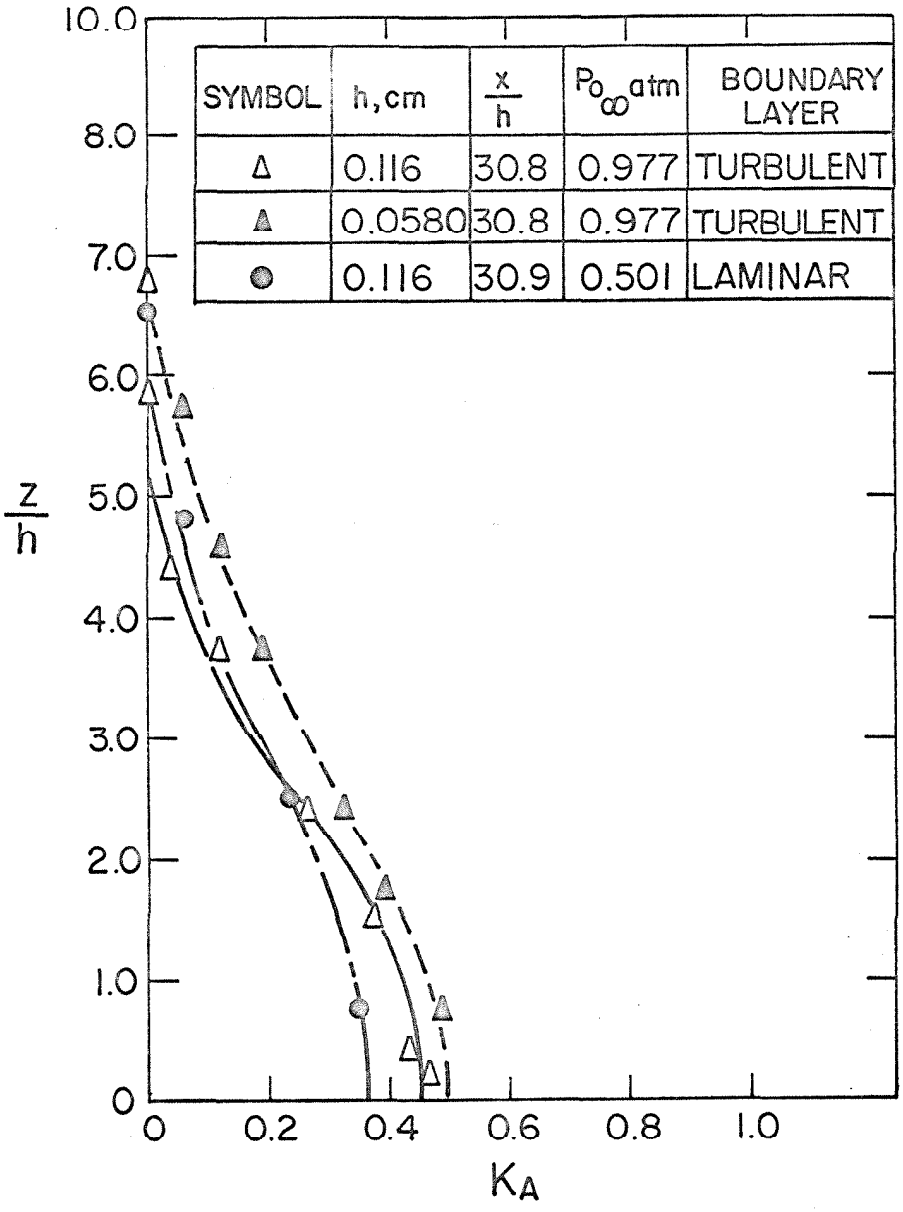

Figure 43. Argon Concentration Profiles for $(x/h) \sim 30$, Slot Injection

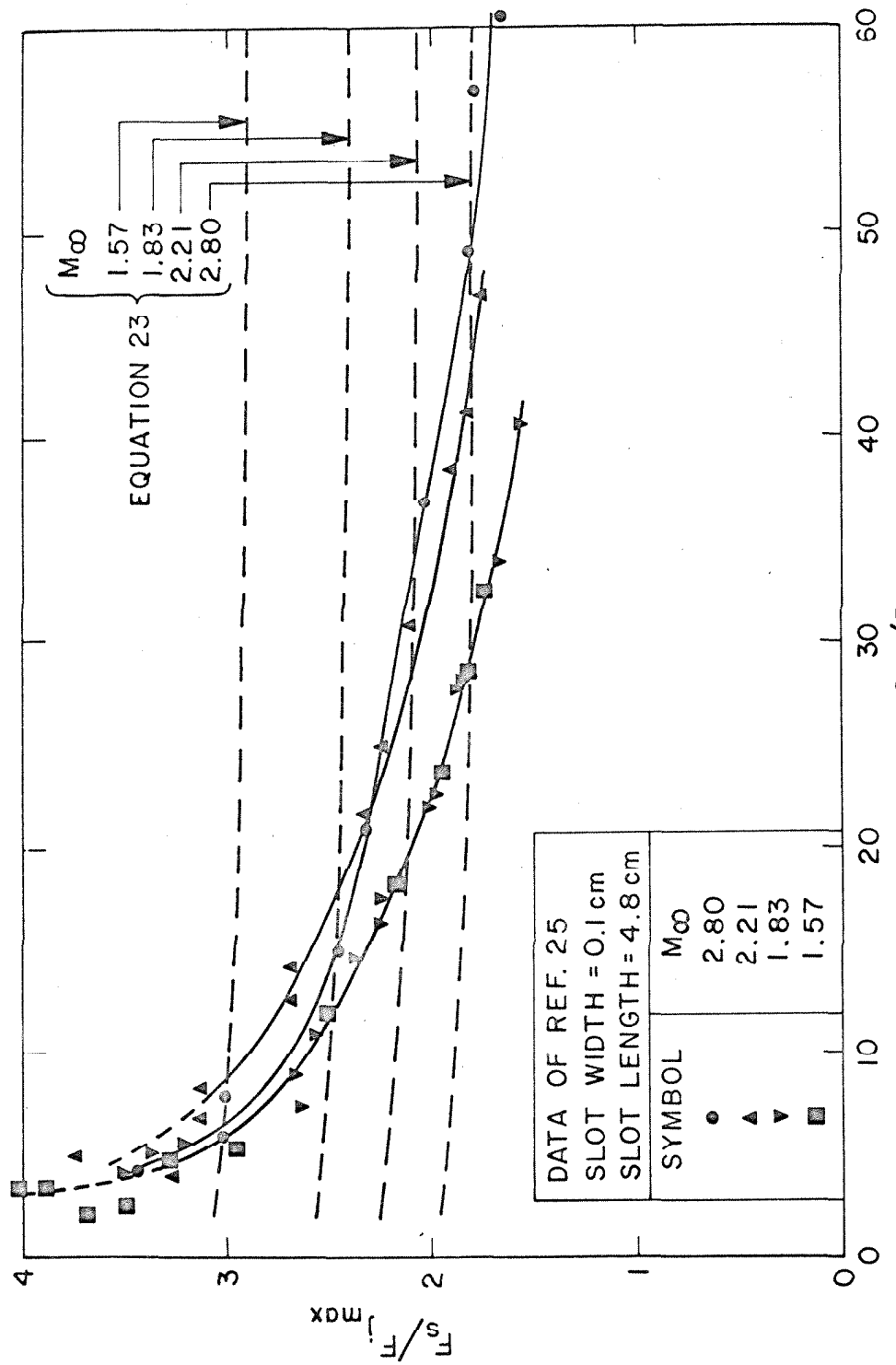

Figure 44. Variation of Non-Dimensional Normal Force Upstream of a Slot with Jet Stagnation Pressure to Free-Stream Static Pressure Ratio. Data from Reference 25

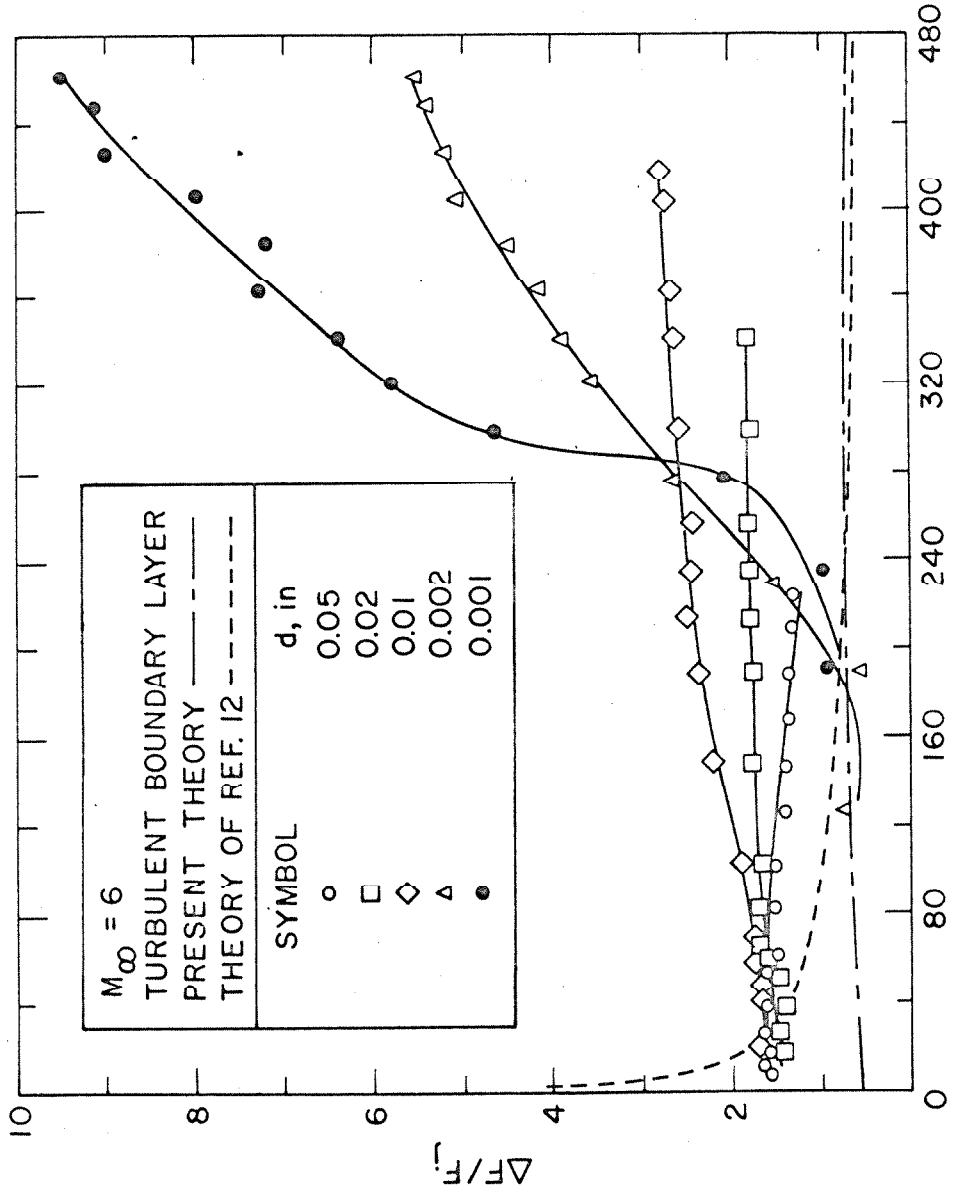

Figure 45. Variation of Non-Dimensional Normal Force Upstream of a Slot with Jet Stagnation Pressure to Free-Stream Static Pressure Ratio. Data from Reference 26

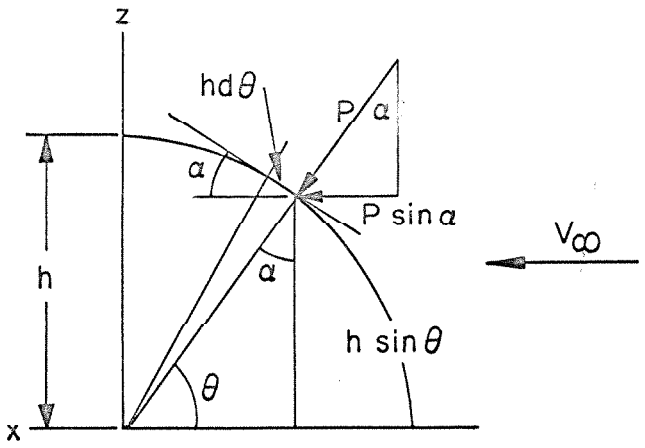

Figure 46a. Sketch for Pressure Integral Derivation, Two-Dimensional Case

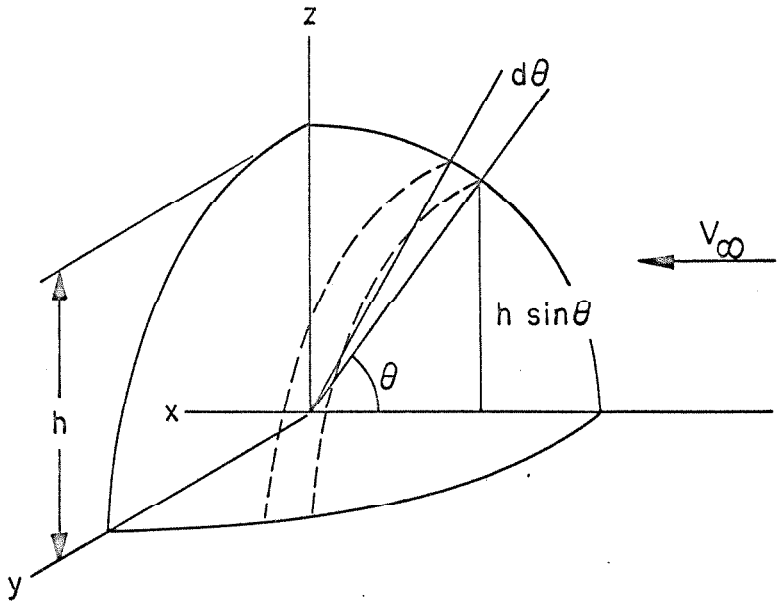

Figure 46b. Sketch for Pressure Integral Derivation, Three-Dimensional Case